The group galaxy population through the cosmic time. Study of the properties of galaxies in the most common high density environment

Ghazaleh Erfanianfar

SIGIL·UNIVERSITAT·LUDOVIC·MAXIM

München, 2013

The group galaxy population through the cosmic time. Study of the properties of galaxies in the most common high density environment

Ghazaleh Erfanianfar

Dissertation
der Fakultät für Physik
der Ludwig–Maximilians–Universität
München

vorgelegt von
Ghazaleh Erfanianfar
aus dem Iran

München, December 2013

Erstgutachter: Prof. Dr. Kirpal Nandra
Zweitgutachter: Prof. Dr. Joseph Mohr
Tag der mündlichen Prüfung: 24. February 2014

Contents

List of Figures

List of Tables

Summary

One of the most fundamental correlations between the properties of galaxies in the local Universe is the so-called morphology-density relation (Dressler 1980). A plethora of studies utilizing multi-wavelength tracers of activity have shown that late type star forming galaxies favour low density regions in the local Universe (e.g. Gómez et al. 2003). In particular, the cores of massive galaxy clusters are galaxy graveyards full of massive spheroids that are dominated by old stellar populations. A variety of physical processes might be effective in suppressing star formation and affecting the morphology of cluster and group galaxies. Broadly speaking, these can be grouped in two big families: (i) interactions with other cluster members and/or with the cluster gravitational potential and (ii) interactions with the hot gas that permeates massive galaxy systems. Galaxy groups are the most common galaxy environment in our Universe, bridging the gap between the low density field and the crowded galaxy clusters. Indeed, as many as 50%-70% of galaxies reside in galaxy groups in the nearby Universe (Huchra & Geller 1982; Eke et al. 2004), while only a few percent are contained in the denser cluster cores. In addition, in the current bottom-up paradigm of structure formation, galaxy groups are the building blocks of more massive systems: they merge to form clusters. As structures grow, galaxies join more and more massive systems, spending most of their life in galaxy groups before entering the cluster environment. Thus, it is plausible to ask if group-related processes may drive the observed relations between galaxy properties and their environment.

To shed light on this topic we have built the largest X-ray selected samples of galaxy groups with secure spectroscopic identification on the major blank field surveys. For this purpose, we combine deep X-ray Chandra and XMM data of the four major blank fields (All-wavelength Extended Groth Strip International Survey (AEGIS), the COSMOS field, the Extended Chandra Deep Field South (ECDFS), and the Chandra Deep Field North (CDFN)). The group catalog in each field is created by associating any X-ray extended emission to a galaxy overdensity in the 3D space. This is feasible given the extremely rich spectroscopic coverage of these fields. Our identification method and the dynamical analysis used to identify the galaxy group members and to estimate the group velocity dispersion is extensively tested on the AEGIS field and with mock catalogs extracted from the Millennium Simulation (Springel et al. 2005). The effect of dynamical complexity,

substructure, shape of X-ray emission, different radial and redshift cuts have been explored on the $L_X - \sigma$ relation. We also discover a high redshift group at z∼1.54 in the AEGIS field. This detection illustrates that mega-second Chandra exposures are required for detecting such objects in the volume of deep fields. We provide an accurate measure of the Star Formation Rate (SFR) of galaxies by using the deepest available *Herschel* PACS and *Spitzer* MIPS data available for the considered fields. We also provide a well-calibrated estimate of the SFR derived by using the SED fitting technique for undetected sources in mid- and far-infrared observations.

Using this unique sample, we conduct a comprehensive analysis of the dependence of the total SFR (Σ SFR), total stellar masses (Σ M_*) and halo occupation distribution (HOD) of massive galaxies ($M_* > 10^{10} M_\odot$) on the halo mass of the groups with rigorous consideration of uncertainties. We observe a clear evolution in the level of star formation (SF) activity in galaxy groups. Indeed, the total star formation activity in high redshift (0.5<z<1.1) groups is higher with respect to the low redshift (0.15<z<0.5) sample at any mass by almost 0.8 ± 0.1 dex. A milder difference (0.35 ± 0.1 dex) is observed between the [0.15-0.5] redshift bin and the groups at $z < 0.085$. This evolution seems to be much faster than the one observed in the whole galaxy population dominated by lower mass halos. This would imply that the level of SF activity is declining more rapidly since z∼1.1 in the more massive halos than in the more common lower mass halos, confirming a "halo downsizing" effect as discussed already in Popesso et al. (2012). The HOD and the total stellar mass-M_{200} relation are consistent with a linear relation in any redshift bin in the M_{200} range considered in our analysis. We do not observe any evolution in the HOD since z∼1.1. Similarly we do not observe evolution in the relation between the total stellar mass of the groups and the total mass, in agreement with the results of Giodini et al (2012). The picture emerging from our findings is that massive groups at $M_{200} \sim 10^{13-14} M_\odot$ have already accreted the same amount of mass and have the same number of galaxies as the low redshift counterpart, as predicted by Stewart et al. (2008). This implies that the most evident evolution of the galaxy population of the most massive systems acts in terms of quenching their galaxy star formation activity. The analysis of the evolution of the fraction of SF galaxies as a function of halo mass or velocity dispersion show that high mass systems seem to be already evolved at z∼1 by showing a fraction of star forming galaxies consistent with the low redshift counterpart at $z < 0.085$. Given the almost linear relation between the ΣSFR and M_{200} in the high-z sample, this implies that most of the contribution to the total SFR of the most massive systems ($M_{200} \sim 10^{14} M_\odot$) is given by few highly star forming galaxies, while in lower mass systems ($M_{200} \sim 10^{13} M_\odot$) is given by many galaxies of average activity. This would be an additional sign of a faster evolution in the more massive systems in terms of star formation activity with respect to lower mass groups. Thus, it would confirm the "halo downsizing" effect. The comparison of our results with the prediction of the Millennium Simulation semi-analytical model confirms the known problem of the models. We confirm the strong bias due to the "satellite overquenching" problem in suppressing significantly the SF activity of group galaxies (more than an order of magnitude) at any redshift with respect to observations. The HOD predicted by the simulations is remarkably in agreement with the observations. But due to the low SF activity of galaxies in massive halos, the models predict also a lower total stellar mass in groups with respect to the observed one at any redshift.

In order to compare the SF activity level of galaxies in different environment, we also define a sample of field galaxies and "filament-like" galaxies. This is done by using the galaxy density field to find isolated galaxies (field) and galaxies in high density region but not associated to any group or more generically to an X-ray extended emission. These two classes of environment in addition to the galaxy group sample are used to study the location of galaxies in SFR-mass plane since $z \sim 1.1$ as a function of the environment. Indeed, several studies have already shown there is a tight correlation between the SFR and the stellar masses of the bulk of the star forming galaxy population at least over the past 10 Gyr. Quiescent galaxies are mainly located under this main sequence (MS) and in a more scattered cloud. Our analysis shows that the Main Sequence of star forming galaxies in the two redshift bins considered ($0.15 < z < 0.5$ and $0.5 < z < 1.1$) is not a linear relation but it shows a flattening towards higher masses ($M* > 10^{10.4-10.6}$ $M_{\odot}$). Above this limit, the galaxy SFR has a very weak dependence on the stellar mass (SFR $\propto$ $\mathrm{M}_*^{0.2-0.3}$). This flattening, to different extent, is present in all environments. At low redshift, group galaxies tend to deviate more from the mean MS towards the region of quiescence with respect to isolated and filament-like galaxies. This environment dependent location of low redshift group galaxies with respect to the mean MS causes the increase of the dispersion of the distribution of galaxies around the MS as a function of the stellar mass. At high redshift we do not find significant evidence for a differential location of galaxies with respect to the MS as a function of the environment. Indeed, in this case we do not observe a significant increase of the dispersion of the distribution of galaxies around the MS as a function of the stellar mass. We do not find evidence for a differential distribution in the morphological type of MS galaxies in different environments. Instead, we observe a much stronger dependence of the mean Sérsic index on the stellar mass. These results suggest that star formation quenching in group galaxies is not due to galaxy structural transformations. It also suggests that while morphology of MS galaxies is more stellar mass dependent, star formation quenching is mostly environment dependent. We conclude that the membership to a massive halo is a key ingredient in the galaxy evolution and that this acts in terms of star formation quenching in group sized halos.

Zusammenfassung

Einer der fundamentalsten Zusammenhänge zwischen den Eigenschaften von Galaxien im heutigen Universum ist das sogenannte Morphologie zu Dichte Verhältnis (Dressler 1980). Eine Fülle von Studien hat in verschiedenen Wellenlängenbereichen mittels Indikatoren für Sternentstehung (englisch kurz: SF) gezeigt, dass in der Entwicklung fortgeschrittene Galaxien, welche Sterne bilden, im heutigen Universum Regionen geringer Dichte bevorzugen (z.B. Gómez et al. 2003). Insbesondere die Zentren massereicher Galaxienhaufen sind Friedhöfe voller elliptischer Galaxien, mit vorwiegend alter Sternpopulation. Eine Reihe von physikalischen Prozessen könnte dafür verantwortlich sein, die Sternentstehung in Galaxien, die Teil von Haufen oder kleineren Gruppen sind zu unterdrücken und deren Morphologie zu beeinflussen. Diese Prozesse können generell in zwei große Gruppen aufgeteilt werden: (i) Wechselwirkungen mit anderen Galaxien des Haufens und/oder dem Gravitationspotential des Haufens selbst und (ii) Wechselwirkungen mit dem heißen Gas, das massereiche Galaxiensysteme durchdringt. In unserem Universum sind Galaxien am häufigsten in Galaxiengruppen anzutreffen, welche die Brücke zwischen einem Feld mit niedriger Dichte und den sehr dichten Galaxienhaufen schlagen. Tatsächlich befinden sich im heutigen Universum etwa 50-70% der Galaxien in Gruppen, während nur ein paar Prozent in den dichteren Zentren der Galaxienhaufen konzentriert sind. Darüber hinaus sind die Galaxiengruppen im aktuellen hierarchischen Modell der Strukturentstehung des Universums die Bausteine massereicherer Systeme: Sie verschmelzen und formen Galaxienhaufen. Während sich diese Strukturen ausbilden werden Galaxien Teil immer massereicherer Systeme und verbringen dabei einen Großteil ihrer Lebensdauer in Galaxiengruppen bevor sie in Galaxienhaufen übergehen. Daher ist es angebracht zu untersuchen, ob Prozesse in Gruppen von Galaxien die beobachteten Verhältnisse von Galaxieneigenschaften und deren Umgebung beeinflussen.

Um dieses Thema genauer zu untersuchen haben wir die größten, aus Röntgenbeobachtungen abgeleiteten, Kataloge von Galaxiengruppen mit guter spektroskopischer Identifikation aus den Durchmusterungen tiefer Felder erstellt. Zu diesem Zweck haben wir tiefe Chandra und XMM-Newton Röntgenbeobachtungen der wichtigsten tiefen Felder (AEGIS, COSMOS, ECDFS und CDFN) kombiniert. Der Katalog der Galaxiengruppen in jedem Feld wurde erstellt indem man ausgedehnte Röntgenemission mit einer Anhäufung von

Galaxien im dreidimensionalen Raum in Verbindung bringt. Dies wird durch die enorm gute spektroskopische Abdeckung der Felder erreicht. Unsere Methode und die dynamische Analyse, welche zur Identifizierung der Galaxiengruppenmitglieder und zur Bestimmung der Geschwindigkeitsverteilung innerhalb der Gruppe benutzt wurde, wurde ausgiebig an den Daten des AEGIS Feldes und an Katalogattrappen, welche aus der Milennium Simulation (Springel et al. 2005) extrahiert wurden getestet. Der Effekt von dynamischer Komplexität, Unterstrukturen, Form der Röntgenemission und verschiedener Beschränkungen in Radius und Rotverschiebung wurden für die Lx-sigma Relation getestet. Wir fanden auch eine hoch rotverschobene Gruppe bei etwa z=1.54 im AEGIS Feld. Dies zeigt, dass Millionen Sekunden an Chandra Beobachtung nötig sind um solche Objekte in einem, von den tiefen Feldern abgedeckten, Volumen zu finden. Wir stellen ein exaktes Maß für die Sternentstehungsrate (englisch kurz: SFR) in den Galaxien zur Verfügung, in dem wir die tiefsten verfügbaren Herschel PACS und Spitzer MIPS Daten verwenden, die für die jeweiligen Felder zur Verfügung standen. Wir geben darüber hinaus eine gut kalibrierte Abschätzung der SFR, welche wir aus der SED Anpassungsmethode für im mittleren und entfernten Infrarot nicht entdeckte Quellen anwenden.

Mit diesem einzigartigen Katalog, führen wir eine umfassende Analyse der Abhängigkeit der Summe der SFR (Σ SFR), der Summe der stellaren Masse (Σ M_*) und der Halo Occupation Distribution (englisch kurz: HOD) massereicher Galaxien ($M_* > 10^{10} M\odot$) von der Masse innerhalb der Halos der Galaxiengruppen durch, unter genauster Berücksichtigung der Unsicherheiten. Wir beobachten eine klare Entwicklung in der SFR der Galaxiengruppen. Tatsächlich ist die SFR in hoch rotverschobenen ($0.5<z<1.1$) Gruppen in allen Massebereichen um etwa 0.8±0.1 dex höher als in denen bei niedriger Rotverschiebung ($0.15<z<0.5$). Ein geringerer Unterschied (0.35±0.1 dex) zeichnet sich zwischen dem [0.15-0.5] Rotverschiebungsbereich und Gruppen unterhalb einer Rotverschiebung von 0.085 ab. Diese Entwicklung scheint viel schneller zu sein als diejenige, die in der gesamten Galaxienpopulation bei niedrigeren Halomassen beobachtet wird. Dies würde bedeuten, dass die SFR seit etwa $z\sim1.1$ in den massereicheren Gruppen stärker abnimmt als in den häufigeren, masseärmeren Gruppen, was ein halo downsizing wie es bereits in Popesso et al. (2012) beschrieben wurde bestätigen würde. Die HOD und die Summe der stellaren Massen M_{200} sind verträglich mit einem linearen Zusammenhang in allen Rotverschiebungsbereichen für den M_{200} Bereich, der in dieser Analyse verwendet wurde. Wir beobachten keine Entwicklung in der HOD seit $z\sim1.1$. In ähnlicher Weise beobachten wir im Verhältnis zwischen der gesamten stellaren Masse einer Gruppe und deren gesamter Masse keine Entwicklung. Dies stimmt mit den Ergebnissen von Giodini et al. (2012) überein. Das Bild, welches sich aus unseren Ergebnissen abzeichnet, ist dass massereiche Gruppen bereits die gleiche Masse und die gleiche Zahl an Galaxien aufgenommen haben wie auch ihre Gegenstücke bei niedriger Rotverschiebung, wie von Stewart et al. (2008) vorhergesagt. Dies bedeutet, dass die stärkste Veränderung der Galaxienpopulation in den massereichsten Systemen sich in der Abschwächung der SFR ihrer Galaxien zeigt. Die Analyse der Veränderung des Anteils der SF Galaxien als Funktion der Halomasse oder Geschwindigkeitsverteilung zeigt ,dass massereiche Systeme um $z\sim1$ bereits in der Entwicklung fortgeschritten sind, im Vergleich zu ihren Gegenstücken bei niedriger Rotverschiebung $z<0.085$. Dies bedeutet durch den annähernd linearen Zusammenhang zwischen ESFR und M_{200} der Gruppen bei hoher Rotverschiebung, dass in den massereichen Systemen ($M_{200} \sim 10^{14} M_\odot$) die SFR von wenigen Galaxien durch starke SFR dominiert wird und in masseärmeren Systemen ($M_{200} \sim 10^{13} M_\odot$) durch eine höhere mittlere SFR bestimmt ist. Dies wäre ein weiterer Hinweis auf eine schnellere nderung der Sternentstehungsaktivität in massereicheren Systemen im Vergleich zu masseärmeren Gruppen. Damit wäre der halo downsizing Effekt bestätigt. Der Vergleich unserer Ergebnisse mit den Vorhersagen des semianalytischen Modells der Millennium Simulation bestätigt dessen bekannten Probleme. Wir bestätigen die starke systematische Abweichung auf Grund des satellite overquenching Problems, welches dazu führt, dass die SFR in Galaxien einer Gruppe im Vergleich zu den Beobachtungen bei beliebiger Rotverschiebung signifikant unterdrückt wird (mehr als eine Größenordnung). Die Vorhersage der HOD durch die Simulationen passt erstaunlich gut zu den Beobachtungen. Aber auf Grund der niedrigen Sternentstehungsaktivität der Galaxien in massereichen Halos, sagen die Simulationen auch eine geringere gesamte stellare Masse als in Gruppen beobachtet vorher.

Um die Sternentstehungsaktivität von Galaxien in verschiedenen Umgebungen zu vergleichen, haben wir auch eine Auswahl an Galaxien im Feld und filamentartigen Galaxien definiert. Diese wurden ausgewählt indem wir die Verteilung der Galaxien auf isolierte Galaxien (Feld) und Galaxien in dichteren Regionen, die keine Zugehörigkeit zu einer Gruppe oder allgemeiner, einer ausgedehnten Röntgenquelle aufweisen, untersuchten. Diese zwei Umgebungsklassen wurden zusammen mit der Auswahl an Galaxiengruppen verwendet um die Lage der Galaxien in der SFR gegen Masse Ebene als Funktion der Umgebung aufzutragen. Tatsächlich haben einige Studien bereits gezeigt, dass es zumindest während der letzten 10 Mrd. Jahre einen engen Zusammenhang zwischen der SFR und den stellaren Massen eines Großteils der Population der Sternentstehungsgalaxien gibt. Galaxien niedriger Sternentstehung (ruhige Galaxien) befinden sich hauptsächlich unter dieser Hauptreihe (englisch kurz: MS) und sind stärker gestreut. Unsere Analyse zeigt dass die Hauptreihe der Sternentstehungsgalaxien in den beiden Rotverschiebungsbereichen, die wir untersuchten ($0.15 < z < 0.5$ und $0.5 < z < 1.1$) keinen linearen Zusammenhang zeigen, sondern ein Abflachen bei höheren Massen (M_* ¿ $10^{10.4-10.6} M_\odot$). Oberhalb dieser Grenze ist die SFR der Galaxien nur sehr schwach von der stellaren Masse abhängig (SFR proportional zu $M_*^{0.2-0.3}$). Diese Abflachung ist in unterschiedlich starker Ausprägung in allen Umgebungen vorhanden. Bei niedriger Rotverschiebung weichen Gruppengalaxien im Vergleich zu isolierten und filamentartigen Galaxien tendenziell weiter von der mittleren MS in Richtung des Bereichs der ruhigen Galaxien ab. Diese umgebungsabhängige Verteilung der Gruppengalaxien bei niedriger Rotverschiebung verursacht eine Dispersion der Verteilung der Galaxien um die MS als Funktion der stellaren Masse. Bei höherer Rotverschiebung finden wir keine signifikante umgebungsabhängige Abweichung der Verteilung der Galaxien um die MS. Tatsächlich finden wir in diesem Fall auch keine signifikante Zunahme der Dispersion der Verteilung der Galaxien um die MS als Funktion der stellaren Masse. Wir finden keinen Beweis für eine Abweichung in der Verteilung der morphologischen Typen der Hauptreihengalaxien in verschiedenen Umgebungen. Stattdessen beobachten wir eine sehr viel stärkere Abhängigkeit des Sersic Index von der stellaren Masse. Diese Ergebnisse deuten an, dass die Abschwächung der Sternentstehung in Gruppengalaxien nicht von Strukturänderungen der Galaxien selbst ausgelöst wird. Dies weist auch darauf hin, dass während die Morphologie der Hauptreihengalaxien mehr von deren stellarer Masse abhängig ist, die Abschwächung der Sternentstehung hauptsächlich von der Umgebung abhängt. Zusammenfassend konnten wir zeigen, dass die Zugehörigkeit zu einem massereichen Halo eine Schlüsselrolle in der Galaxienentwicklung spielt und dass sich diese in der Abschwächung der Sternentstehung in den Halos von Galaxiengruppen auswirkt.

Chapter 1

Introduction

1.1 Structure Formation

The goal of the structure formation theory is to explain how the observable structures in the Universe originated out of an almost perfectly homogeneous initial Universe. The main idea of modern cosmology (e.g. see Peacock 1999) is that of a Universe which was initially extremely homogeneous and hot except for very tiny perturbations. Primordial density fluctuations were exponentially amplified during a phase of inflation (Guth 1981). There are many viable theories to explain inflation but how it starts and eventually stops is still matter of debate. When the perturbations approach an amplitude of order unity, the growth of perturbations becomes nonlinear. The treatment of the nonlinear structure formation is very difficult and can only be treated by rough models except for simple cases. A simple but relatively useful toy model for the treatment of the nonlinear growth of perturbations is the spherical top hat model (Peebles 1980). Suppose a homogeneous spherical overcritical perturbation of mass M within an otherwise critical homogeneous expanding background Universe. The perturbation is initially expanding with the background, but due to its overcritical mass its expansion will slow down until it entirely decouples from the expansion of the background. From this moment the perturbation starts to contract and will finally form a compact object of mass M. For a perfectly spherical overdensity the mass would actually collapse to a single point, in reality, of course, such perfect symmetry does not exist and it occurs instead extreme "shell crossing" (Gunn 1977) and "violent relaxation" (Lynden-Bell 1967) until a pressure supported, virialized object has formed - a halo. The formation of the dark matter (DM) halos can be regarded as the first of a two-step process for the evolution of galaxies (White & Rees 1978). In the second step, the baryons fall into the DM halos, where they become shock heated, and form galaxies by cooling down.

Structure formation is thought to act via hierarchical growth from primordial fluctuations. In the currently standard hierarchical structure formation scenario, objects are thought to form via gravitational collapse of peaks in the initial primordial density field. First, smaller structures collapse and then they incorporate in larger collapsing structures

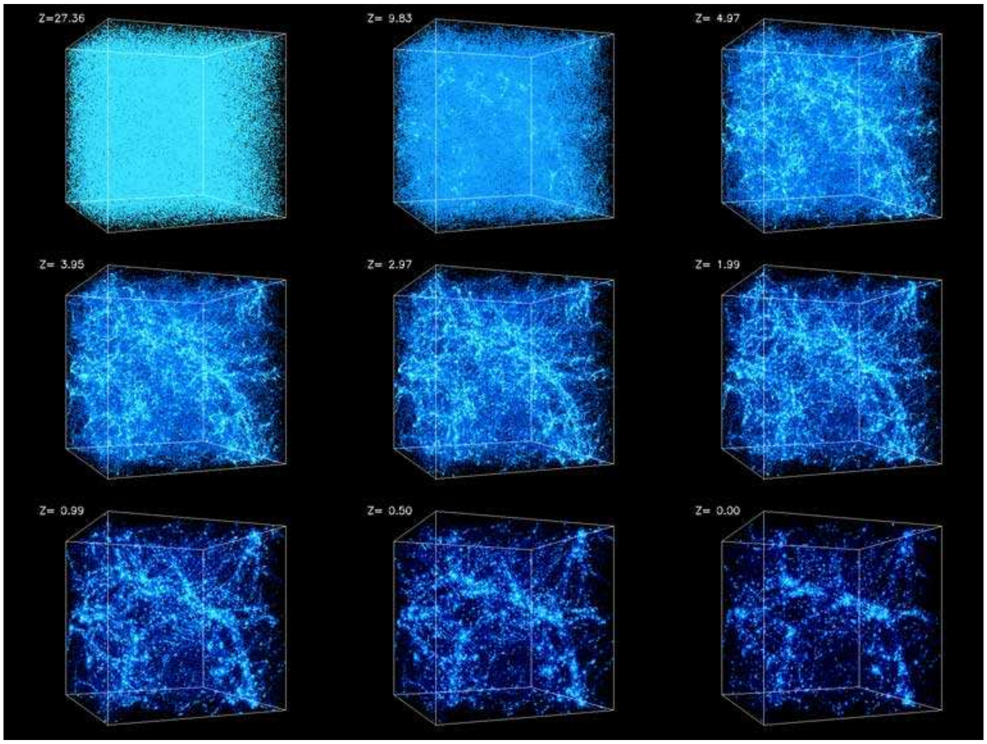

Figure 1.1: The formation of clusters and large-scale filaments in the Cold Dark Matter model with dark energy. Each frame portrays the evolution of structures in a 43 million parsecs (or 140 million light years) box, from redshift of 30 to the present epoch.

in a *bottom − up* scenario. Galaxies in high-density regions of the Universe will collapse earlier and may evolve more rapidly than galaxies in low-density regions (e.g. Kauffmann 1995).

The overall theory including the formation of galaxies is generally very complex. However, since the physics of DM is relatively simple due to their weak interaction, the evolution of the DM part can be studied easily and is well understood today. The dominant mass component is (unidentified) collisionless cold dark matter, which also determines the dynamics of the baryons on large scales where hydrodynamic forces are unimportant compared with gravity. The complex physics takes place on the smaller scales where baryons have collapsed to form galaxies which in turn affect their own evolution and that of their neighbours by feedback processes.

The hierarchical structure formation scenario has been extensively investigated using N-body simulations (e.g. Angulo et al. 2012; Springel et al. 2005; Springel & Hernquist 2003; White & Rees 1978). These simulations have become sophisticated to the point where they can reproduce observations of large scale structures with high precision. An example is given by Fig. 1.2, where we show the comparison of the filamentary structures observed in different redshift surveys (in blue) and the Millennium simulation (in red) of Springel, Frenk & White (2006).

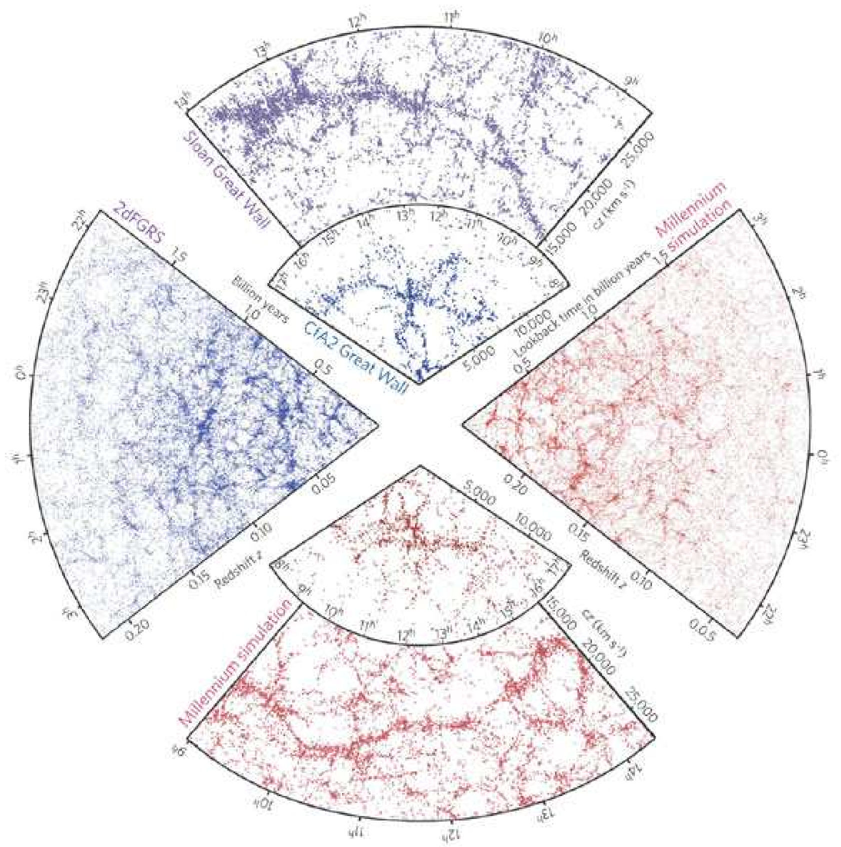

Figure 1.2: Comparison between filamentary structures observed in SDSS and 2dFGRS surveys (in blue) and mock galaxy surveys constructed using semi-analytic technique. Springel, Frenk & White (2006)

1.1.1 Semi-analytical models of galaxy formation

Due to the complicated physics related to galaxy formation and evolution, simple rules that can be easily changed to study the importance of different physical processes are very useful. Semi-analytical models (SAMs) of galaxy formation try to encode simplistic rules for the formation and evolution of galaxies within a cosmological framework. A SAM is a collection of physical recipes that describe an inflow of gas, how gas can cool and heat up again, how stars are formed within galaxies, how stellar populations evolve and how black holes grow using simplified physics (White & Frenk 1991; Cole 1991; Lacey & Silk 1991; Kang et al. 2005; Baugh 2006; De Lucia & Blaizot 2007). SAMs can also easily include different feedback effects: stellar winds, active galactic nuclei (AGN) or supernovae (SNe) feedbacks (e.g. Croton et al. 2006; Somerville et al. 2008; Ricciardelli & Franceschini 2010), for example. Thus, SAMs attempt to describe all the gas physics that goes into galaxy formation and evolution, but is not modelled in the dark matter only simulation.

Because of their nature, SAMs can be used to explore ideas of galaxy formation and evolution and to understand which physical processes are the most important in the life of a galaxy by changing the recipes describing the physics.

The backbone of a SAM is the evolution of dark matter halos. This evolution is usually parametrized with dark matter halo merger trees that allow the hierarchical nature of gravitational instabilities to be explicitly taken into account (Baugh et al. 1998)). Dark matter merger trees explain how the dark matter halos form via mergers of smaller halos. They provide the introduction of the baryonic component which reacts gravitationally to the growing network of dark matter potential wells.

After a cosmological model has been chosen and the merger trees have been generated the baryonic processes must be taken into account. A SAM typically includes the following steps: 1) follow the hot and cold gas and stars, the three baryonic components, and adopt a recipe for disk formation; 2) define a recipe for the conversion rate between the three components, including star formation and feedback effects; 3) keep track of the metallicity of each component; 4) convert the star formation history and metallicity of the stellar populations into luminosities; and 5) adopt a recipe for galaxy-galaxy mergers.

1.2 Star Formation

A galaxy generally is observed and defined by its stars. Hence, how stars form is an essential question which any theory of galaxy formation should address. In galaxy-sized halos, the baryonic gas can cool within a time which is shorter than the age of the halo. Consequently the gas lose pressure support and move towards the center of the halo potential well, cousing its density to increase. As soon as its density exceeds that of the dark matter in the central part of the halo, the cooling gas becomes self-gravitating and collapse under its gravity. Self-gravitating gas, in the presence of efficient cooling, is unstable and can collapse catastrophically. Finally, this cooling process may lead to the formation of dense, cold gas clouds within which star formation can occur (Mo, van den Bosch & White 2010).

Understanding of star formation in a cosmological framework is extremely challenging as it spans a large order of magnitudes in mass and density from the gas in galaxy-sized halo to a typical star. However, for the purpose of galaxy formation and evolution, it is enough to understand the properties of the stellar population in a volume which is comparable to that of a galaxy.

Because the complexity involved in physics of SF, SAMs often derive the star formation rate (SFR) of a galaxy using a simple relation

$$\dot{\rho}_\star = \epsilon_{SF} \frac{\rho_{cold}}{\tau_\star} \tag{1.1}$$

where ϵ_{SF} is a efficiency of star formation, ρ_{cold} is the density of the cold gas and $\tau_\star$ is the characteristic timescales. However, several different form of above equation have been developed from a constant $\tau_\star$ to models that are proportional to the dynamic time of the galaxy and taking into account, for instance, the circular velocity and/or radius of disc. In any model, the above law is varying with the empirical law, for which it has been assumed that the SFR is controlled by the self-gravity of the gas (Schmidt 1959).

One of the property closely tied to SF in galaxies is the initial mass function (IMF, e.g. Chabrier 2003) which represent the number of stars of a given mass that forms. The form of IMF is of fundamental importance for many areas of astrophysics and a topic of considerable debate (e.g. Schmidt 1959; Chabrier 2003; van Dokkum 2008). IMF measurement is difficult as it requires to the conversion of the observed luminosity function of a stellar population at present day to its mass function at birth. In the best estimation for Galactic disk, IMF has a power-law slope at $m \lesssim 1M_\odot$ and turns over at lower masses (Kroupa 2001; Chabrier 2003). This turnover can be modelled by a broken power-law (Kroupa 2001) or by a log-normal distribution with a characteristic mass(Chabrier 2003). In SAMs, usually assumed IMF is universal while modelling star formation. Note, however, a number of different evidence exist in support of evolving and non-universal IMF (e.g. van Dokkum & Conroy 2010; Lucatello et al. 2005; Tumlinson 2007a,b; van Dokkum 2008).

1.2.1 Observational information on SF

The past decade has witnessed a remarkable stream of new observational information on star formation. These new data are providing a comprehensive reconstruction of the fundamental evolutionary phases and physical processes that lead to the formation of individual stars in interstellar clouds, while extending the reach of integrated measurements of star-formation rates (SFRs) to the most distant galaxies known. The new data have also stimulated a parallel renaissance in theoretical investigation and numerical modelling of the star-formation process (e.g. Kennicutt & Evans 2012). These new observations led to major advancement in the calibration and validation of diagnostic methods for measuring SFRs in galaxies. Whereas measuring uncertainties of factors of two or larger in SFRs was commonplace ten years ago, new diagnostics based on multiwavelength data are reducing these internal uncertainties by up to an order of magnitude in many cases. These methods have also reduced the impact of many systematic errors, in particular uncertainties due to dust attenuation, though others such as the IMF remain important limiting factors. As individual stars are unresolved in all but the closest galaxies so most information on the star formation properties of galaxies comes from integrated light measurements in the ultra-violet (UV), far-infrared (FIR) or nebular recombination lines as the direct tracers. In following, I present a brief discussion about different SFR diagnostics and then I will explain in more detail the method which we use in this work.

Integrated Colors and Spectra

When galaxy types change, several changes in the spectrum will appear. Fig. 1.3 illustrates these changes for elliptical, different types of spiral and irregular galaxies. Although the integrated spectra contain contributions from the full range of stellar spectral types and luminosities, the dominant contributors at visible wavelengths are intermediate-type main sequence stars and giants. As a consequence, the integrated colors and spectra of normal galaxies fall on a relatively tight sequence, with the spectrum of any given object dictated by the proportion of early- to late-type stars or, alternatively, by the ratio of young (<1

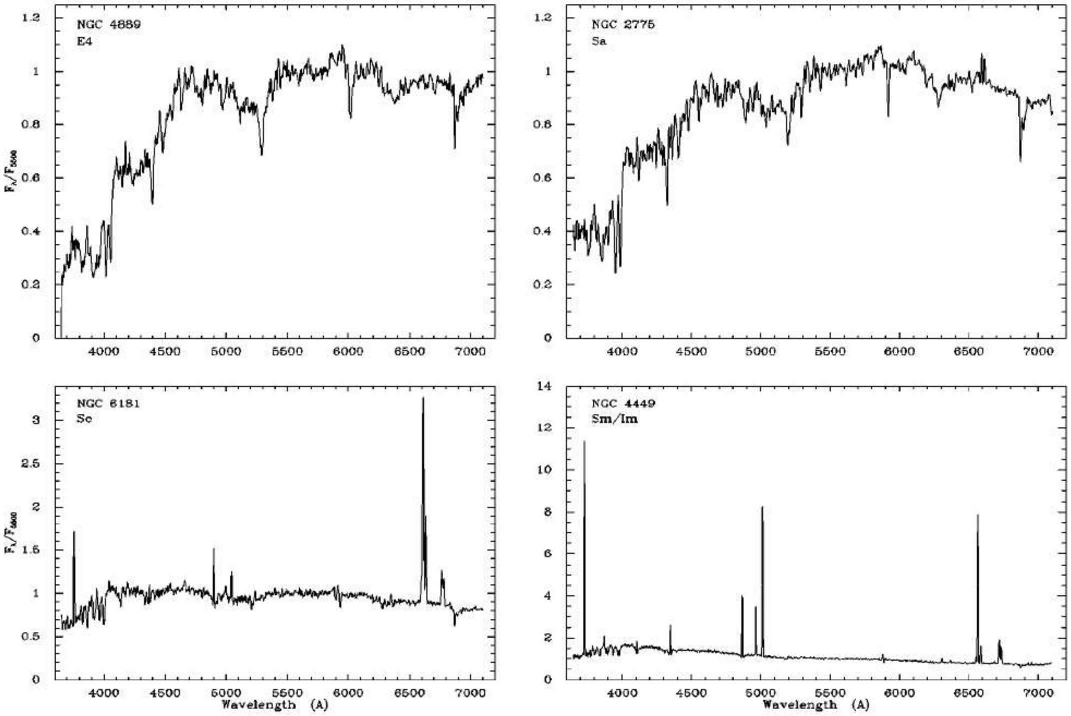

Figure 1.3: Integrated spectra of elliptical, spiral, and irregular galaxies, from Kennicutt (1998). The fluxes have been normalized to unity at 5500 $\AA$.

Gyr) to old (3-15 Gyr) stars. This makes it possible to use the observed colors to estimate the fraction of young stars and the mean SFR over the past 10^8-10^9 years. The scaling of the SFR to continuum luminosity is a smooth function of the color of the population, and this can be calibrated using an evolutionary synthesis model. Synthesis models are used in all of the SFR diagnostics. A grid of stellar evolution tracks is used to derive the effective temperatures and bolometric luminosities for various stellar masses as a function of time, and these are converted into broad band luminosities (or spectra) using stellar atmosphere models or spectral libraries. The individual stellar templates are then summed together, weighted by an initial mass function (IMF), to synthesize the luminosities, colors, or spectra of single-age populations as functions of age. These isochrones can then be added in linear combination to synthesize the spectrum or colors of a galaxy with an arbitrary star formation history, usually parametrized as an exponential function of time. Although a single model contains at least four free parameters (the star formation history, galaxy age, metal abundance, and IMF), the colors of normal galaxies are well represented by a one-parameter sequence with fixed age, composition, and IMF, varying only in the time dependence of the SFR (e.g. Larson & Tinsley 1978; Charlot & Bruzual 1991). The SFRs derived in this way are relatively imprecise and are prone to systematic errors from reddening or from an incorrect IMF, age, or metallicity of star formation history (Larson & Tinsley 1978). Nevertheless, the method offers a useful means of comparing the average

SFR properties of large samples of galaxies when absolute accuracy is not required.

Ultraviolet Continuum

To combat the limitations described above, one can use observations in wavelength range where the integrated spectrum is dominated by young stars, so that the SFR scales linearly with luminosity. The optimal wavelength range is 1250-2500 $\AA$. For extragalactic studies, this subject has been revolutionized by the launch of the *Galaxy Evolution Explorer* (GALEX) mission (Martin et al. 2005). The conversion between the UV flux over a given wavelength interval and the SFR can be derived using the synthesis models described earlier. The main advantages of this technique are that it is directly tied to the photospheric emission of the young stellar population. However, this method also suffers from some limitations. The primary disadvantage of the UV is its severe sensitivity to interstellar dust obscuration. The availability of new data from GALEX and other facilities has stimulated a fresh look at this problem.

Emission Line Tracers

As Fig.1.3 shows, the most significant change in the spectra of different galaxy types emerge from a rapid increase in the strengths of the nebular emission lines. These lines mostly re-emit the integrated stellar luminosity of galaxies and they are a direct probe of the young massive stellar population. Most applications of this method have been based on measurements of the H_α line but for moderate redshifts, the bluer visible line, in particular [OII] forbidden line have been used as well. An evolutionary synthesis model usually have been used to convert ionizing flux to SFR and there are many different calibration for that in the literature (e.g. Kennicutt 1998; Jansen, Franx & Fabricant 2001; Kewley, Geller & Jansen 2004; Moustakas, Kennicutt & Tremonti 2006). This feature is subject to severe systematic uncertainties from excitation variations in galaxies and dust obscuration. The uncertainties of the [OII] based SFRs are much larger than H_α based one. There are also some different emission lines discussed in literature as SFR tracers like Lyα, Ne[II], Ne[III] and C[II] (for a review see, e.g. Kennicutt & Evans 2012).

Infrared emission

Measurement of the infrared (IR) emission is essential to have a comprehensive picture of SFR as a significant fraction of the starlight in the Universe is absorbed and re-emits in IR, at wavelengths of roughly 10-300 μm. The new facilities such as the *Spitzer Space Telescope* (Werner et al. 2004), and the *Herschel Space Observatory* (Pilbratt et al. 2010) provided a detailed information in this field. During the past decades, It has been more evident that a major component to comprehend galaxy evolution is represented by dust and re-emitted at mid- and far-infrared wavelengths. As we have already mentioned, the derivation of the cosmic star formation history from other SFR diagnostics suffers from uncertainties in the obscuration corrections in the dust component. (e.g. Lilly et al. 1996; Madau et al. 1996.

The mid-infrared emission in galaxies, in particular the emission detect in 8 μm and 24 μm Spitzer bands, has been analyzed by a number of authors(e.g. Alonso-Herrero et al. 2006; Boselli, Lequeux, & Gavazzi 2004; Calzetti et al. 2005, 2007;Förster Schreiber et al. 2004; Pérez-González et al. 2006; Relaño et al. 2008; Rieke et al. 2009; Roussel et al. 2001; Salim et al. 2009; Wu et al. 2005; Zhu et al. 2008).

In the next section, we describe the most recent facility, $Herscel$ satellite and give a brief overview about science result which provided using $Herschel$ and *Spitzer* data.

1.3 The Herschel satellite

Since three years ago, *Herschel Space Telescope*, with higher sensitivity and longer wavelengths than *Spitzer*, provided more powerful tools for probing the evolution of the rate at which galaxies have assembled their gas and dust components. The Herschel satellite is designed to explore the "cool Universe" during its expected 3.5 year mission life-time (Pilbratt et al. 2010). $Herschel$ is equipped with a 3.5 m main mirror and marks the beginning of a new generation of "space giants". Its science payload consists of three instruments: $PACS$ and $SPIRE$, both cameras and spectrometers that allow Herschel to perform imaging in six different "colors" in the far-infrared, and $HIFI$, a spectrometer with extremely high spectral resolution. In particular, the Photoconducting Array Camera and Spectrometer $PACS$ (Poglitsch et al. 2010) provides $Herschel$ with far-infrared imaging and spectroscopic capabilities from 60 to 210 μm. In fact, PACS photometer addresses a wide range of key questions of current astrophysics concerning the origins of stars, planetary systems, galaxies, and the evolution of the Universe. One of the major Herschel Guaranteed Time (GT) extragalactic projects is the PACS Evolutionary probe (PEP) deep extragalactic survey. This survey planned to answer the main questions about the cosmic infrared background (e.g. Berta et al. 2011) and the nature of its constituents, determine the cosmic evolution of dusty star formation and of the infrared luminosity function (IR LF), illuminate the relation of far-infrared emission and environment, and determine clustering properties. PEP is focused on PACS 70, 100, and 160 μm observations. PEP encompasses the most important blank fields: COSMOS (2 deg^2), Lockman Hole, EGS and ECDFS (450-700 arcmin^2), GOODS-N and GOODS-S ($\sim$200 arcmin^2).

1.4 Herschel and Spitzer science results

The launch of the *Spitzer Space Telescope* and *Herschel Space Observatory* opened a new era for infrared (IR) and far infrared (FIR) astronomy. The high sensitivity of these new facilities, has enabled people to address many aspect of observational astronomy. In the following, we briefly describe those areas that we believe the *Spitzer* and $Herschel$ have made the greatest impact in extragalactic research and are also related to this work.

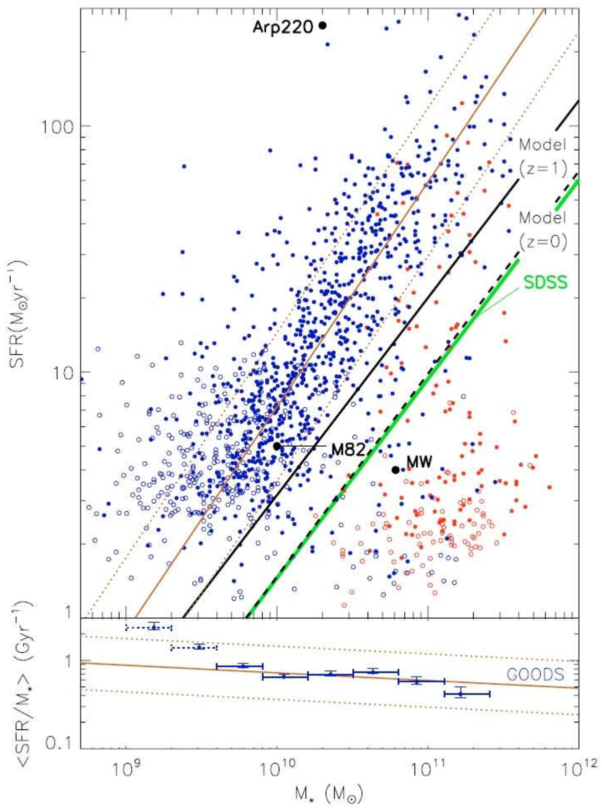

Figure 1.4: Relationship between SFR and specific SFR (SFR/M_*) with stellar mass in z $\sim$ 0.8-1.2 galaxies from Elbaz et al. (2007). Red and blue symbols are for red and blue galaxies as defined by their colors. A Salpeter IMF is assumed. The plain brown line shows the best fit for MS to blue GOODS galaxies and the dashed brown lines mark the 68% confidence level of the fit.

1.4.1 The SFR-M plane "Main Sequence"

Location of galaxies on the SFR-M plane give us valuable clues to trace the evolution of galaxies during the cosmic time and different environment. Deep galaxy surveys have found consistently that the star formation rate per unit stellar mass (M_*) depends strongly on both M_* and redshift, with the bulk of star formation occurring earlier in massive galaxies than in less massive systems. Noeske et al. (2007b,a) investigate the SFR as a function of redshift in the Extended Groth Strip (EGS). Using the *Spitzer* 24-μm fluxes and optical emission line spectroscopy to determine SFRs, they find a clear band of SFRs as a function of galaxy mass referred to as a "main sequence" of star formation in galaxies, which, at a given redshift, increases with galaxy mass. This smooth sequence suggests that the same set of few physical processes governs SF in galaxies, unless quenching occurs for particular reasons. The evolution of SF along the MS appears to be dominated by a gradual decline of SFR in individual galaxies since z$\sim$1 , rather than by an evolving frequency or amplitude of starbursts. Thus, the dominant process that governs SF since z$\sim$1 is likely a gradual one,

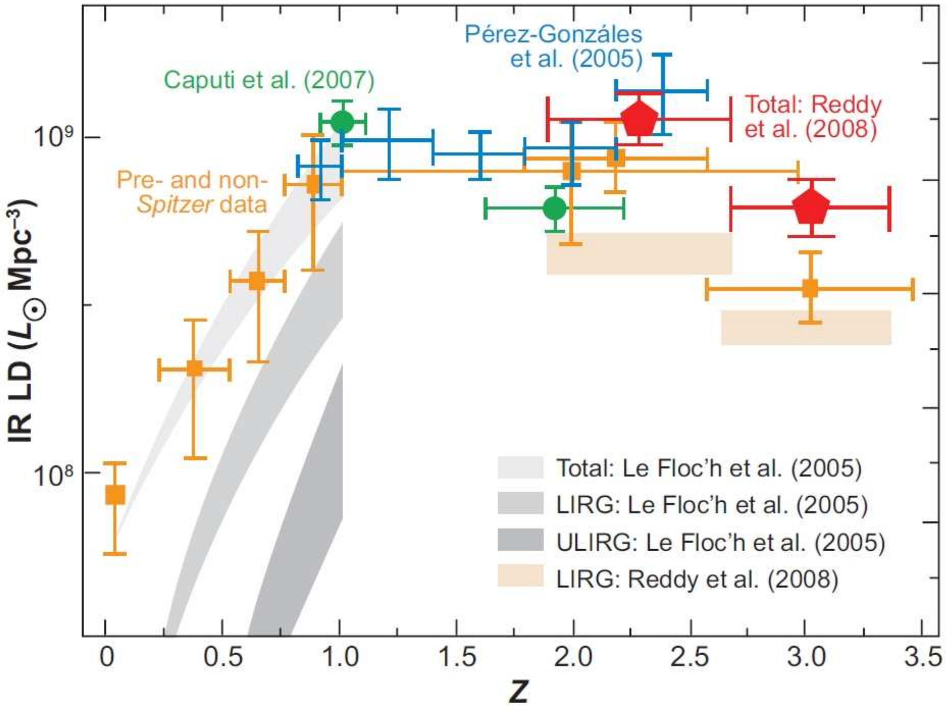

Figure 1.5: The infrared Luminosity density (IR LD) as a function of redshift (Reddy et al. 2008; Soifer, Helou & Werner 2008). The orange points show pre- and non-*Spitzer* data. The *Spitzer*-based data contain results from Reddy et al. (2008), Caputi et al. (2007), Pérez-González et al. (2005) and Le Floc'h et al. (2005). The bands indicate the total, LIRG, amd ULIRG contribution to the total IR LD at $z < 1$, as determined by Le Floc'h et al. (2005)

.

and possibility could be represented by the gas exhaustion (Noeske et al. 2007b). Elbaz et al. (2007); Daddi et al. (2007) show this sequence exist at higher redshifts up to z∼2 (Figure 1.4).

1.4.2 The SFR history of the Universe

The determination of the history of star formation in the Universe has been a major trust of observational cosmology and galaxy evolution studies for decades. Starting with the pioneering work of Lilly et al. (1996) and Madau et al. (1996), people derived the SFR as a function of look-back time using optical and UV observations. It was quickly realized that such determinations highly suffer from the effects of dust obscuration on the brightness of galaxies in the rest-frame UV.

Pérez-González et al. (2005) and Le Floc'h et al. (2005) derive the SFR history from 24-μm measurement of *Spitzer* by establishing the IR luminosity function as a function of redshift and then converting this to SFR per Mpc^3. These results find an increase in the IR

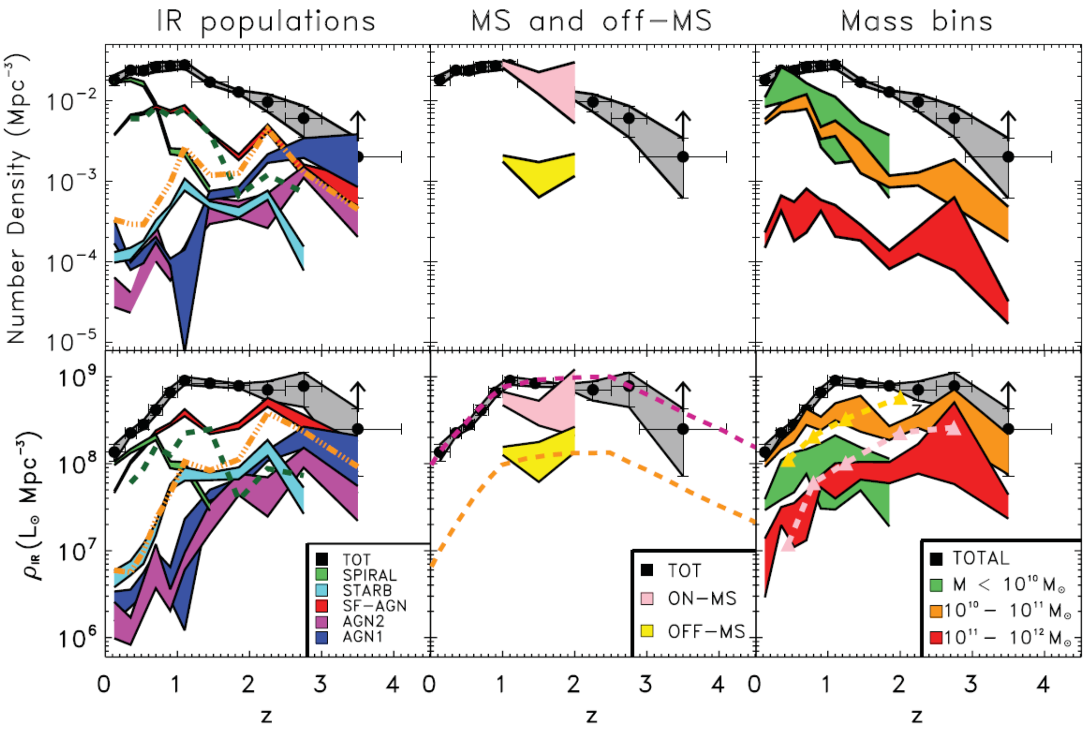

Figure 1.6: Top: evolution of the comoving number density of PEP sources up to redshift ∼4 (black filled circles with error-bars within 1σ uncertainty region, represented by the gray filled area) as studied in Gruppioni et al. (2013). *Bottom*: Redshift evolution of the total IR luminosity density (ρ_{IR}) to z = 4. The black filled circles and the gray dashed area in all the three panels represent the PEP derived ρ_{IR} and its 1σ uncertainty region. The left panels show the number density (*top*) and the luminosity density (*bottom*) of the IR populations. The middle panels - the uncertainty regions of the relative contributions of the off- and on- SFR-mass main sequence sources. The *right* panels show the relative contribution of sources with different stellar masses.

luminosity density and, thus, SFR per Mpc^3 by an order of magnitude between z=0 and z∼1. Pérez-González et al. (2005) find that the SFR per Mpc^3 increase till $z \sim 1.5$, and then flattens to $z \sim 3$. These works are consistent with the evolution of UV-based SFR (Lilly et al. 1996; Madau et al. 1996) where the UV-based analysis apply the large corrections for dust extinction. Figure 1.5 shows the IR luminosity density (SFR) versus redshift from these works as well as other works which pushed the determinations to still higher redshifts. Bai et al. (2007) and Marcillac et al. (2007) find similar evolution with redshift in cluster member galaxies. Le Floc'h et al. (2005) expand the contribution to the IR luminosity into lower luminosity systems ($\mathrm{L}_{IR} < 10^{11} L_{\odot}$), luminous IR galaxies (LIRGs, $10^{11} L_{\odot} < \mathrm{L}_{IR} < 10^{12} L_{\odot}$) and ultra-luminous IR galaxies (ULIRGs, $\mathrm{L}_{IR} > 10^{12} L_{\odot}$). For $z < 0.7$, they find that lower luminosity systems dominate, but for $z > 0.7$, LIRGs dominate the energy production, producing ∼ 70% of the total IR energy density at z∼1. The contribution from ULIRGs is rising steeply with redshift, being negligible (< 3% of the total) at z <

and 20 % of the energy at z $\sim$ 1.

However, with the rather uncertain extrapolation of L_{IR} from the galaxy total 24 μm flux at $z > 1.5$, the study of the infrared luminosity function built with PACS data at 70, 100 and 160 μm can better constrain the evolution of the contribution to the SFR density of the Universe of different classes of galaxies. Gruppioni et al. (2013) find very close agreement in the evolution of the total IR luminosity density from PEP with previous works based on IR data. As well as other previous findings, they show the rapid rise from z$\sim$0 to z$\sim$1, followed by a flattening at higher redshifts. They also indicate the intermediate-redshift (1<z<3) flattening is followed by a high-redshift decline , which starts around z $\sim$ 3. Moreover, they illustrate that the evolution derived for the global IR LF, derived in the PEP fields, is indeed a combination of different evolutionary paths: the IR population does not evolve all together as a single population, as it is often assumed in the literature, but it is composed by different galaxy classes evolving differently. Indeed they clarify the relative contribution of different classes of galaxies to global IR number density and luminosity density evolution (ρ_{IR}), as shown in 1.6. Their most interesting finding is, perhaps, the derivation of the relative contribution to ρ_{IR} of galaxies on the SFR-mass Main Sequence (see previous discussion) and off-MS sources. The former always dominate, though their contribution keeps nearly constant between z = 0.5 and z = 2.5, while the contribution to ρ_{IR} of the latter increases significantly with z (from 10% at 0.5 < z < 1.2, to > 20% at 1.8 < z < 2.5). A quite different evolution in the contribution to ρ_{IR} is also observed from galaxies in different stellar mass range, reflecting the downsizing scenario (ρ_{IR} peaks at higher redshift with increasing mass). Intermediate-mass objects ($\log(M/M_{\odot})$ = 10-11) always dominate the IR luminosity density, increasing up to z $\sim$ 1, then remaining nearly constant at higher redshifts (at least up to $\sim$ 2.8), while the contribution of most massive objects increases even more rapidly with z (at z = 2 it was $\sim$5 times higher than today) and continues to grow up to z = 3.

1.5 General properties of Galaxy Groups

1.5.1 The overall picture

A galaxy group is a concentration of galaxies, embedded in an extended dark matter halo. Ideally, group member galaxies are physically bound together due to their mutual gravitational attraction and the presence of the dark matter halo. Galaxy groups are less massive, gravitationally bound system than galaxy clusters and they are not simply scale-down versions of the rich cluster (e.g. Ponman, Cannon & Navarro 1999; Mulchaey 2000; Ponman, Sanderson & Finoguenov 2003; Voit 2005; Sun 2012). Because of shallow gravitational potential, galaxy groups are systems where the roles of complex baryon physics (e.g. cooling, galactic winds and AGN feedback) become significant. Galaxy groups typically contain less than $\sim$ 50 members in a size of few megaparsec. As no clear cut-off in number of members exists between groups and clusters, better quantities to discriminate between groups and clusters are mass and size, though, these do not provide clear cut-off values either. Groups have total mass (including dark matter mass) in the range $M = 10^{12.5} - 10^{14} M_{\odot}$ (Huchra & Geller 1982) about an order of magnitude less massive than galaxy clusters. Typical groups are also about a few times smaller than galaxy clusters (e.g. Einasto et al. 2003b; Koester et al. 2007).

Groups of galaxies are important laboratories to study galaxy evolution and formation. They are in the stage between the field and the densest environment in the Universe, massive clusters (Zabludoff & Mulchaey 1998) and as many as 50%-70% of all galaxies reside in galaxy groups (Turner & Gott 1976; Geller & Huchra 1983; Eke et al. 2005). Furthermore, since galaxy groups have low velocity dispersions but sufficiently high densities, galaxy evolution process such as transformation and merging occur more frequently in groups rather than clusters where galaxies have larger velocity dispersion.

1.5.2 Detection methods

There are a number of different methods for detecting groups of galaxies: searches in optical data via the red-sequence method (e.g. Gladders & Yee 2005; Koester et al. 2007), X-ray emission from hot intra group gas (e.g. Finoguenov et al. 2010),cosmic shear due to weak gravitational lensing maps (e.g. Miyazaki et al. 2007), and spectroscopic group samples (Gerke et al. 2012; Knobel et al. 2012). While spectroscopic surveys reveal the largest and deepest group catalogues, the detection of group X-ray emission has been proven to ensure that objects are virialized, and with the deepest X-ray survey available to date, the limits to which X-ray emission can be detected are reaching the level of low-mass groups.Moreover, compared to shear maps, X-rays probe a wider range in mass and redshift (Leauthaud et al. 2010). In the following section we describe each method and mention their strengths and weaknesses.

Red sequence method

There is a very well-defined, nearly horizontal sequence when one plots the color of cluster and group galaxies versus their magnitude. This red sequence is populated mainly by the early-type galaxies in galaxy systems. The scatter of early-type galaxies around this sequence is very small, suggesting that mainly early-type galaxies in clusters and groups have the same color, only weekly depending on luminosity. Even more surprising is the fact that the color-magnitude diagrams of different systems at the same redshift define a very similar red sequence. This sequence is redder at higher redshifts. In fact, by detection of red-sequence of clusters and groups one can with a good precision (with a typical accuracy of $\Delta z \sim 0.1$) estimate the redshift of the system. The accuracy of redshift estimate strongly depends on the choice of filters for color of the system. Since the most prominent spectral feature of early-type galaxies is the 4000-$\AA$ break, the redshift is estimated best if this break is located right between two of a color bands used.

This tight sequence suggests that the stellar population of member galaxies have very similar ages. The only age that is singled out is the age of the Universe itself.

X-ray emission from hot Intra Group Medium (IGM)

The X-ray radiation from massive clusters of galaxies has first been discovered with UHURU X-ray satellite, launched in 1970. With the later X-ray imaging satellites like Einstein, ROSAT, XMM-Newton, Chandra and Suzaku, X-ray emission was also detected from lower mass clusters and groups. While there were hints from Einstein observations that some groups of galaxies might contain a hot intra group medium, it was not until the 1990s that the presence of diffuse gas in groups was firmly established. Group studies were aided by the launch of two important X-ray telescopes, ROSAT (the ROentgen SATellite) and ASCA (Advanced Satellite for Cosmology and Astrophysics). Both of these telescopes were capable of simultaneous X-ray imaging and spectroscopy in the energy range appropriate for poor groups. In addition, the field of view for both telescopes was large enough that nearby groups could effectively be studied.

In many cases, the X-ray emission from intra group medium is extended, often beyond the optical extent of the group. X-ray spectroscopy suggests the emission mechanism is a combination of thermal bremsstrahlung and line emission from highly ionized trace elements. The spatial and spectral properties of the X-ray emission suggest the entire volume of groups is filled with hot, low-density gas. This gas component is referred to as the intra group medium, in analogy to the diffuse X-ray emitting intra cluster medium found in rich clusters (e.g. Forman & Jones 1982).

The X-ray luminosity, as one of the easiest properties of the hot gas to measure, carries important information on the gas distribution. Arnaud & Evrard (1999) show that X-ray luminosity of the hot gas in groups and clusters can be written as:

$$E(z)^{-1}L_X = f_{gas}^2(T)[E(z)M(T)]\Lambda(T,Z)\hat{Q}(T) \tag{1.2}$$

Where $E(z) = \sqrt{\Omega_M(1+z)^3 + \Omega_\Lambda}$, f_{gas} is the gas fraction and M is the total mass. Λ is the cooling function which is mainly T dependent for $KT > 2keV$ and abundance (Z) dependent at $KT < 2keV$. $\hat{Q}(T)$ is the structure function that is equal to $\langle\rho_{gas}^2\rangle/\langle\rho_{gas}\rangle^2$ averaging over the cluster atmosphere.

Spectroscopic group samples

Huchra & Geller (1982) introduced a simple early method for identifying groups and clusters in the Center for Astrophysics (CfA) redshift survey by searching for nearby neighbour galaxies around each galaxy. This technique is known as the friends of friends or percolation method. In its simplest form, it defines a linking length b and links every galaxy to those neighboring galaxies a distance b or less away (*friends*). This procedure generates complexes of galaxies linked together via their neighbors (*friend of friends*); these complexes are identified as groups and clusters. Different versions of this algorithm have been used in literature to identify groups especially in local redshift surveys (e.g. Eke et al. 2004) and percolation techniques have also long been used to identify virialized dark matter halos within N-body simulations.

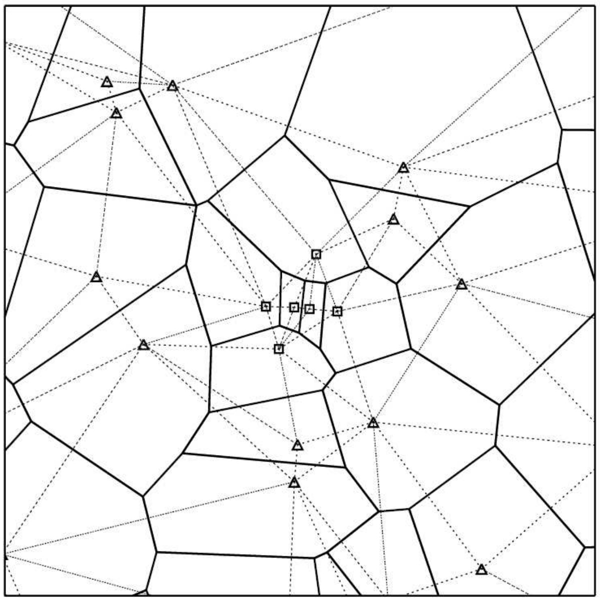

Figure 1.7: The schematic diagram of Voronoi-Delaunay method. The triangles show a randomly generated uniform background and the squares show a small galaxy group. Dotted lines show the Delaunay mesh, which links each point to its nearest neighbor (Gerke et al. 2005).

Unfortunately, working in redshift space can lead to serious problems for this algorithm. The finger-of-God effect requires that we stretch the linking volume into an ellipsoid or cylinder along the line of sight, which increases the possibility of spurious links. Since the percolation method weights each galaxy equally while creating links, then places all linked galaxies into a given group or cluster, such false links can lead to catastrophic failures, in which the group finder “hops” between several nearby groups, merging them together into a single, falsely detected massive cluster. On the other hand, shrinking the linking volume to prevent this problem increases the chances that a given structure will be broken into several smaller structures by the group finder or missed entirely. These problems have been studied in detail by Nolthenius & White (1987) and Frederic (1995).

Various other group-finding methods have been developed to combat such difficulties. Tully (1980, 1987) used the so-called hierarchical group-finding scheme, originally introduced by Materne (1978), to find nearby groups. The hierarchical grouping procedure used is computationally interesting, but in the context of the current model of structure formation it seems to lack theoretical motivation. The SDSS team has also introduced a group-finding algorithm called C4 (Nichol 2004), which searches for clustered galaxies in a seven-dimensional space, including the usual three redshift-space dimensions and four photometric colors, on the principle that galaxy clusters should contain a population of galaxies with similar observed colors. Kepner et al. (1999) introduced a three-dimensional adaptive matched filter algorithm that identifies clusters by adding halos to a synthesized background mass density and computing the maximum-likelihood mass density. White &

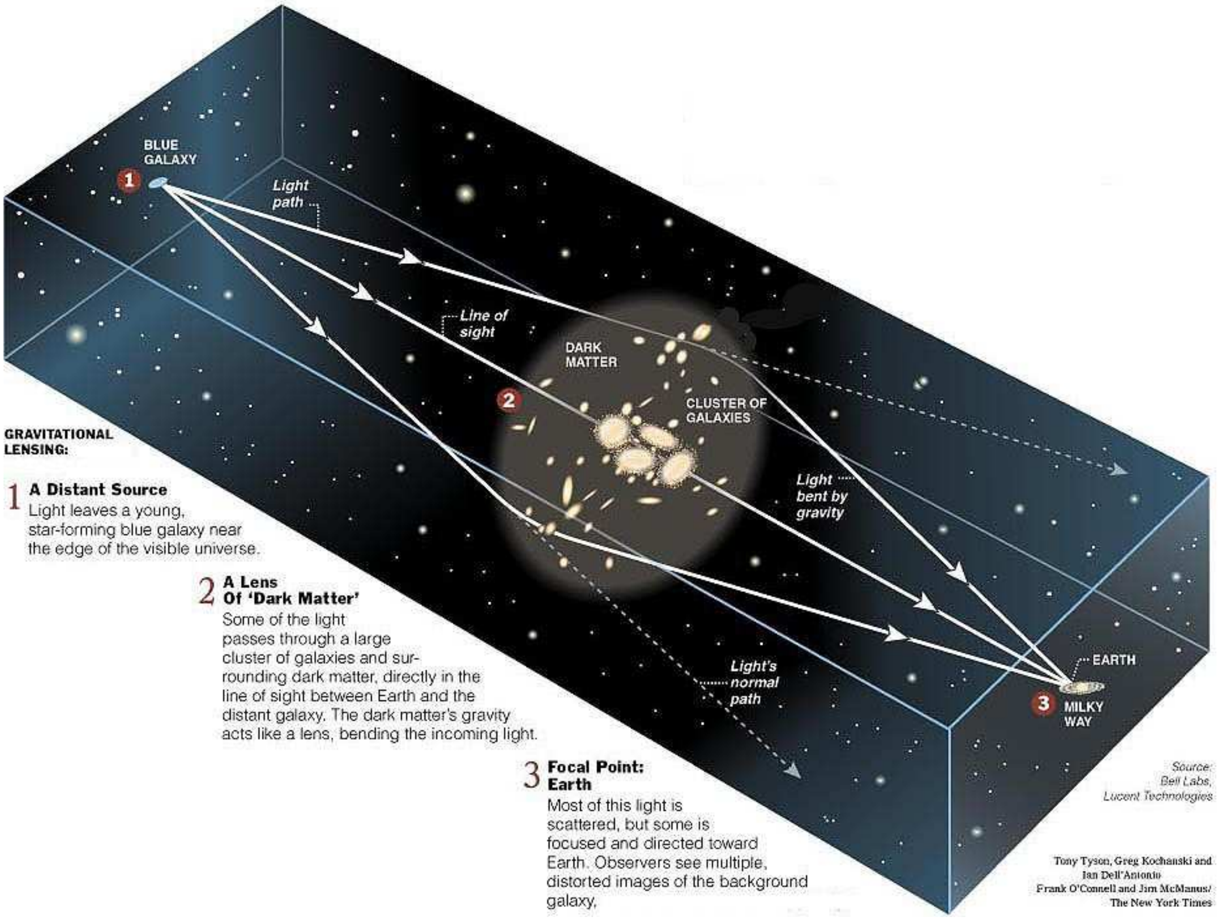

GRAVITATIONAL LENSING:

1 **A Distant Source**
Light leaves a young, star-forming blue galaxy near the edge of the visible universe.

2 **A Lens Of 'Dark Matter'**
Some of the light passes through a large cluster of galaxies and surrounding dark matter, directly in the line of sight between Earth and the distant galaxy. The dark matter's gravity acts like a lens, bending the incoming light.

3 **Focal Point: Earth**
Most of this light is scattered, but some is focused and directed toward Earth. Observers see multiple, distorted images of the background galaxy,

Source: Bell Labs, Lucent Technologies

Tony Tyson, Greg Kochanski and Ian Dell'Antonio
Frank O'Connell and Jim McManus/ The New York Times

Figure 1.8: Illustration of gravitational lensing effect.

Kochanek (2002) found that this algorithm is extremely successful at identifying clusters in spectroscopic redshift surveys, and recently, Yang et al. (2005) have introduced a group finder that combines elements of the matched filter and percolation algorithms. Finally, Marinoni & Hudson (2002) developed a group-finding algorithm the VDMthat makes use of the Voronoi partition and Delaunay triangulation of a galaxy redshift survey to identify high-density regions. By performing a targeted, adaptive search in these regions, the VDM avoids many of the pitfalls of simple percolation methods (Gerke et al. 2005).

Weak gravitational lensing

Inhomogeneities in the matter distribution perturb the paths of photons that are emitted by distant galaxies. The result is equivalent as if we are viewing these sources through a piece of glass with a spatially varying index of refraction: the images appear slightly distorted and magnified. Both effects can be measured in principle, and can be used to determine (projected) masses, because the amplitude of the distortion provides a direct measure of the gravitational tidal field, independent of the nature of the dark matter or

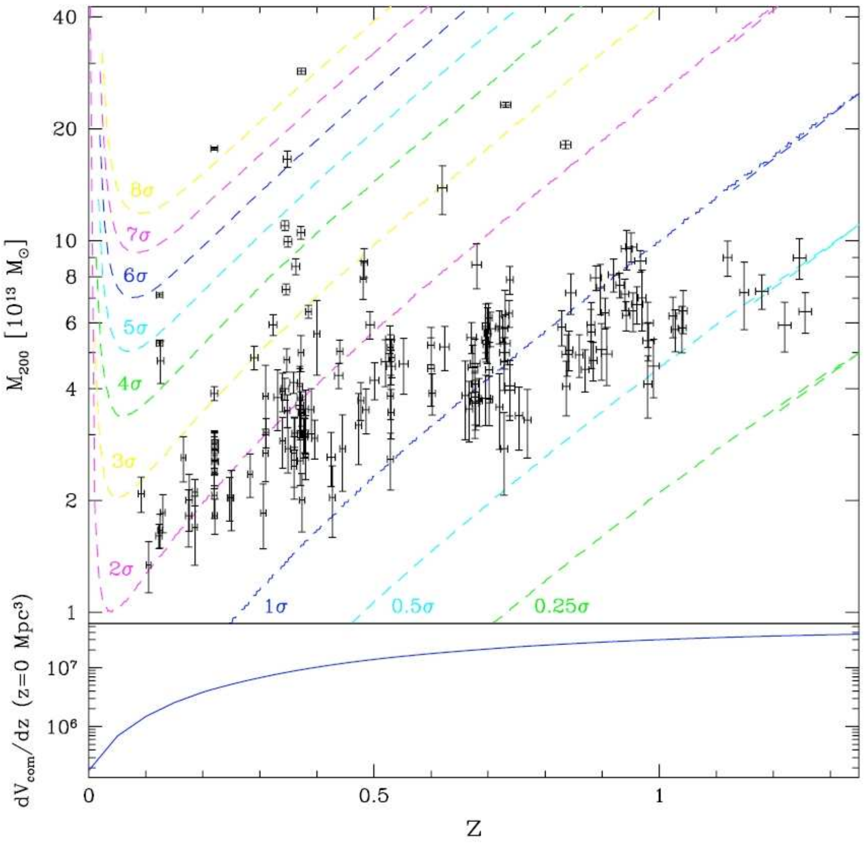

Figure 1.9: Theoretically computed lensing detection significance (dashed curves) of X-ray structures (data points) in the COSMOS field as a function of mass and redshift from Leauthaud et al. (2010)

the dynamical state of the system of interest. This is particularly useful for clusters and groups of galaxies, which are dynamically young and often show signs of merging (see e.g. Hoekstra & Jain 2008; Hoekstra et al. 2013, for a review). This technique is the simplest in terms of the underlying physics and is the only method for which the total halo mass can be directly probed, independently of both the baryons and the dynamical state of the system. Historically, Zwicky (1937) in his remarkable paper on the Coma cluster, proposed that cluster masses could be measured through gravitational lensing of background galaxies. That method did not become practical for six more decades but is now one of the primary means for measuring cluster mass. Measuring the weak-lensing distortion of any single galaxy is almost impossible because the exact shape of the unlensed galaxy is generally unknown. Alternatively, observers must measure the shear distortion of the whole field of background galaxies, under the assumption that any intrinsic departures of galaxy images from circular symmetry are uncorrelated (e.g. Tyson, Wenk & Valdes 1990; Kaiser & Squires 1993; Hoekstra et al. 1998; Mellier 1999; Bartelmann & Schneider 2001; Voit 2005). However, shear maps can only detect the most massive systems ($M > 10^{14}$ $M_\odot$) and are limited to moderate redshifts because the lensing weight function peaks mid way between the source and the observer, with galaxy shapes increasingly difficult to measure at z > 1.

Among group detection methods, X-rays are perhaps the cleanest and the most complete one. First, X-ray emission depends on the square of the gas density (eq. 1.2) and so X-rays pick up the cores of dense structures more accurately and are less prone to projection effects unlike spectroscopic finders. Second, unlike red-sequence technique which rely on galaxy properties, X-rays yield a complete sample of groups and clusters, irrespective of their galaxy content. Finally, X-rays probe a wider range in mass and redshift than shear maps which are fundamentally limited by the shape of the lensing weight function. Upper panel of Fig. 1.9 shows the expected lensing detection significance of X-ray structures in COSMOS as a function of mass and redshift (Leauthaud et al. 2010). The lower panel in Fig. 1.9 shows the comoving volume probed by the survey per unit redshift. In fact, Fig. 1.9 demonstrates that lensing alone cannot detect low mass or high redshift objects. Instead one must resort to other detection techniques such as X-rays. Note that although the low redshift lensing sensitivity is relatively good, the volume probed is also quite limited.

1.5.3 Mass of galaxy groups from the projected phase-space distribution of groups members

With the advent of multi-object spectroscopy, a large number of redshifts for members galaxies has become available. This large amount of data provides the observational material for the analysis of cluster and group mass distribution. Knowledge of mass distribution of groups and clusters especially in relation to the distributions of different system components indicate the way these systems and their components form and evolve (see, e.g. El-Zant et al. 2004). There are different ways to determine the mass profile of a group or cluster as we briefly mentioned in previous section (X-ray emission from hot intra group medium and Weak lensing). Another way to determine the mass profile of a group is by the use of its member galaxies as tracer of the gravitational potential.

In order to determine mass distribution of groups and clusters using the projected phase-space distribution of its member galaxies, we can use the Jeans analysis (see, e.g. Binney & Tremaine 1987) or the "Caustic" method introduced by Diaferio & Geller (1997). Both Jeans and Caustic method sample the total and not just the dark mass of a system. The reliability of the different estimators of mass distribution can be assessed via numerical simulations, and via direct comparison with different mass estimators. Numerical simulations indicate both Jeans and caustic method produce reliable mass estimates.

1.5.4 Different species of groups: a brief overview

Loose groups

Loose groups of galaxies are often simply referred to as groups. They are the most common class of groups with a space density of $\sim 10^{-5}$ Mpc^{-3} (Nolthenius & White 1987). They comprise ~ 50 members, including large number of faint dwarf galaxies, in a diameter of up to $\sim$ 1.5 Mpc. Thus, as the name implies, loose groups are an intermediate in scale between compact groups and rich clusters. Tucker et al. (2000) finds a median line-of-sight velocity dispersion of 164 km/s and median virial mass $\sim 1.9 \times 10^{13} h^{-1}$ $M_\odot$ for loose groups. However, Einasto et al. (2003a) argue that loose groups in the neighbourhood of a rich cluster are typically 2.5 times more massive and 1.6 times more luminous than loose groups on average. Furthermore, Einasto et al. (2003a) find that these groups have velocity dispersions of about 1.3 times larger than the loose groups on average. The immediate neighbourhood of a loose group can therefore have a significant impact on the group properties and dynamics. Hence, a nearby large cluster can enhance the evolution of the neighbouring loose group making it difficult to draw common values for the properties of loose groups that would apply to all of them. Due to their relatively small velocity dispersions and intermediate sizes, loose groups can be important when galaxies that may merge in the future are being identified and studied. For example, Mamon (1986) was the first to suggest that compact groups might be transient unbound cores of loose groups. Indeed, further studies have confirmed that loose groups are associated with compact groups, and that loose groups are often the birth places of compact groups (e.g. Diaferio, Geller & Ramella 1994).

Poor groups

Most galaxies in the local Universe, including the Galaxy, belong to a poor groups of galaxies (Zabludoff & Mulchaey 1998). Poor groups typically contain fewer than five bright ($\lesssim$ M*) galaxies and that the total number of group members is less than in a typical loose group. However, with the recent deeper redshift surveys new and faint galaxies around poor groups bringing them closer to the definition of loose groups.

However, the total number of members may not be that important for groups. Instead, the fraction of early-type galaxies in the poor groups has been found to vary significantly, ranging from that characteristic of the field ($\sim$ 25%) to that of rich clusters ($\sim$ 55 %) (Zabludoff & Mulchaey 1998) in disagreement with many loose groups. The relatively high early-type fraction in some poor groups is indeed surprising because most poor groups have low galaxy number density, thus, the effects of disruptive mechanisms such as galaxy harassment (Moore et al. 1996) are assumed to be weaker than in rich or compact groups. Conversely, the kinematics of poor groups makes them preferred sites for galaxy-galaxy mergers, which may alter the morphologies and star formation histories of some group members (Zabludoff & Mulchaey 1998), providing a possible explanation for the relatively large number of elliptical galaxies.

The dynamical status of poor groups is still matter of debate (e.g. Zabludoff & Mulchaey 1998; Mahdavi et al. 1999 and references therein). The higher galaxy densities than in the field and lower velocity dispersions than in cluster cores, make them favourable sites for galaxy-galaxy mergers (Barnes 1985). Consequently, one would assume that if poor groups are old structures several mergers should have taken place. Thus, if some or even all poor groups are gravitationally bound, why do we observe them at all? One possible explanation is that bound poor groups are collapsing for the first time, and in such, they will eventually face the same destiny as loose groups, that is being eventually associated with compact groups.

Compact groups

A compact group (CG) of galaxies contains a small number of members in which the typical intergalactic separation is of the order of the scale of the galaxies. The most well studied CG catalogue is probably the Hickson Compact Groups (HCGs) (e.g. Hickson 1982). HCGs are compact configurations of relatively isolated systems of typically four or five galaxies in close proximity to one another (Fig. 1.10). There are also some hints for their peculiarities in terms of morphology or kinematics, starbursts or even AGN activity (for a complete review, see Hickson 1997). Furthermore, HCGs have been found to contain large quantities of diffuse gas and to be dynamically dominated by dark matter (for predictions of X-ray properties, see Diaferio, Geller & Ramella 1995). They have also been found to trace the largescale structure, but to prefer low-density environments. HCGs may form as subsystems within looser galaxy associations and evolve by gravitational processes. Hence, while compact groups are associated with loose groups and filaments, these tend to be low-density and sparsely populated systems.

A CG is more likely to consist of similar type galaxies than would be expected for a random distribution (Hickson 1997, and references therein). However, they significantly have lower fraction of late-type galaxies than in the field. Zepf & Whitmore (1993) found that elliptical galaxies in compact groups tend to have lower internal velocity dispersions than do ellipticals of similar properties in other environments. Moreover, elliptical galaxies of CGs have been found to lie off the fundamental plane defined by ellipticals in other environments. This suggests that the velocity dispersion is of greater physical relevance to the formation and evolution of galaxies in CGs, than is the apparent physical density. The strong galaxy interactions in CGs are expected to induce mergers of group members (for early simulations, see Mamon 1987). The dynamical timescales of CGs have however been argued and range from relatively short ($\sim 0.1\mathrm{H}_0^{-1}$) (e.g. Diaferio, Geller & Ramella 1994) to longer ones $\sim \mathrm{H}_0^{-1}$ (e.g. Governato, Tozzi & Cavaliere 1996). If the merger timescales are somewhere between the two extremes, it is likely that CGs are rather short lived. To explain this, it has been suggested that CGs may be continuously replenished through dynamical evolution of loose groups. This provides a reasoning for the existence of CGs, but what will they become in the course of evolution? One potential scenario was described by Borne et al. (2000) who suggest that the evolutionary progression from CGs can lead first to pairs followed by ultra-luminous infrared galaxies (ULIRGs) and finally to elliptical galaxies. Thus, it is possible that CGs are the progenitors for ULIRGs. Note, however, that it has also been suggested that the eventual collapse of the CG due to mergers could lead to the formation of a fossil group (e.g. Vikhlinin et al. 1999; Mulchaey & Zabludoff 1999).

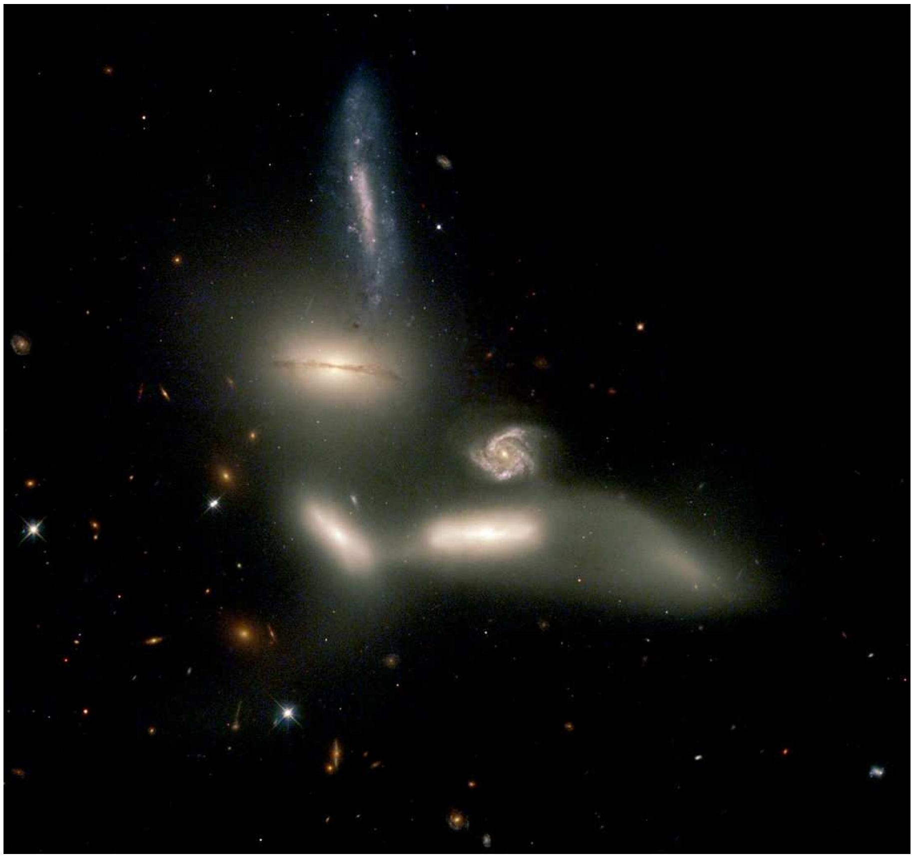

Figure 1.10: A Hubble Space Telescope (HST) image of the compact group HCG 79.

Fossil groups

A fossil system is defined as a spatially extended X-ray source with an Xray luminosity from diffuse, hot gas of $L_{X,bol} \geq 10^{42} h_{50}^{-2} ergs^{-1}$, while the optical counterpart is a system of galaxies with $\Delta m_{12} \geq 2$, where Δm_{12} is the magnitude gap between the brightest and the second brightest galaxy in the R-band within half the projected virial radius of the group centre Jones et al. (2003). The optical criterium is supposed to guarantee that the system is dominated by an E or cD type galaxy and that other members of the system can only cause small perturbations to the total potential well of the system. The first fossil group was discovered by Ponman et al. (1994) using Röntgen satellite (ROSAT) X-ray data. Since the discovery of fossil groups Khosroshahi, Ponman & Jones (2007) compiled a list of seven fossil groups based on Chandra X-ray Observatory data and Santos, Mendes de Oliveira & Sodré (2007) used SDSS data to identify 34 candidates. Fossil groups have also been studied theoretically using cosmological N-body simulations (e.g. Dónghia et al. 2005). Interestingly, based on the results of different studies fossil groups have been interpreted in different ways. Jones et al. (2003) describe fossil groups as old, undisturbed systems which have avoided infall into galaxy clusters, but where galaxy merging of most of the L^* galaxies has occurred. Khosroshahi, Ponman & Jones (2007) suggest that fossil groups

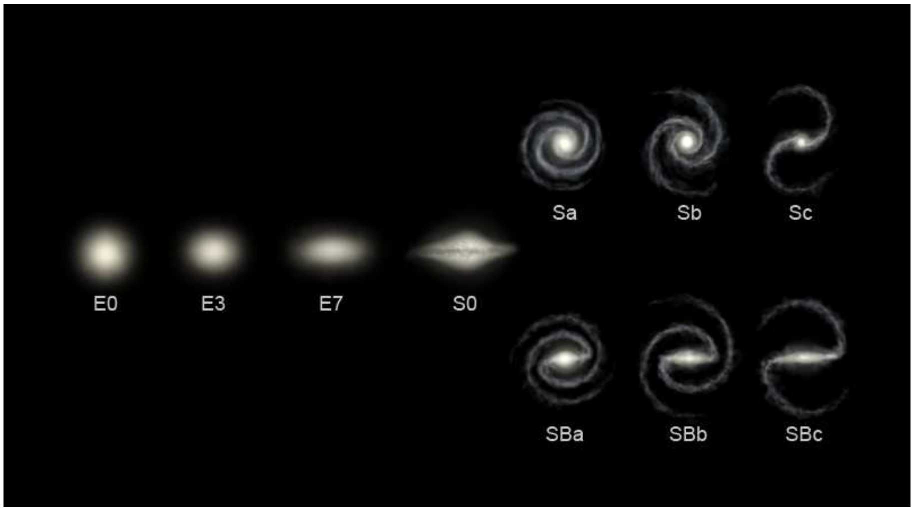

Figure 1.11: Types of galaxies according to the Hubble classification scheme. An E indicates a type of elliptical galaxies; an S is a spiral; and SB is a barred-spiral galaxies.(Image: Ville Koistinen)

have formed early, while Vikhlinin et al. (1999) and Mulchaey & Zabludoff (1999) suggest that fossils can be the result of galaxy merging within a compact group. In contrast, it has also been suggested that fossil groups are the remnants of what was initially a poor group of galaxies that has been transformed to this old stage of galaxy evolution in low density environments with compact groups acting as likely way station in this evolution (Eigenthaler & Zeilinger 2009). In cosmological N-body simulations fossil groups represent undisturbed, early forming systems in which large and massive galaxies have merged to form a single dominant elliptical galaxy (Dariush et al. 2007; von Benda-Beckmann et al. 2008). Given the different interpretations, it is clear that more work is required before fossil groups can be considered as fully understood.

1.6 The galaxy population in group environment

Groups are the most common environment of galaxies in the present day Universe, containing 50%-70% of the galaxy population (Geller & Huchra 1983; Eke et al. 2005). This naturally implies that processes taking place in the group environment can affect the colors, star formation history and morphologies of their member galaxies.

One of the most fundamental correlations between the properties of galaxies and their host environment in the local Universe is the so-called morphology-density relation (Dressler 1980). The morphology-density relation expresses the link between the occurrence of specific Hubble types (Fig. 1.11) and the local density. This relation shows that disc-dominated galaxies tend to reside in lower density region of the Universe, opposite to elliptical and lenticular galaxies (Fig. 1.12). Postman & Geller (1984) extended this relation to group regime and strengthened the hypothesis of group environment effect on

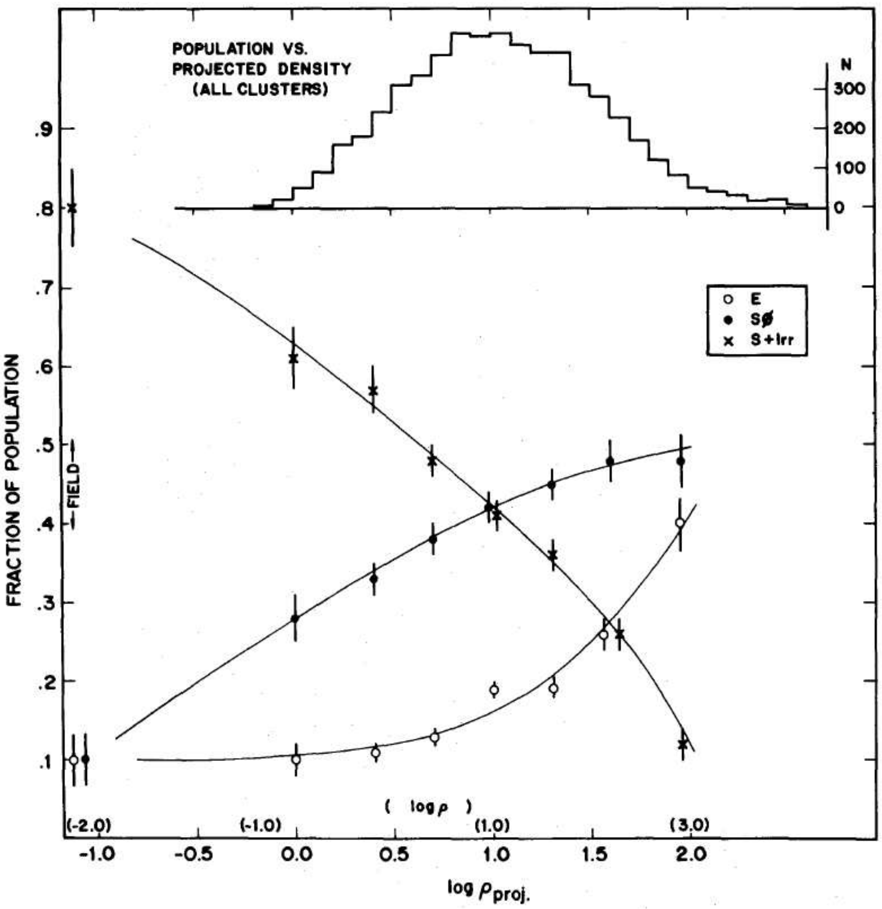

Figure 1.12: Morphology-density relation (Dressler 1980). The fraction of elliptical and lenticular galaxies (Es and S0s) increases as a function of projected density while the fraction of Spiral and Irregular galaxies (S+Irr) decreases with increasing density.

its galaxy population. Another pieces of empirical evidence supporting this claim was the observation by Butcher & Oemler that galaxy clusters consist of a higher fraction of blue galaxies at progressively higher redshift, the so-called Butcher-Oemler effect (Butcher & Oemler 1978, 1984). Since these early papers, Butcher-Oemler effect has been confirmed photometrically and spectroscopically (e.g. Rakos & Schombert 1995; Margoniner et al. 2001; Goto et al. 2003; Lavery & Henry 1986, 1988; Poggianti et al. 2006, 1999), and has been extended to galaxy groups (e.g. Allington-Smith et al. 1993; Wilman et al. 2005; Gerke et al. 2007; Cucciati et al. 2010). The blue colors of galaxies mostly created when galaxies are involved in merging or tidal interactions which indicate that Butcher-Oemler effect is a proxy of the transformation of spiral galaxies to Elliptical/S0.

An alternative way to study the effect of the environment on the member galaxies is through the analysis of the SFR-density relation. Lewis et al. (2002) used Two-Degree Field Galaxy Redshift Survey (2dFGRS; Colless et al. 2001) to show there is an anti-correlation between SFR and local projected density in cluster of galaxies up to 2 virial radii from the cluster center. Gómez et al. (2003) confirmed similar results in groups of galaxies using Sloan Digital Sky Survey (SDSS; Stoughton et al. 2002). This relation indicate the cores of dense environment are full of massive spheroidal systems which are dominated by old stellar population, while the lower density environments are mostly populated by gas rich spirals. The existence and the behavior of this relation at z∼ 1 is still a subject of debate. Elbaz et al. (2007) and Cooper et al. (2008) observed the reversal of SFR-density relation at z∼1 in GOODS and DEEP2 fields, respectively. Popesso et al. (2011), using $Herschel\ PACS$ data, show that the reversal is mainly due to higher fraction of AGN which exhibit slightly higher SFR with respect to galaxies at the same stellar mass. Kovač et al. (2010a) indicate that galaxy star formation and color transformation rates are higher in groups environment than in lower density regions at z∼1. Caputi et al. (2009) show that luminous infrared galaxies (LIRGs, $L_{IR}= 10^{11} - 10^{12}L_{\odot}$) are more often found in overdense environment, while ultra-luminous infrared galaxies (ULIRGs, $L_{IR} > 10^{12}L_{\odot}$) prefer under-dense region using zCOSMOS data set (Lilly et al. 2007). On the contrary, Feruglio et al. 2010, using photometric redshift to define local density, do not find any dependence of the fraction of LIRG on the environment. However these scenario can become more complicated by interplay of mass and density.

There are many different physical processes which can play a role in driving morphology-density and SFR-density relation. In the following, we discussed some of these major physical processes.

Dynamical friction. A massive galaxy moving at velocity v through a background of DM particles with mass density ρ experiences a drag force decelerating the galaxy in the direction of motion (Chandrasekhar 1943). This "dynamical friction" happens because the galaxy accelerates the DM particles behind it, leaving an overdense concentration of background particles in the wake of the galaxy. Thus the galaxy steadily looses speed in respect to the group center and thus spirals towards it according to $\dot{v} \propto \rho M v^{-2}$. This drag force is independent of the mass of individual background particles, but proportional to the galaxy mass. An immediate consequence is that the central galaxy frequently experiences mergers with other galaxies falling to the center termed galactic "cannibalism" (Hausman & Ostriker 1978) and provides a straightforward explanation for the existence of the huge cD galaxies in the centres of many rich clusters.

Galaxy merging. Mergers occurs more frequently in the group environment and the outskirt of the clusters than in the field (e.g. Caldwell et al. 1993; Moss & Whittle 1993; Gnedin 2003). A critical parameter for the occurrence of a merger between galaxies is their relative velocity which should be smaller than the relative escape velocity of the galaxies. It can be shown that the merger rate Γ in a group despite the relatively high galaxy density is roughly proportional to 1/v (Spitzer & Baade 1951; Peacock 1999). This leads to the expectation that the merger rate is higher in a group with the smaller velocity dispersion. Rich clusters having a velocity dispersion of ∼1000 km/s are therefore less prone to mergers compared to small groups with velocity dispersions of a few hundred km/s. Merger or tidal interactions can destroy galactic discs and convert spiral and irregular galaxies to bulge dominated ellipticals and lenticulars (Toomre & Toomre 1972; Farouki & Shapiro 1981).

Galaxy harassment. A process which can also significantly alter the morphology of galaxies are multiple high-speed encounters between galaxies without merging ("galaxy harassment", Moore et al. 1996). Galaxy harassment leads to disk deformation in spiral and S0 galaxies and detectable tidal tales, stripping of the outer galactic halos, or trigger star formation activity (Richstone 1976) and should be much more frequent than real galaxy mergers.

Ram pressure stripping. Interactions with the dense intracluster gas of density σ, a galaxies moving through this medium with velocity v feels ram pressure $p_{ram} \simeq \sigma v^2$ (Gunn & Gott 1972). This pressure can sweep interstellar medium out of a galaxy and so "quench" its star formation immediately.

Strangulation. A similar process is "strangulation". When galaxies falling into the DM halo lose their warm outer envelope of gas (Balogh, Navarro & Morris 2000). This leads to cut of the supply of cold gas in the galaxy and thus a gradual decrease of star formation.

1.6.1 The "Nature" vs. "Nurture" scenario

There is a complex interplay between stellar mass of galaxies and their environment which make the scenario of environment effects on galaxy population more complicated. The main debate now centers on the role of galaxy "internal" versus "external" processes as driving mechanisms of the galaxy evolution, or, according to an old-fashion approach, the "nature" versus "nurture" scenario. In the current paradigm of galaxy formation the "internal" processes are mainly linked to the co-evolution of the host galaxy and its central black hole (Di Matteo, Springel & Hernquist 2005; Croton et al. 2006; De Lucia et al. 2006; Hopkins et al. 2006). However, the nature versus nurture dichotomy seems now to be an ill-posed problem. Indeed, in the current paradigm of galaxy formation these physical processes turn out to be coupled with a history bias that is an integral part of the hierarchical structure formation of cosmic structure (De Lucia et al. 2012). Recent studies have demonstrated that halos in overdense regions form statistically earlier and merge more rapidly than halos in regions of the Universe of average density (Gao et al. 2004). This differential evolution is bound to leave an 'imprint' on the observable properties of galaxies that inhabit different regions at any cosmic epoch (De Lucia et al. 2012). This aspect makes the interpretation of the observational evidences even more difficult. In fact, binning galaxies according to their stellar mass does not suffice to disentangle the role of nature and nurture. For instance, two galaxies of identical mass at some cosmic epoch can end up having different stellar masses if one of them falls on to a cluster and the other remains in a region of average density.

A first attempt to investigate from the observational point of view the inter-relationships between stellar mass, star-formation rate and environment comes from Peng et al. (2010) in the SDSS, zCOSMOS surveys. With a purely empirical approach, they show a) two distinct processes, mass (internal) quenching and environment (external) quenching are both operating since z∼1, b) environment-quenching occurs as large-scale structure develops and is more effective on satellite galaxies, c) mass-quenching is more efficient for central, generally more massive galaxies. This is supported observationally by the study of star-formation histories of galaxies in the Virgo cluster (Gavazzi et al. 2002), galaxies with higher H-band luminosities being characterized by shorter time-scale of star formation. Moreover, Pipino et al. (2011) also support this scenario by analysis the chemical abundances in elliptical galaxies. However, the limit of Peng et al. (2010) analysis is mainly in the definition of the environment that relies on the local galaxy density, which is only a poor proxy of the DM halo mass.

1.7 Aims and Outline of the Thesis

As mentioned above, groups of galaxies are important laboratories to study galaxy evolution and formation. They are the most common environment in local universe as they encompass more than half of nearby galaxies. Massive galaxies ($\sim 10^{10} - 10^{11} M_{\odot}$) favour high density regions like groups and clusters and the most contribution to the star formation density of the universe is provided by these galaxies. Additionally, the star formation activity in groups can be suppressed with respect to galaxies in lower density environment like field galaxies.

Much work has already been done in order to shed light on the undersatnding of the relation between galaxy formation and evolution and the environment. Most recently, Popesso et al. (2012), Iovino et al. (2010) and Kovač et al. (2010a) suggested that evolution of SF activity in group galaxies is faster than field since z∼1. However, there is still a lack of comprehensive study in this area. Taking into account all these elements, the aim of this thesis is to proof whether the membership of a galaxy to a group is sufficient to quench the SF activity of a galaxy. This will show if the structure formation process itself can be one of the major causes of the decline of the SF rate density of the Universe since redshift 1-2. For this aim, providing a complete and clean sample of galaxy groups with reliable membership is of great importance. So, the first part of this thesis is dedicated to create a new X-ray galaxy groups and their membership catalog in All-wavelength Extended Groth strip International Survey (AEGIS). Taking advatage of deep X-ray surveys and new multiwavelength data, in the second and third part of this thesis, we build a larger sample of groups by combining X-ray samples in deep X-ray fields and assign membership in a consistent way. Using this unique sample, we study the evolution of star fomation rate activity and density in group environment based on a pure spectroscopically membership. At the end we also provide a very comprehensive picture on the SFR-M plane in different envrionment.

The outline of this thesis is described in the following: in Chapter 2, we present a catalog of X-ray galaxy groups and their membership which is the results of a search for extended X-ray sources from 800-ks Chandra coverage of the All-wavelength Extended Groth Strip International Survey (AEGIS); in Chapter 3, We provide the analysis of the evolution of the total star formation activity, total stellar mass and halo occupation distribution (HOD) by using one of the largest X-ray selected sample of galaxy groups with secure spectroscopic identification on the major blank fields (ECDFS, CDFN, COSMOS, AEGIS) up to z$\sim$1; in Chapter 4, we examine whether the position of bulk of SF galaxies depends on environment. we also analyse the dispersion of the MS in different bins of stellar mass and check whether this depends on the environment; a brief summary and the most important conclusions for this work are outlined in Chapter 5.

Chapter 2

X-RAY Groups of Galaxies in the AEGIS deep and wide fields

G. Erfanianfar, A. Finoguenov, M. Tanaka, M. Lerchster, K. Nandra, et al.

ApJ, **765**(2013), 117

Abstract

We present the results of a search for extended X-ray sources and their corresponding galaxy groups from 800-ks Chandra coverage of the All-wavelength Extended Groth Strip International Survey (AEGIS). This yields one of the largest X-ray selected galaxy group catalogs from a blind survey to date. The red-sequence technique and spectroscopic redshifts allow us to identify 100% of reliable sources, leading to a catalog of 52 galaxy groups. The groups span the redshift range $z \sim 0.066 - 1.544$ and virial mass range $M_{200} \sim 1.34 \times 10^{13} - 1.33 \times 10^{14} M_{\odot}$. For the 49 extended sources which lie within DEEP2 and DEEP3 Galaxy Redshift Survey coverage, we identify spectroscopic counterparts and determine velocity dispersions. We select member galaxies by applying different cuts along the line of sight or in projected spatial coordinates. A constant cut along the line of sight can cause a large scatter in scaling relations in low-mass or high-mass systems depending on the size of cut. A velocity dispersion based virial radius can more overestimate velocity dispersion in comparison to X-ray based virial radius for low mass systems. There is no significant difference between these two radial cuts for more massive systems. Independent of radial cut, overestimation of velocity dispersion can be created in case of existence of significant substructure and also compactness in X-ray emission which mostly occur in low mass systems. We also present a comparison between X-ray galaxy groups and optical galaxy groups detected using the Voronoi-Delaunay method (VDM) for DEEP2 data in this field.

2.1 Introduction

Groups of galaxies are important laboratories to study galaxy evolution and formation. They are in the stage between the field and the densest environment in the universe, massive clusters (Zabludoff & Mulchaey 1998) and as many as $50\% - 70\%$ of all galaxies reside in galaxy groups (Turner & Gott, 1976; Geller & Huchra, 1983; Eke et al., 2005).

It is valuable to study galaxy groups over a range of cosmic time to understand the effect of the group environment on the galaxy population. Several efforts have been made to identify groups and clusters up to redshift one and beyond (e.g., Stanford et al. 2006; Eisenhardt et al. 2008; Bielby et al. 2010; Tanaka, Finoguenov & Ueda 2010). The faint X-ray emission and low galaxy number densities of galaxy groups make such environments difficult to distinguish from the field compared to massive galaxy clusters at higher redshifts. We have a relatively good knowledge and samples of galaxy groups in the local universe (e.g. Mulchaey & Zabludoff 1998) but there is a lack of similar samples of galaxy groups which have both sufficiently deep X-ray data and counterparts with optical spectroscopy at high redshift. In the presence of advances in deep X-ray surveys, extended X-ray emission provides a reliable signal to detect such environments at high redshifts.

There are a number of different methods for detecting groups of galaxies: searches in optical data via the red-sequence method (e.g. Gladders & Yee 2005; Koester et al. 2007); the Sunyaev-Zeldovich (SZ) effect on the cosmic microwave background, CMB (e.g. Sunyaev & Zeldovich 1972; Carlstrom, Holder & Reese 2002; LaRoque et al. 2003; Benson et al. 2004); X-ray emission from hot intracluster gas (e.g. Böhringer et al. 2000; Vikhlinin et al. 2009; Finoguenov et al. 2010); cosmic shear due to weak gravitational lensing maps (e.g. Miyazaki et al. 2007; Massey et al. 2007); and spectroscopic group samples (e.g. Gerke et al. 2012; Miller et al. 2005; Knobel et al. 2009). While spectroscopic surveys reveal the largest and deepest group catalogs, detection of the group X-ray emission has been proven to ensure objects are virialized, and with the deepest X-ray survey available to date, the limits to which X-ray emission can be detected are reaching the level of low-mass groups. Moreover, compared to shear maps, X-rays probe a wider range in mass and redshift (Leauthaud et al. 2010).

In this paper, with recent deep Chandra data (Nandra et al. in prep), we search for galaxy groups in a wide range of redshift in the Extended Groth Strip (EGS). In previous work, searching for galaxy groups in Chandra data with a nominal exposure time of 200 ks and $\sim 0.67 deg^2$ coverage of EGS field yielded a discovery of seven high significance galaxy groups in this field (Jeltema et al. 2009). We now add new Chandra data with approximately 800 ks exposure time covering $\sim 0.25 deg^2$ field Figure (3.1). Furthermore, EGS is one of the four fields in Deep Extragalactic Evolutionary Probe 2 (DEEP2) spectroscopy survey (Davis et al. 2003; Newman et al. 2012) and it is the only field which has been targeted for extensive spectroscopic data in DEEP3 (Cooper et al. 2011, 2012). The DEEP2 and DEEP3 coverage of EGS are magnitude limited but not color selected, yielding a large sample of spectroscopic galaxies at all redshifts enabling us to identify our groups optically and determine their velocity dispersions.

This paper is laid out as follows: section 2 presents a brief description of AEGIS survey

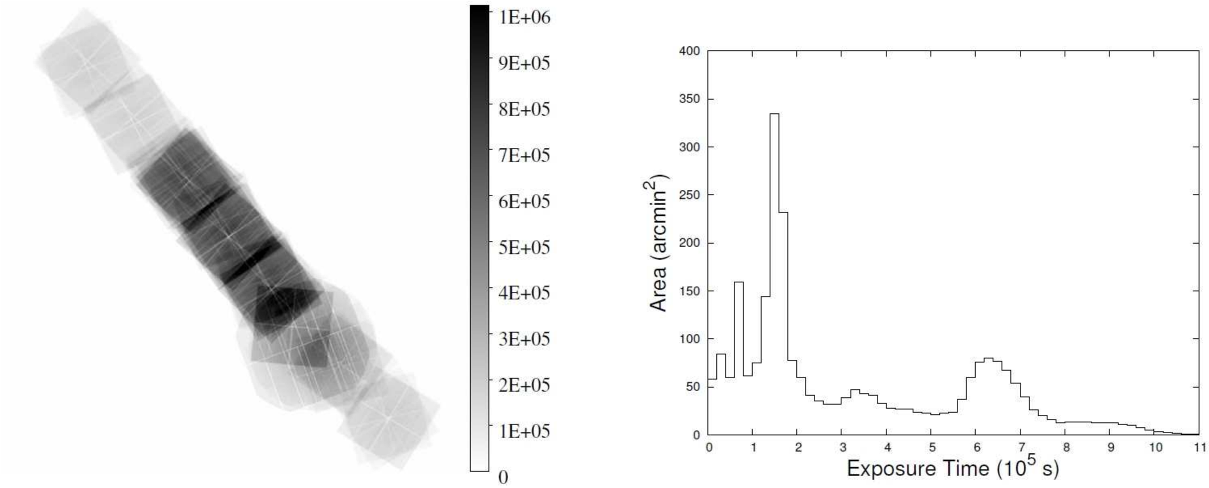

Figure 2.1: The exposure map (left panel) and the distribution of exposure time (right panel) in Chandra and XMM coverage of EGS.

and our data, section 3 describes our method for group identification. We present our identified group catalog in section 4. In section 5 we present spectroscopic group membership and dynamical properties of th groups. We make a comparison between the X-ray groups and optical groups which are identified from Voronoi-Delaunay method (VDM) in the DEEP2 spectroscopic dataset in section 6. Throughout this paper a ΛCDM cosmology with $\Omega_m = 0.27$, $\Omega_\Lambda = 0.73$ and $H_0 = 100h$ km s^{-1} Mpc^{-1} where h=0.71 is assumed.

2.2 THE AEGIS SURVEY

The All-Wavelength Extended Groth Strip International Survey (AEGIS) brings together deep imaging data from X-ray to radio wavelengths and optical spectroscopy over a large area (0.5-1 deg^2). This survey includes: Chandra/ACIS X-ray (0.5-10 keV), GALEX ultraviolet (1200-2500 $\AA$), CFHT/MegaCam Legacy Survey optical (3600-9000 $\AA$), CFHT/CFH12K optical (4500-9000 $\AA$), Hubble Space Telescope/ACS optical (4400-8500 $\AA$), Palomar/WIRC near-infrared (1.2-2.2 μm), Spitzer/IRAC mid-infrared (3.6, 4.5, 5.8, 8 μm, VLA radio continuum (6-20cm) and a large spectroscopic dataset using the DEIMOS spectrograph on the Keck II 10m telescope in an area with low extinction and low Galactic and zodiacal infrared emission (Davis et al. 2007). In the following section we will describe the various data sets used in this analysis.

2.2.1 X-ray data

Our very deep Chandra survey used the Advanced CCD Imaging Spectrometer (ACIS-I) in three contiguous fields covering a total area of 0.25 deg^2 (Nandra et al. in prep) and a series of eight pointings covering a total area of approximately $0.67deg^2$ in the Extended Groth Strip. Laird et al. (2009) provided the details for the latter survey and the X-ray point sources catalog. The total exposure time is approximately 3.4 Ms with nominal exposure of 800 ks in each three central fields.

We also used the XMM-Newton observations of the field (ObjIDs 0127921001, 0127921101, 0127921201, 0503960101), which were processed and co-added following the prescription of Bielby et al. (2010). The total time of XMM observations is 100ks and its contribution to the final coverage can be seen in Figure 3.1 as a roundish area in the southern part of the survey. Here we present the X-ray extended sources catalog based on the Chandra and XMM observations in EGS.

In the Chandra analysis, we have applied a conservative event screening and modeling of the quiescent background. We have filtered the light-curve events using the lc clean tool in order to remove normally undetected particle flares. The background model maps have been evaluated with the prescription of Hickox & Markevitch (2006). We estimated the particle background by using the ACIS stowed position [1] observations and rescaling them by the ratio of the hard band (9.5−12keV) fluxes. The cosmic background flux has been evaluated by subtracting the particle background maps from the real data and masking the area occupied by the detected sources. We applied the method which has been used in Finoguenov et al. (2009) to search for extended sources and as a result we found 56 extended sources in EGS strip. Briefly, X-ray data have been obtained from X-ray mosaics made from coaddition of the $XMM-Newton$ and *Chandra* data. After background subtraction and point source removal for each observation and each instrument separately, the residual images were co-added, taking into account the difference in the sensitivity of each instrument to produce a joint exposure map. To detect the sources we run a wavelet detection at $32''$ and $64''$ spatial scales, similar to the procedure described in Finoguenov et al. (2007, 2009).

2.2.2 Photometric Data

The EGS field is located at the center of the third wide field of the Canada-France-Hawaii Telescope Legacy Survey (CFHTLS-Wide3, W3)[2] which is covered in u^*, g', r', i' and z' filters down to i'=24.5 with photometric data for 366,190 galaxies (Brimioulle et al. 2008). The EGS field also contains the CFHTLS Deep 3 field (Davis et al. 2007), which covers 1 deg^2 with *ugriz* imaging to depths ranging from 25.0 in z to 27 in g. For this work, we

---

[1] http://cxc.cfa.harvard.edu/contrib/maxim/acisbg

[2] Based on observations obtained with MegaPrime/MegaCam, a joint project of CFHT and CEA/DAPNIA, at the Canada-France-Hawaii Telescope (CFHT) which is operated by the National Research Council (NRC) of Canada, the Institut National des Science de l'Univers of the Centre National de la Recherche Scientifique (CNRS) of France, and the University of Hawaii. This work is based in part on data products produced at TERAPIX and the Canadian Astronomy Data Centre as part of the Canada-France-Hawaii Telescope Legacy Survey, a collaborative project of NRC and CNRS

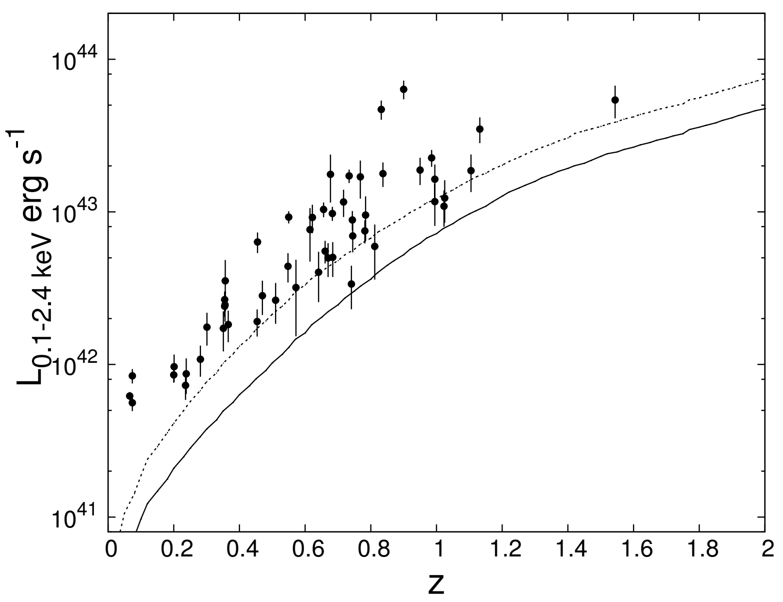

Figure 2.2: X-ray luminosity as a function of redshifts for X-ray galaxy groups in EGS. The error bars are based only on the statistical errors in the flux measurements. The solid line and dashed line are the flux detection limits associated with 10 and 50% of the search area respectively.

have used the T0006 release of the CHTLS Deep data [3]. The CFHTLS Deep field also contains near-infrared coverage in the JHK bands via the WIRCam Deep Survey (WIRDS - Bielby et al. 2012). This covers 0.4 deg^2 of the D3 field and provides deep imaging to $\sim$ 24.5 (AB) in the three NIR bands. Photometric redshifts in the region covered by the NIR data were determined using the `Le Phare` code as described in Bielby et al. (2010).

2.2.3 Spectroscopic Data

The DEEP2 Redshift Survey has targeted $\sim 3.5\ deg^2$ within four fields on the sky using the DEIMOS multi-object spectrograph (Faber et al. 2003) on the Keck II Telescope (Davis et al. 2003). All the DEEP2 targets have $18.5 \leq R \leq 24.1$. The EGS is one of these four fields. Compared to other DEEP2 fields, the EGS spectroscopy is magnitude limited, but not color-selected, giving the advantage of a sample of galaxies at all redshifts (Davis et al. 2007). In addition, this region of sky has been targeted for extensive spectroscopy with DEEP3 (Cooper et al. 2011, 2012). The DEEP2 and DEEP3 catalogs have about 23,822 unique objects in total(with -2≤redshift quality≤4) and 16,857 objects with reliable redshifts (with redshift quality≥3). In addition to DEEP2 and DEEP3, EGS is located in Sloan Digital Sky Survey [4] coverage so we have additional spectra for our low redshift

---

[3] http://terapix.iap.fr/cplt/T0006-doc.pdf

[4] Funding for the SDSS and SDSS-II has been provided by the Alfred P. Sloan Foundation, the Participating Institutions, the National Science Foundation, the U.S. Department of Energy, the National

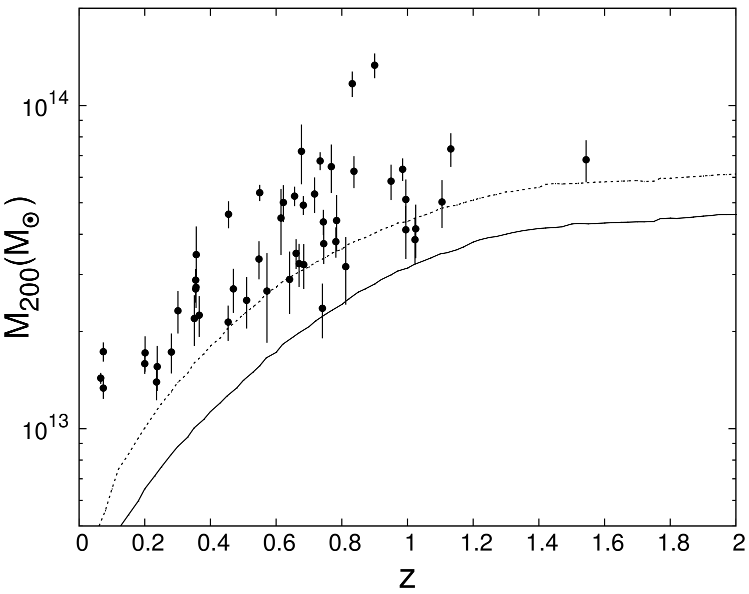

Figure 2.3: X-ray masses as a function of redshifts for X-ray galaxy groups in EGS. The error bars are based only on the statistical errors in the flux measurements. The solid line and dashed line are the flux detection limits which associate with 10 and 50% of search area respectively.

galaxies. We also used redshifts of spectroscopic galaxies obtained in follow-up observations of the DEEP2 sample with the Hectospec spectrograph on the Multiple Mirror Telescope (MMT; Coil et al. 2009).

2.3 Optical Identification

To identify the groups in redshift space, we used galaxies with good redshift quality in DEEP2 and DEEP3 to construct our initial redshift catalog. Using this catalog, imaging data, and position of X-ray extended sources, we assigned a redshift to each X-ray source visually where the spatial distribution of galaxies in the sky coincide with the X-ray emission. For those sources for which we found more than one counterpart and the X-ray shape allows to securely seprate the contribution from several counterparts, we define a new ID in our X-ray catalog. The detected sources areas searched for flux extension down to 90% confidence level which is subsequently used for flux estimation.

We also used the refined red-sequence technique, described in Finoguenov et al. 2010, to confirm the overdensity of red galaxies within or near those X-ray sources which have a lack of spectroscopic data. In brief, we selected galaxies with $|z - z_{phot}| < 0.2$ and within a physical distance of 0.5 Mpc from the center of X-ray emission at the given redshift. Then,

---

Aeronautics and Space Administration, the Japanese Monbukagakusho, the Max Planck Society, and the Higher Education Funding Council for England. The SDSS Web Site is `http://www.sdss.org/`.

using a Gaussian weight, we count galaxies around the model red-sequence and find overdensities. Since different observed colors are sensitive to red galaxies at different redshifts, we adopt the following combination of colors and magnitudes.

For those groups which lie in D3 field in CFHTLS :
0.0<z<0.3 : $u^* - r'$ color and r' magnitude
0.3<z<0.6 : $g' - i'$ color and i' magnitude
0.6<z<1.0 : $r' - z'$ color and z' magnitude
1.0<z<1.5 : $i' - J$ color and J magnitude
1.5<z<2.0 : $z' - Ks$ color and Ks magnitude

For those in the W3 field:
0.0<z<0.3 : $u^* - r'$ color and r' magnitude
0.3<z<0.6 : $g' - i'$ color and i' magnitude
0.6<z : $r' - z'$ color and z' magnitude

We note that Bielby et al. (2010) mistakenly quoted their filter combinations to identify red-sequence signals. They used the same filters as in our D3 field. Using the red-sequence technique and the spectroscopic data, we could identify redshifts for 52 extended X-ray sources. We have spectroscopic redshifts for 49 galaxy groups and more than two spectroscopic members for 46 galaxy groups.

We also assigned a flag for each extended source that describes the quality of the identification. Flag=1 indicates confident redshift assignment and significant X-ray emission and also good centering, while for Flag=2 the centering has a large uncertainty. In the cases when a single X-ray source has been matched to several optical counterparts the assigned flag is equal to 2 or larger. For Flag=3 we have no spectroscopic confirmation but good centering and for Flag=4 we have unlikely redshifts due to the lack of spectroscopic objects and red galaxies and also a large uncertainty in centering. We assigned Flag=5 for the 13 unreliable cases for which we could not identify any redshift. They can be split into the following categories.

Some of the X-ray extended sources do not have spherical and symmetric morphologies and some exhibit a secondary peak in X-ray distribution. Initially, we expect this results from overlapping systems but visual inspection of optical data and the red-sequence method indicate a single significant group for some of these. So, we classify the second shallow peak in X-rays as substructure inside those real groups. Furthermore, sources on the edge of X-ray coverage with low signal to noise and no optical counterparts could be explained as residual background level in the images or bright X-ray clusters outside the field of view. We note that two RCS-2 clusters (Gilbank et al. 2011) are located $10'$ west from the edge of the survey. In the few cases of bright stars near the X-ray emission, we could not match galaxy counterparts to the extended emission. We assigned Flag=5 for all of these cases and they are not included in the final sample.

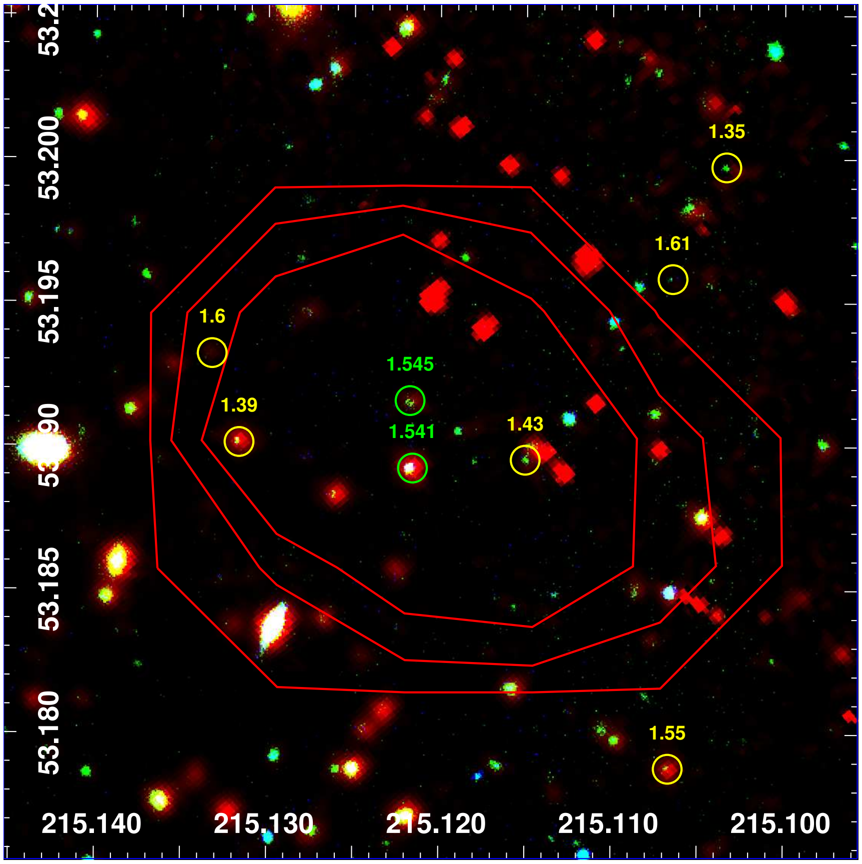

Figure 2.4: RGB image of galaxy group at z=1.54 with ID = EGSXG J1420.4+5311 using channel 2 (4.5 microns) of Spitzer/IRAC and z' and r' bands from W3 field of CFHTLS. The contours show the X-ray emission. The green circles show spectroscopic redshifts and the yellow circles indicate galaxies located at $1.3 < z_{photo} < 1.7$ within r_{200} of the group. Many of the red points are artifacts in the ch2 image and they don't have any corresponding sources in z' and r' bands.

2.4 A Catalog of identified X-ray groups

In this section, we describe our catalog of 52 X-ray galaxy groups detected in AEGIS (Table 1). The group identification number, RA and Dec. of the peak of X-ray emission in Equinox J2000.0 are listed in Column 1, 2 and 3. In Column 4 the mean of red-sequence redshifts which is substituted with the median of spectroscopic redshifts in case there is a spectroscopic redshift determination for the group member galaxies is listed. We provide the group flux in the 0.5–2 keV band in Column 5 with the corresponding 1σ error. The rest-frame luminosity in the 0.1–2.4 keV is given in Column 6. Column 7 lists the estimated total mass, M_{200}, computed following Leauthaud et al. 2010 and assuming a standard evolution of scaling relations: $M_{200}E_z = f(L_xE_z^{-1})$ where $E_z = (\Omega_M(1+z)^3 + \Omega_\Lambda)^{1/2}$. The corresponding r_{200}, $M_{200} = \frac{4}{3}\pi r_{200}^3(200\rho_{critical})$, in arcminutes is given in Column 8.

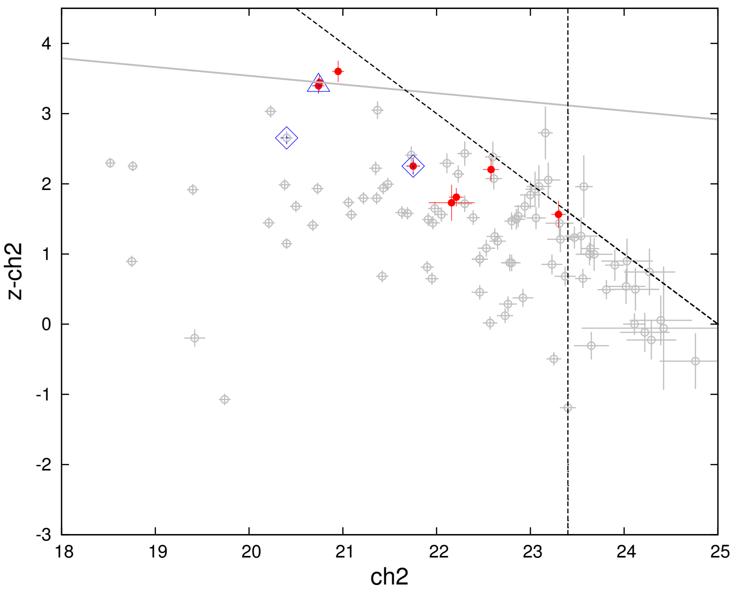

Figure 2.5: Color-magnitude diagram for EGSXG J1420.4+5311 based on Spitzer/IRAC and CFHTLS data. All the galaxies within r_{200} of the group are plotted here. The filled circles show galaxies with $1.3 < z_{photo} < 1.7$. The diamonds and triangle indicate secure and possible spectroscopic members respectively. The grey line shows model red-sequence for z=1.5. The 50% completeness for Channel 2 magnitude and z-ch2 color are shown as vertical and slanted dashed lines respectively.

Column 9 lists the flag for our identification, as described in section 3. The number of spectroscopic member galaxies inside r_{200} is given in Column 10 (see §5). Column 11 lists flux significance which provides insight on the reliability of both the source detection and the identification. The velocity dispersion estimated from X-ray luminosities is given in column 12.

Figures 3.2 and 3.5 show the luminosity and mass of groups as a function of their redshifts respectively.

2.4.1 A galaxy group candidate at z=1.54

During the optical group identification using spectroscopic data, we have discovered a high-z group candidate at z=1.54 (Figure 3.4). The X-ray signal is measured with a significance of 4.1σ. This group has two sepectroscopic members with good flags in the hot halo of the group. One of the spectroscopic members show AGN activity in its expectra and also detected as a X-ray point source in our analysis. The point source emission has been removed from the flux estimates. As it is a Chandra-detected group, the resolution allows us to exclude the AGN contamination down to a factor of 10 below the level of the detection of the extended emission itself. We estimate a cluster mass of $M_{200} = 6.8 \times 10^{13} M_{\odot}$, an X-ray luminosity of $L_X = 5.4 \times 10^{43}$ erg s^{-1} and a virial radius of $r_{200} = 0.015°$. A red-sequence finder using channel 2 (4.5 micron) from Spitzer/IRAC and z' band from CFHTLS has also detected a signal around z=1.5 (Figure 2.5). Since we did not have a deep z-band image for this group, there was a strong limit on our color-magnitude diagram and thus the red-sequence signal and therefore we called it a group candidate. The uniqueness of this candidate group arises from availability of ultra deep X-ray image but the system is marginally covered by Spitzer/IRAC data and is out of coverage of Deep fields in AEGIS (CFHTLS D3, Hubble/ACS and CANDELS).

2.5 Spectroscopic group member galaxies

We search for galaxies associated with our identified X-ray sources based on their redshifts and positions. We perform this selection in different ways and explore the effects on the dynamical velocity dispersion, mass, and $L_x - \sigma$ scaling relation of the groups.

First, we assume an initial velocity dispersion of 500 km/s for each group and calculate the redshift range for the group members from equation 1 (Wilman et al. 2005; Connelly et al. 2012):

$$\delta(z)_{max} = 2\frac{\sigma(v)_{obs}}{c} \tag{2.1}$$

This $\delta(z)_{max}$ is then converted into a spatial distance using equation 2 and 3:

$$\delta(r)_{max} = \frac{c\delta(z)_{max}}{b \cdot H_{71}(z)} \tag{2.2}$$

with $b = AspectRatio = 9.5$

$$\delta(\theta)_{max} = 206265'' \frac{\delta(r)_{max}}{h_{71}^{-1}Mpc} \cdot (\frac{D_\theta}{h_{71}^{-1}Mpc})^{-1} \tag{2.3}$$

where D_θ is angular diameter distance.
Considering the center of the X-ray emission as the center of the groups, we selected groups members which lie within our redshift and angular limits (equation 4 and equation 5).

$$|z - z_{group}| < \delta(z)_{max} \tag{2.4}$$

$$\delta(\theta) < \delta(\theta)_{max} \tag{2.5}$$

We recompute the observed velocity dispersion of the groups, $\sigma(v)_{obs}$ using the "gapper" estimator method which gives more accurate measurement of velocity dispersion for small size groups (Beers, Flynn & Gebhardt 1990; Wilman et al. 2005) in comparison to the usual formula for standard deviation, $\sigma^2 = \langle v^2 \rangle - \langle v \rangle^2$. According to the formula

$$\sigma(v)_{obs} = 1.135c \times \frac{\sqrt{\pi}}{N(N-1)} \sum_{i=1}^{n-1} \omega_i g_i \tag{2.6}$$

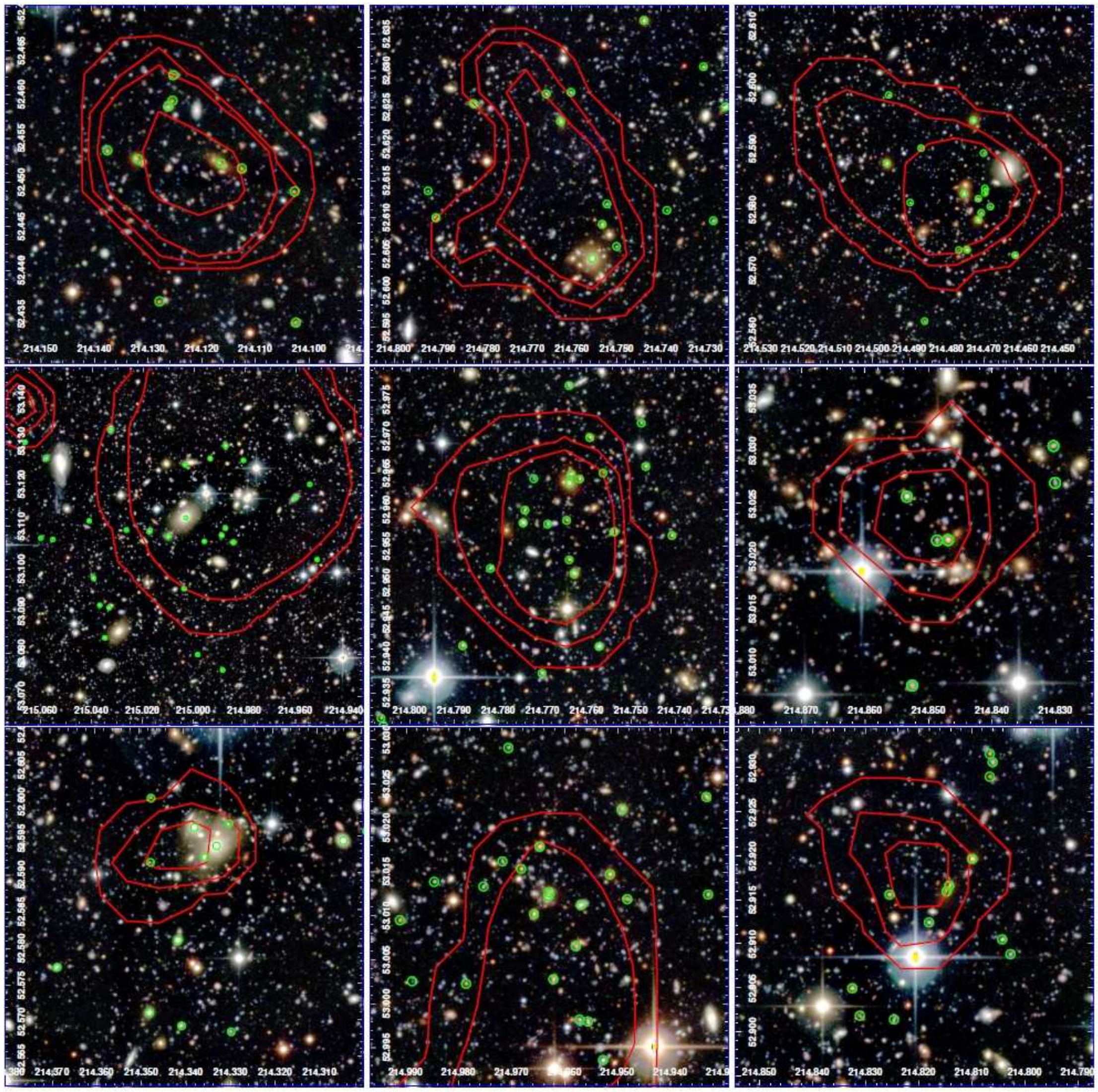

Figure 2.6: CFHTLS D3 RGB images of X-ray galaxy groups using g', r' and i' bands of the groups with contours indicating levels of X-ray emission (in red) and spectroscopic members of the groups inside the virial radius estimated from X-rays. From upper left to lower right, the group IDs are: EGSXG J1416.4+5227, EGSXG J1419.0+5236, EGSXG J1417.9+5235, EGSXG J1420.0+5306, EGSXG J1419.0+5257, EGSXG J1419.4+5301, EGSXG J1417.3+5235, EGSXG J1419.8+5300, and EGSXG J1419.2+5255. The horizontal and vertical axes show the right ascension and declination respectively.

where $w_i = i(N-i)$, $g_i = z_{i+1} - z_i$ and N is the total number of spectroscopic members. In this way we measure the velocity dispersion using the line-of-sight velocity gaps where the velocities have been sorted into ascending order. The factor 1.135 corrects for the 2σ clipping of the Gaussian velocity distribution. We then consider the r-band luminosity-weighted centroid in projected space as the center of the group and the mean redshift of the galaxy members as the group redshifts and again find the galaxy members. We repeat the entire process until we obtain a stable membership solution. For all the groups, we reach such a stable membership after 2 iterations. At the end, we calculated the rest-frame and intrinsic velocity dispersion according to

$$\sigma(v)_{rest} = \frac{\sigma(v)_{obs}}{1+z} \tag{2.7}$$

$$\langle \Delta(v) \rangle^2 = \frac{1}{N} \sum_{i=1}^{N} \Delta(v)_i^2 \tag{2.8}$$

$$\sigma(v)_{intr}^2 = \sigma(v)_{rest}^2 - \langle \Delta(v) \rangle^2 \tag{2.9}$$

The intrinsic velocity dispersion, $\sigma(v)_{intr}$, is computed by removing the effect of measurement errors of component galaxies from the rest-frame velocity dispersion, $\sigma(v)_{rest}$ (equations 8 and 9). Then we calculated errors for our velocity dispersions using the Jackknife technique (Efron 1982). The error is $[\frac{N}{N-1}\sum(\delta_i^2)]^{\frac{1}{2}}$ where $\delta_i = \sigma(v)_{obs} - \sigma(v)_{obs,excluding\, i_{th}\, member}$. We then applied two different optical and X-ray based cuts for the radius used to select member galaxies. Using $\sigma(v)_{intrinsic}$ derived from member galaxies after iterating, we computed r_{200} for the optical cut as Carlberg, Yee & Ellingson (1997):

$$r_{200} = \frac{\sqrt{3}\sigma_{intr}}{10H(z)} \tag{2.10}$$

Where

$$H(z) = H_0 E(z) \tag{2.11}$$

For the X-ray defined radial cut, we used $r_{200,x}$ from the main catalog(see § 4). We then calculated the intrinsic velocity dispersion for all groups based on equations 6, 7, 8 and 9 for the members with the optical and X-ray based radial cuts. In Figure 2.6 we present a gallery of RGB images of the X-ray galaxy groups within the D3 field of CFHTLS.

In the second way, we pick the spectroscopic galaxies with positions within the $r_{200,x}$ of the X-ray centers and their redshifts match to $\Delta z_1 = 0.001 \times (1+z_G)$ and $\Delta z_2 = 0.0025 \times (1+z_G)$ which corresponds to typical minimum and maximum velocity dispersions of a group. Table 2 shows a sample of spectroscopic galaxy members based on $0.0025 \times (1+z_G)$ selection. Then we computed intrinsic velocity dispersions for the member galaxies based on the X-ray virial radius and two different redshift cuts (Δz_1 & Δz_2).

In all cases, we considered galaxy groups with more than 10 members when we use the “gapper”estimator to have a more relaible measurement of velocity dispersion(e.g. Zabludoff & Mulchaey 1998; Girardi & Mezzetti 2001). Figure 2.7 shows velocity dispersions of X-ray galaxy groups derived by “gapper”estimator method and from X-ray emission.

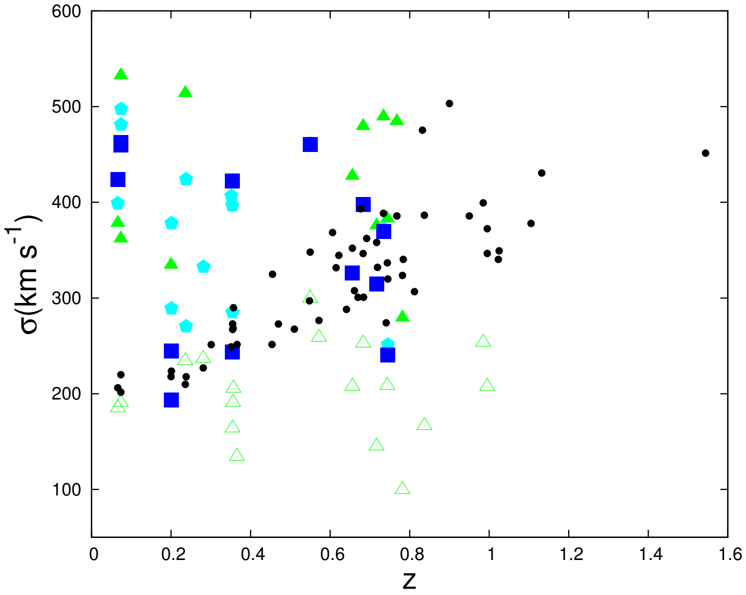

Figure 2.7: Velocity dispersion as a function of redshift. The black filled circles show the velocity dispersions estimated from X-ray luminosities using scaling relations for all the groups. The filled and empty triangles show velocity dispersions for the groups with Δz_2 and Δz_1 respectively. The pentagons show the velocity dispersion for the groups with optically determined radial cut after iterations and the squares show the velocity dispersion for the groups with X-ray radius cut after iterations.

2.5.1 The relation between X-ray luminosity and dynamical velocity dispersion

Figures 2.8 and 2.9 show the X-ray luminosity versus velocity dispersion for different methods. These plots include all the galaxy groups with Flag=1 and 2. We also plot the $L_x - \sigma$ relation (dashed line) expected from scaling relations obtained for a sample of groups with similar luminosities in the $0 < z < 1$ redshift range in COSMOS (Leauthaud et al. 2010).

Velocity dispersions can be biased to higher values for low mass systems when we select members based on large Δz as we may include outliers in our calculation and conversely can be biased to lower values for high mass systems if we select member galaxies within low Δz along the line of sight as we are then ignoring some parts of the group (Figure 2.8). Furthermore, tracking the groups while we use different Δz to choose member galaxies reveals an average systematics error $\sim$ 190 km/s.

Figure 2.9 shows the $L_x - \sigma$ relation for galaxy groups which members are selected based on two different radial cuts. It is obvious from Figure 2.9 that different radial cuts can cause a change in scatter of $L_x - \sigma$ relation but, in the case of high mass systems, there is no apparent change in scatter of this relation. In addition, low X-ray luminosity systems show significant deviations from the scaling relation in both X-ray and optically based radial cuts.

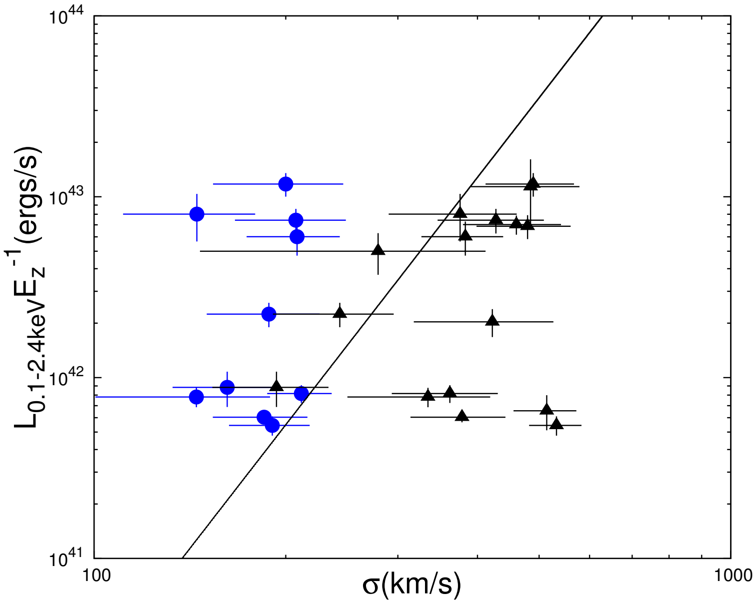

Figure 2.8: $L_X - \sigma$ relation for X-ray groups. The blue circles and the black triangles are corresponding to groups which members match to Δz_1 and Δz_2 respectively. The solid line show our expectation for $L_X - \sigma$ relation from scaling relations.

We looked at the quality flags, dynamical complexity and the X-ray compactness in comparison to the virial radius for the groups in order to study the group properties and their effects on the relation.

As we expect, Figures 2.10 and 2.11 illustrate galaxy groups with Flag=2 have significant deviations from the relation compared to galaxy groups with Flag=1 (similar to what Connelly et al. 2012 found for the intermediate redshift X-ray selected groups).

To search for substructure in our groups, we apply the Dressler-Shectman (DS; Dressler & Shectman 1988). We use the DS test as in Hou et al. (2012) which implement it for group size systems. In brief, we consider each individual galaxy in the group plus the N_{nn} nearest members to it with $N_{nn} = \sqrt{n}_{mem}$ and calculate mean velocity and velocity dispersion for them ($\bar{v}^i_{local}, \sigma^i_{local}$). Then we compute the deviations for each galaxy from the mean velocity ($\bar{v}$) and velocity dispersion (σ) of the whole group with n_{mem} galaxies:

$$\delta_i^2 = (\frac{N_{nn}+1}{\sigma^2})[(\bar{v}^i_{local} - \bar{v})^2 - (\sigma^i_{local} - \sigma)^2] \tag{2.12}$$

where $1 \leq i \leq n_{members}$. Then Δ statistics were computed using:

$$\Delta = \sum_{i=1} \delta_i \tag{2.13}$$

To identify substructure, we used a probability (P-values) threshold for the DS test so we run 10,000 Monte Carlo simulations for each group. In each Monte Carlo run, the

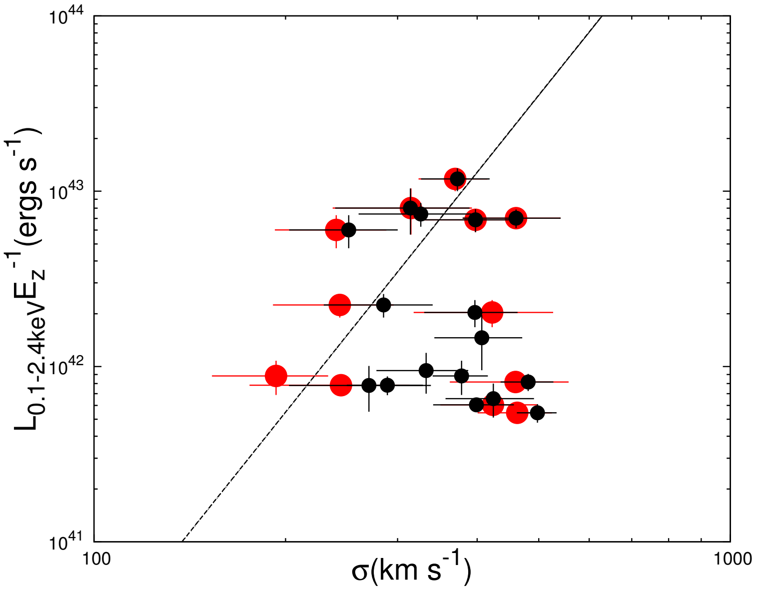

Figure 2.9: $L_X - \sigma$ relation for X-ray groups which members lie within a dynamically based virial radius (black circles) and X-ray based virial radius (red circles).

observed velocities are randomly shuffled and reassigned to member positions and $\Delta_{shuffled}$ is computed. The probabilities are given by

$$P = \sum(\Delta_{shuffled} > \Delta_{observed})/n_{shuffle} \tag{2.14}$$

$n_{shuffle}$ is the number of the Monte carlo simulations which in our case is 10,000. A system is then considered to have significant substructure with 99 percent confidence level when $P < 0.01$. In total, we found 2 galaxy groups of 17 in optically based radial cut groups and 1 group of 12 in X-ray based radial cut galaxy groups with significant substructure which are marked with stars in Figure 2.10 and 2.11.

Figure 2.12 shows the optical images for three galaxy groups which have the largest deviations from the scaling relation in Figure 2.10. All of them have Flag=1 and subtructure is not detected using the DS test. The two left images in Figure 2.12 have less than 10 members given an X-ray based virial radius cut and are not included in Figure 2.11. We compared the extension of X-ray emission to virial radius extracted from X-rays and optical velocity dispersion for galaxy groups. As Figure 2.13 shows there is a population of the group galaxies which the fraction of the extension of X-rays to virial radius is less than 20% in optically based radial cut and less than 15% in X-ray based radial cut. These populations are dominated by some galaxy groups with Flag=2 and two galaxy groups from left in Figure 2.12 with an over-luminous galaxy close to the X-ray center.

We explored the $L_x - \sigma$ relation in more detail for three of the groups with large deviations from the scaling relation (Figure 2.12). EGSXG J1418.3+5227 with $L_x = 1.08 \times 10^{42}$ erg s^{-1}, has $\Delta m_{12} = 2$ where Δm_{12} is the r-band magnitude difference between the first and the second brightest galaxy located in half of the virial radius of the group.

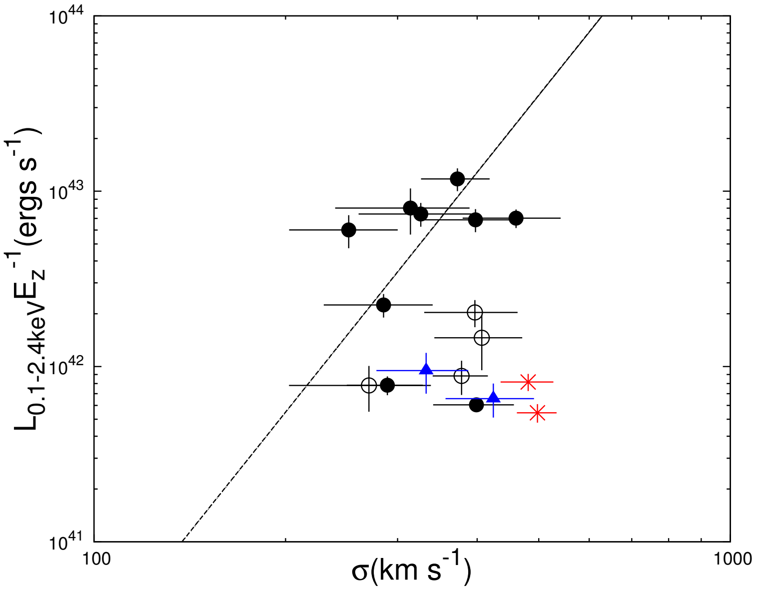

Figure 2.10: $L_X - \sigma$ relation for X-ray groups which members lie within a dynamically based virial radius. The red stars show groups which have substructure detected by DS test, blue triangles are the compact X-ray systems, and open circles show the groups with Flag=2. The solid line shows our expected $L_X - \sigma$ relation derived from scaling relations.

These conditions result in the classification of this group as a fossil galaxy group candidate (Jones et al. 2003). As fossil galaxy groups are believed to be the final result of galaxy merging in normal groups, we expect a sufficiently deep potential well and high X-ray luminosity for these systems (Ponman et al. 1994; Jones, Ponman & Forbes 2000). As a consequence, we expect fossil groups be more X-ray luminous than normal groups for a given velocity dispersion (Khosroshahi, Ponman & Jones 2007) but instead we find the opposite. Moreover, Osmond & Ponman (2004) applied a radius of 60 kpc as a threshold for detectable X-ray emission to separate galactic haloes from group-scale haloes using different studies of bright isolated galaxies (O'Sullivan, Ponman & Collins 2003; O'Sullivan & Ponman 2004). The radius of detectable X-ray emission (at which the group emission fell to the background level) for EGSXG J1418.3+5227 is more than this threshold and about 95 kpc. However, the nature of this X-ray extended source with such unexpectedly low X-ray emission compared to the velocity dispersion is still a matter of interest.

In the cases of EGSXG J1417.3+5235 and EGSXG J1417.7+5241, both having large numbers of spectroscopic member galaxies, the estimation of velocity dispersion can't be the main uncertainty. EGSXG J1417.3+5235 satisfies all the three criteria (population, isolation and compactness) for a compact group (Hickson 1982). For compactness criterion, Hickson (1982) establish that the sum of member galaxies' magnitude averaged over the smallest circle containing the cores of most luminous galaxies in a compact group should be less than 26 in POSS-I E band, $\mu_E < 26$ mag arcsec^{-2}. He use POSS-I E band for the cut on the surface brightness of his local groups which roughly corresponds to r-band

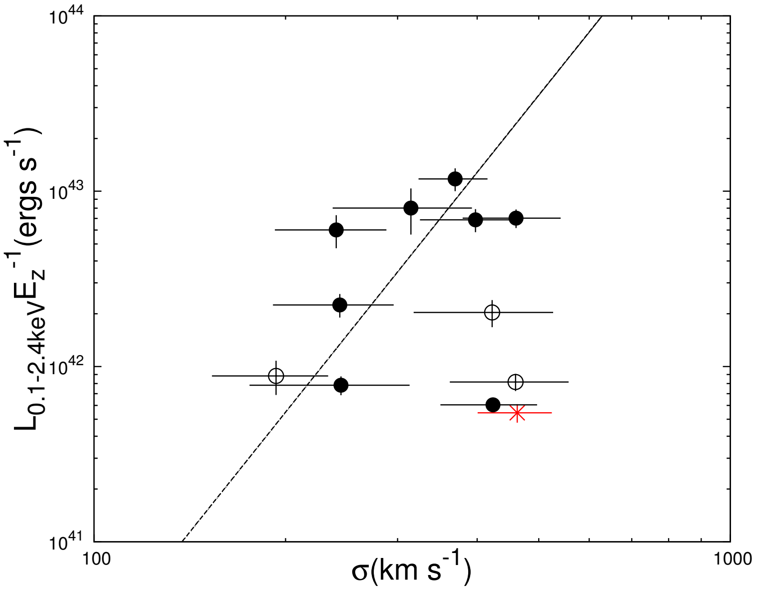

Figure 2.11: $L_X - \sigma$ relation for X-ray groups given a raidal cut based on X-ray. The red stars show groups which have substructure detected by DS test, blue triangles are the compact X-ray systems and open circles show the groups with Flag=2. The solid line show our expectation for $L_X - \sigma$ relation from scaling relations.

(e.g. Díaz-Giménez et al. 2012). As all his compact groups are in the local universe, we should apply the k-correction to the r-band magnitude of the member galaxies of EGSXG J1417.3+5235 at z=0.236. All galaxies which we use for computing surface brightness are on the red-sequence, therefore, we calculate the k-correction to the r-band magnitude using the stellar population model of Maraston et al. (2009) for red galaxies. Using the k-corrected magnitudes, this group satisfies compactness criterion. It also has high concentration in X-ray emission (Figure 2.13), while having low mass, so leading to steep X-ray profile. However, Helsdon & Ponman (2000) find the loose and compact local groups lie in a similar position on the $L_X - \sigma$ relation. Figure 2.15 shows the histogram of velocity distribution of member galaxies and the expected Gaussian distribution from scaling relations for EGSXG J1417.3+5235.

Excluding these three groups, the Flag=2 groups and also the group with substructures, the $L_x - \sigma$ relation of our sample is consistent with the $L_x - \sigma$ relation expected from scaling relations obtained from COSMOS (Leauthaud et al. 2010).

2.5.2 X-ray mass vs. Dynamical mass

We also estimated dynamical mass for the galaxy groups using r_{200} (eq. 10) and the intrinsic velocity dispersion as in Balogh et al. (2006) and Carlberg et al. (1999):

$$M_{dyn} = \frac{3}{G}\sigma^2 r_{200} \tag{2.15}$$

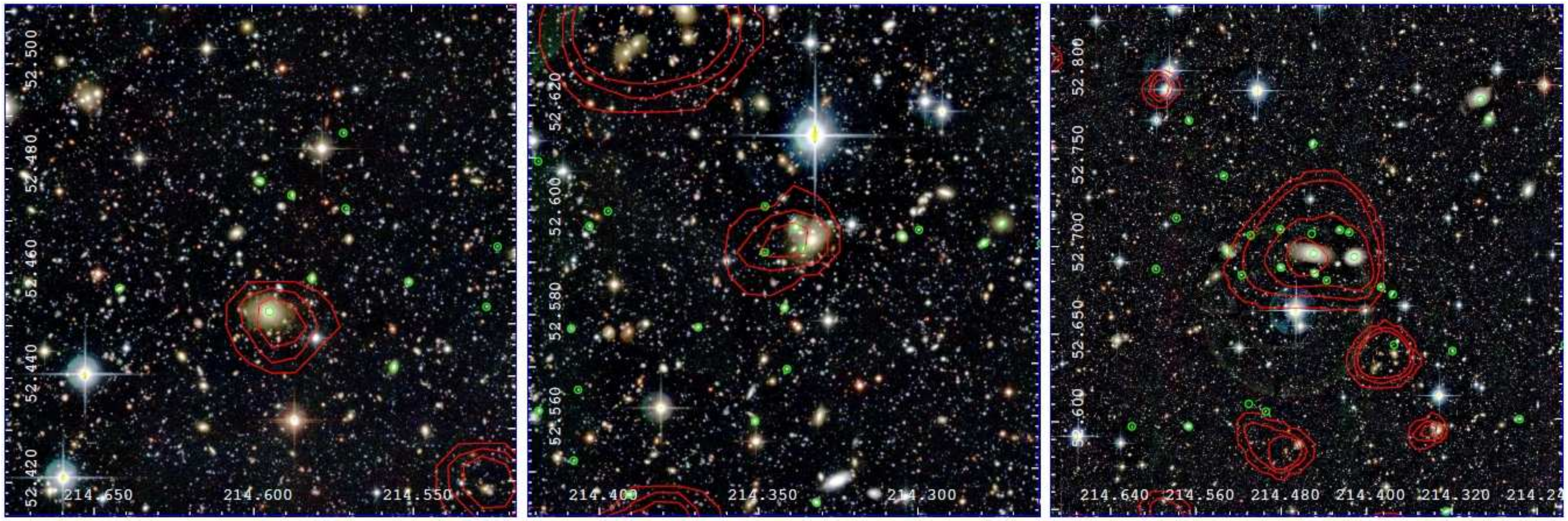

Figure 2.12: CFHTLS D3 RGB images of X-ray galaxy groups using g', r' and i' bands of the groups with contours indicating levels of X-ray emission (in red) and spectroscopic members (in green). The groups ID from left to right are: EGSXG J1418.3+5227, EGSXG J1417.3+5235 and EGSXG J1417.7+5241.

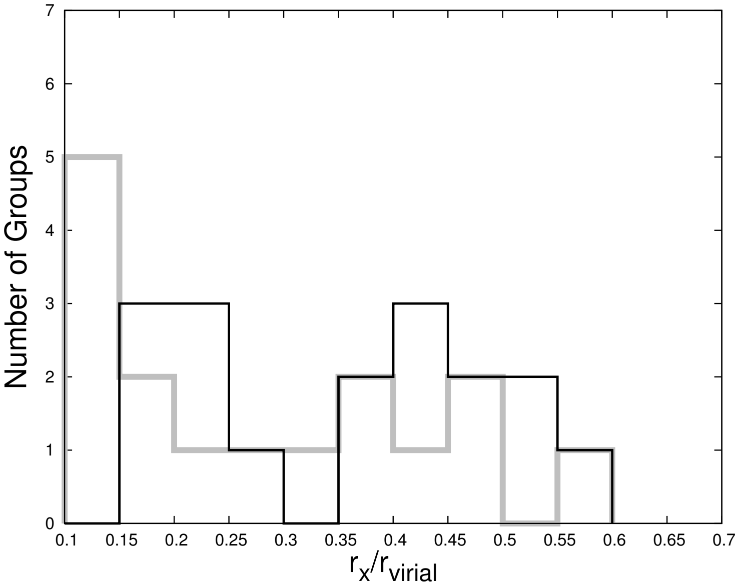

Figure 2.13: Fraction of X-ray extent to virial radius for an X-ray based virial radius (black line) and optically based virial radius (grey line).

As we expect from the $L_x - \sigma$ relation of the groups (Figures 2.10 and 2.11) we find much better agreement between dynamical mass and X-ray mass for high mass systems (Figure 2.15). For low mass systems with low quality flag (Flag=2) and substructure, the disagreement between these two masses is more substantial. In addition, the errors on dynamical mass are increased in X-ray based r_{200} as the groups have less members in this case compared to that of an optically based r_{200}.

2.6 Comparison to optical groups

The optical group catalog is derived from DEEP2 DR4 dataset using the Voronoi-Delaunay method (VDM) group finder (Gerke et al. 2012) and includes groups in all DEEP2 fields. It yields 1165 groups with more than two observed members in the EGS field. We look at the distribution of redshifts for our X-ray and optically selected groups and in Figure 2.16 show the normalized distribution of redshifts for both samples. X-ray groups are preferentially found at z>0.6, compared to optical groups, but in general the two distributions are similar. We also compared velocity dispersions of both samples. In order to have a reliable comparison we take into account only optical groups with our X-ray detection limit. Figure 2.17 shows the distribution of rest-frame velocity dispersion for galaxy groups with more than five members. For X-ray galaxy groups, we plot both velocity dispersions derived from X-ray properties and gapper estimator method. Velocity dispersion of optical groups are the observed velocity dispersion derived using the gapper algorithm. We converted them to rest-frame velocity using Eq. 7 for the comparison.

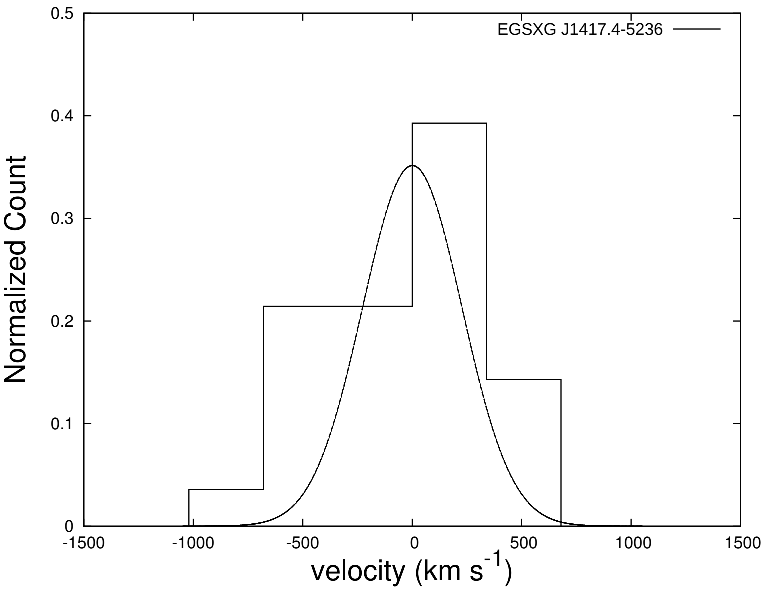

Figure 2.14: The solid line shows the histogram of velocity distribution of EGSXG J1417.3+5235. The dashed Gaussian curve is the expected velocity distribution from scaling relation for this group.

We searched for the high velocity tail of the distribution of the optical group velocity dispersion in the X-ray data. This high velocity tail arises from galaxy groups with less than ten members which are actually part of a bigger group or on the edge of the X-ray coverage of EGS. Ignoring this tail, in general these distributions are also similar.

2.7 Summary and Discussion

We have searched for X-ray extended sources in AEGIS. We identified X-ray galaxy groups corresponding to extended X-ray emissions and presented the galaxy groups catalog. The catalog is reaching fluxes of 10^{-15} ergs s^{-1} cm^{-2} with 52 systems detected by Chandra. Previously Chandra catalogs at such depths contain half a dozen objects per field (Giacconi et al. 2002; Bauer et al. 2002). The DEEP2 and DEEP3 redshift surveys which provide the most complete sample at intermediate redshift and the largest accurate data sets at $z \sim 1$, combined with deep X-ray imaging from Chandra in EGS field, bring a deep study of galaxy groups to a new level. Spectroscopic member galaxies are selected by applying different cuts: two X-ray based and optically based virial radius and two cuts along the line of sight. We examined the $L_x - \sigma$ relation for each cut and discussed the effects of them on the relation. We explored substructure in the groups by applying the Dressler-Shectman test and discussed its effect on the overestimation of velocity dispersion. We also looked at the compactness of the X-ray emission of the groups and its effect on the scaling relation.

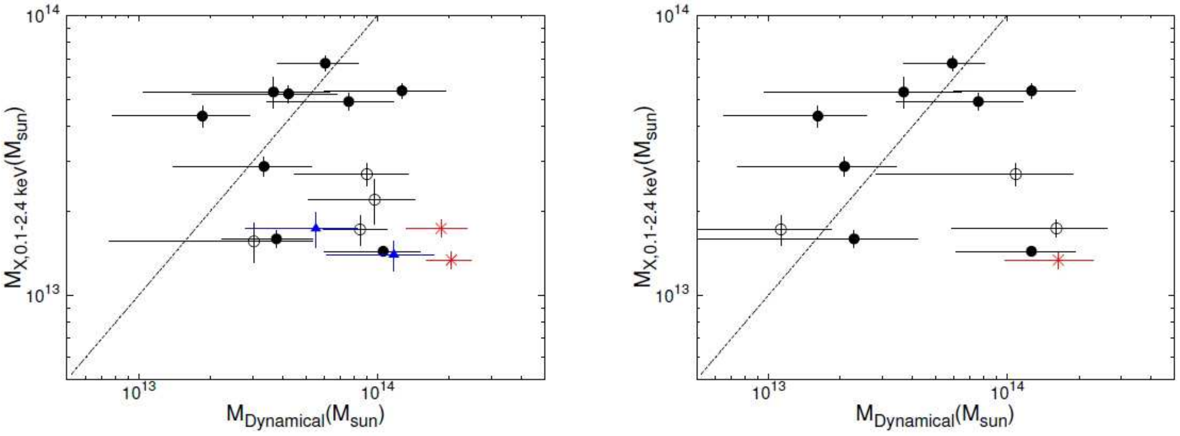

Figure 2.15: X-ray mass versus dynamical mass for the X-ray galaxy groups. Left plot shows the galaxy groups with member selected within velocity dispersion based r_{200}. The right one shows galaxy groups with members within X-ray based r_{200}. The red stars show groups which have substructure detected by DS test, blue triangles are the compact X-ray systems and open circles show the groups with Flag=2. The dashed line is the one-to-one relation.

A comparison between dynamical mass and X-ray mass of the groups is also done. Finally, X-ray galaxy groups are compared with optical galaxy groups which are identified from VDM groups. Our results show:
1) Our detection of a high-z group illustrates that megasecond Chandra exposures are required for detecting such objects in the volume of deep fields. Smaller exposures, as Pierre et al. (2012), only yields a marginal detection. 2) For a sample of groups with a wide range of X-ray luminosities, choise of a constant Δz for member selection can cause a large scatter in $L_x - \sigma$ relation. 3) Choice of X-ray based virial radius or optically based virial radius does not have significant effect on the scatter around $L_x - \sigma$ relation for groups with high X-ray luminosities. 4) Substructure in groups can inflate velocity dispersion as outliers are also included in galaxies with dynamical complexity. 5) We find a compact group at z=0.24 with a concentrated X-ray emission with high velocity dispersion in comparison to X-ray luminosity. 6) X-ray galaxy groups and optical galaxy groups from VDM are nearly similar in both redshift and velocity dispersion distributions.

We would like to thank David Wilman, Annie Hou and Antonis Georgakakis for helpful discussions about the dynamical properties and AGN contamination of X-ray groups. We also thank Felicia Ziparo and Steve Willner for useful comments on the manuscript. This project has been supported by the DLR grant 50OR1013 to MPE. MT acknowledges the support by World Premier International Research Center Initiative (WPI Initiative), MEXT, Japan and by KAKENHI No. 23740144. This work was also supported in part by National Science Foundation grants AST 00-71198, 05-07483, 08-08133 to UCSC and AST 00-71048, 05-07428, and 08-07630 to UCB and AST 08-06732 to U. Pittsburgh.

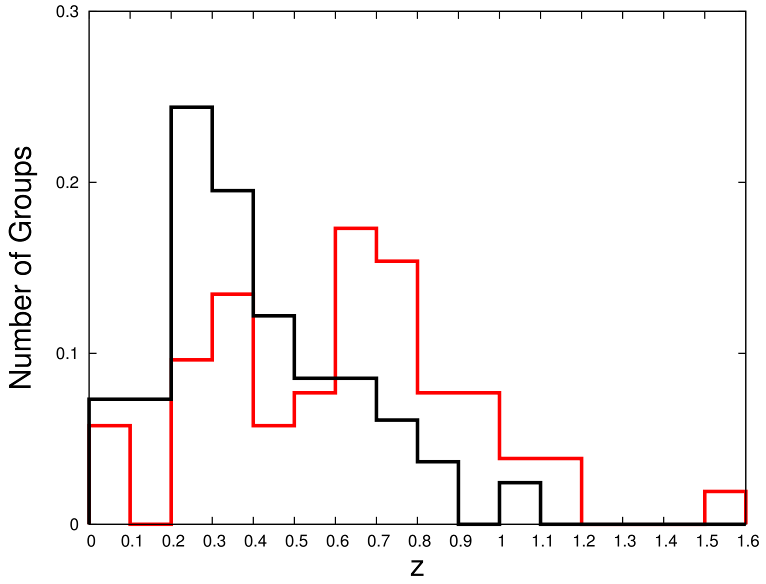

Figure 2.16: Normalized distribution of redshift for X-ray galaxy groups (in red) and optical galaxy groups (in black) inside of our flux detection limits in EGS.

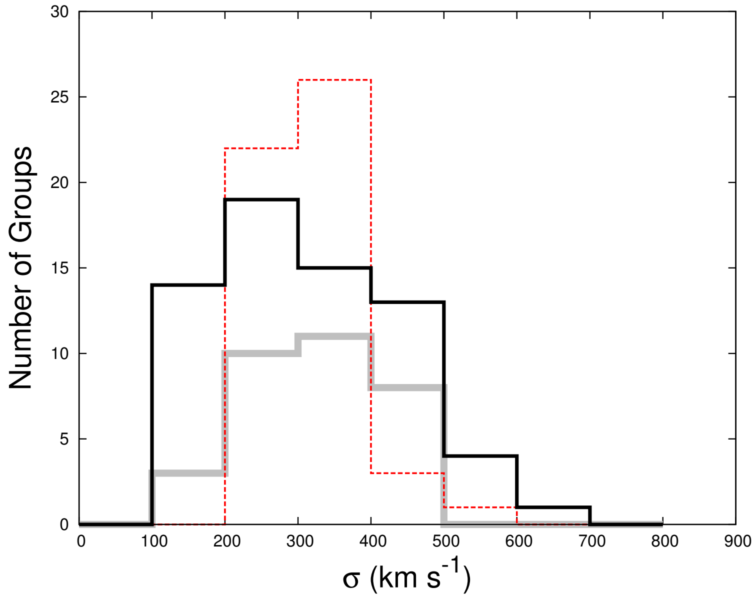

Figure 2.17: Distribution of velocity dispersion for optical and X-ray galaxy groups. The black line shows the distributions of velocity dispersion of optical VDM groups. The dashed red and thick grey lines are corresponding to distributions of velocity dispersion estimated from X-rays and dynamical velocity dispersion for X-rays groups.

Table 2.1: A sample of group member galaxies.

Group ID	RA	Dec.	z
EGSXG J1417.5+5238	214.38009	52.63223	0.7199
EGSXG J1417.5+5238	214.36919	52.62006	0.7201
EGSXG J1417.5+5238	214.36626	52.65201	0.7157
EGSXG J1417.5+5238	214.41671	52.62889	0.7173
EGSXG J1417.5+5238	214.40832	52.62752	0.7193
EGSXG J1417.5+5238	214.40229	52.62471	0.7170
EGSXG J1417.5+5238	214.40131	52.63039	0.7168
EGSXG J1417.5+5238	214.39906	52.64248	0.7151
EGSXG J1417.5+5238	214.39653	52.64163	0.7161
EGSXG J1417.5+5238	214.39236	52.62690	0.7167
EGSXG J1417.5+5238	214.39221	52.63439	0.7156
EGSXG J1417.5+5238	214.38562	52.63828	0.7168
EGSXG J1417.5+5238	214.34541	52.63622	0.7167
EGSXG J1419.6+5251	214.90556	52.85547	0.6675
EGSXG J1419.6+5251	214.94009	52.85377	0.6713
EGSXG J1419.6+5251	214.92459	52.85621	0.6711
EGSXG J1419.6+5251	214.91483	52.84952	0.6692
EGSXG J1419.6+5251	214.90534	52.85083	0.6702
EGSXG J1419.6+5251	214.90136	52.85234	0.6681

Table 2.2: AEGIS X-ray Galaxy Groups

ID	RA	DEC	z	Flux $[10^{-14} erg cm^{-2} s^{-1}]$	L_X $[10^{42} erg s^{-1}]$	M_{200} $[10^{13} M_\odot]$	r_{200} [arcmin]	Flag	N(z)	Flux Significance	σ_X
EGSXG J1414.8+5209	213.71657	52.16481	0.455	0.50±0.08	6.35±0.98	4.61±0.44	1.8	4	3	6.50	325
EGSXG J1414.8+5212	213.71946	52.21343	0.301	0.38±0.09	1.76±0.43	2.32±0.35	2.0	2	3	4.11	251
EGSXG J1415.0+5204	213.76555	52.07685	0.074	2.77±0.33	0.56±0.07	1.34±0.10	5.7	1	28	8.49	202
EGSXG J1415.4+5220	213.85106	52.34112	0.074	4.22±0.46	0.84±0.09	1.73±0.12	6.2	2	19	9.19	220
EGSXG J1415.6+5221	213.91018	52.36540	0.622	0.33±0.07	9.20±1.94	5.01±0.65	1.5	4	9	4.73	345
EGSXG J1416.1+5224	214.02791	52.41598	0.571	0.13±0.07	3.19±1.67	2.67±0.82	1.3	1	6	1.92	277
EGSXG J1416.2+5205	214.07123	52.09987	0.832	0.91±0.13	46.87±6.79	11.68±1.06	1.6	2	1	6.90	475
EGSXG J1416.3+5213	214.07507	52.22752	0.641	0.12±0.04	4.02±1.46	2.90±0.64	1.2	4	7	2.76	288
EGSXG J1416.3+5229	214.07862	52.49943	0.356	0.36±0.08	2.46±0.55	2.74±0.38	1.8	2	8	4.44	268
EGSXG J1416.3+5214	214.08759	52.23544	0.366	0.25±0.06	1.83±0.43	2.25±0.32	1.7	4	8	4.27	251
EGSXG J1416.4+5227	214.12227	52.45173	0.837	0.30±0.06	17.81±3.26	6.26±0.71	1.3	1	7	5.46	386
EGSXG J1416.6+5228	214.15991	52.47882	0.812	0.09±0.04	5.94±2.34	3.17±0.75	1.1	3	5	2.54	307
EGSXG J1416.6+5222	214.17417	52.37189	0.510	0.15±0.04	2.63±0.79	2.50±0.45	1.4	2	5	3.35	267
EGSXG J1416.6+5229	214.17480	52.48355	0.238	0.33±0.09	0.87±0.23	1.56±0.25	2.1	4	6	3.82	218
EGSXG J1416.8+5210	214.20403	52.17700	0.900	1.04±0.15	63.55±8.95	13.33±1.17	1.6	3	0	7.10	503
EGSXG J1417.0+5226	214.25416	52.44758	1.023	0.08±0.02	10.89±2.90	3.85±0.63	1.0	1	5	3.75	340
EGSXG J1417.2+5215	214.31665	52.25140	0.470	0.20±0.05	2.82±0.72	2.71±0.42	1.5	3	0	3.95	273
EGSXG J1417.3+5235	214.34115	52.59349	0.236	0.27±0.05	0.73±0.14	1.39±0.17	2.1	1	9	5.07	210
EGSXG J1417.4+5237	214.37150	52.63047	0.355	0.39±0.05	2.66±0.34	2.88±0.23	1.9	1	14	7.72	273
EGSXG J1417.5+5238	214.38305	52.63655	0.717	0.29±0.06	11.61±2.36	5.32±0.67	1.4	2	13	4.93	358
EGSXG J1417.5+5232	214.38819	52.53527	0.985	0.25±0.03	22.59±2.87	6.35±0.51	1.2	2	6	7.87	399
EGSXG J1417.7+5228	214.44405	52.47140	0.995	0.16±0.04	16.36±4.08	5.12±0.79	1.1	1	5	4.01	372
EGSXG J1417.7+5241	214.44751	52.69237	0.066	3.92±0.24	0.62±0.04	1.43±0.06	6.5	1	23	16.27	206
EGSXG J1417.9+5226	214.47592	52.43701	0.684	0.13±0.03	5.04±1.30	3.22±0.51	1.2	4	3	3.88	301
EGSXG J1417.9+5235	214.48176	52.58382	0.683	0.27±0.03	9.76±1.04	4.92±0.33	1.4	1	11	9.42	346
EGSXG J1417.9+5225	214.48632	52.42462	0.995	0.10±0.03	11.68±3.58	4.13±0.77	1.0	3	5	3.26	347
EGSXG J1417.9+5231	214.49046	52.52231	0.661	0.16±0.03	5.52±0.93	3.49±0.37	1.3	1	6	5.91	308
EGSXG J1418.0+5222	214.50330	52.36890	0.950	0.22±0.04	18.79±3.81	5.83±0.73	1.2	3	0	4.94	386
EGSXG J1418.1+5225	214.52697	52.41944	0.548	0.21±0.05	4.40±0.96	3.35±0.45	1.4	1	3	4.59	297
EGSXG J1418.3+5227	214.59199	52.45022	0.281	0.27±0.06	1.08±0.25	1.73±0.24	1.9	2	7	4.36	227
EGSXG J1418.5+5252	214.62561	52.86899	1.025	0.10±0.03	12.31±3.83	4.15±0.79	1.0	2	1	3.21	349
EGSXG J1418.8+5248	214.70147	52.80696	0.741	0.06±0.02	3.37±1.07	2.36±0.45	1.0	1	4	3.15	274
EGSXG J1419.0+5236	214.76363	52.61357	0.550	0.45±0.04	9.25±0.85	5.38±0.31	1.7	1	11	10.86	348
EGSXG J1419.0+5257	214.76810	52.95626	0.656	0.32±0.04	10.37±1.15	5.24±0.36	1.5	1	16	9.02	352
EGSXG J1419.2+5255	214.82121	52.91803	0.782	0.14±0.02	7.51±1.29	3.79±0.41	1.2	3	10	5.80	324
EGSXG J1419.4+5301	214.85110	53.02358	0.745	0.15±0.03	6.95±1.52	3.74±0.50	1.2	1	6	4.57	320
EGSXG J1419.6+5251	214.91782	52.85103	0.670	0.14±0.03	4.99±1.24	3.24±0.50	1.2	1	6	4.01	301
EGSXG J1419.7+5246	214.93393	52.77711	0.784	0.18±0.06	9.53±3.10	4.41±0.87	1.2	1	6	3.07	340
EGSXG J1419.8+5300	214.96203	53.01138	0.744	0.19±0.03	8.85±1.29	4.36±0.40	1.3	1	14	6.87	337
EGSXG J1420.0+5258	215.00399	52.97709	0.454	0.15±0.03	1.91±0.39	2.14±0.27	1.4	1	7	4.95	251
EGSXG J1420.0+5306	215.00462	53.11241	0.200	0.48±0.05	0.85±0.10	1.59±0.11	2.5	2	19	8.93	218
EGSXG J1420.2+5308	215.06885	53.13864	1.105	0.13±0.04	18.62±5.14	5.03±0.85	1.0	2	3	3.63	378
EGSXG J1420.4+5311	215.12046	53.19035	1.544	0.18±0.04	54.10±13.11	6.80±1.01	0.9	2	3	4.13	451
EGSXG J1420.5+5308	215.14733	53.13952	0.734	0.41±0.04	17.19±1.75	6.74±0.43	1.5	1	17	9.84	388
EGSXG J1420.8+5306	215.20148	53.10867	0.355	0.35±0.05	2.41±0.36	2.71±0.25	1.8	2	14	6.73	267
EGSXG J1421.3+5308	215.32631	53.14764	0.351	0.26±0.08	1.72±0.51	2.19±0.39	1.7	2	7	3.40	249
EGSXG J1421.4+5308	215.34650	53.13477	0.201	0.54±0.11	0.97±0.20	1.72±0.21	2.5	2	15	4.96	224
EGSXG J1421.5+5302	215.38609	53.04315	0.677	0.53±0.18	17.62±6.11	7.22±1.52	1.6	2	5	2.88	393
EGSXG J1422.0+5328	215.51144	53.47268	0.357	0.51±0.19	3.54±1.30	3.46±0.77	2.0	1	6	2.71	290
EGSXG J1422.6+5321	215.66020	53.36037	0.768	0.36±0.10	16.95±4.73	6.47±1.10	1.4	1	9	3.58	388
EGSXG J1423.0+5326	215.76783	53.44306	0.615	0.28±0.11	7.66±2.94	4.49±1.04	1.5	2	3	2.60	332
EGSXG J1423.6+5328	215.92348	53.47078	1.132	0.27±0.05	34.88±6.68	7.34±0.87	1.2	1	5	5.22	431

Chapter 3

The evolution of star formation activity in galaxy groups

G.Erfanianfar , P. Popesso, A. Finoguenov, S. Wuyts, D. Wilman, A. Biviano, et al.

Submitted to MNRAS

Abstract

In this paper, we study the evolution of the total star formation activity, total stellar mass and halo occupation distribution (HOD) in massive halos since z$\sim$1.1 by using one of the largest X-ray selected sample of galaxy groups with secure spectroscopic identification in the major blank field surveys (ECDFS, CDFN, COSMOS, AEGIS). We make extensive use of mock catalogs to check the robustness of our method in determining the group velocity dispersion and membership, and check also the possible biases induced by the spectroscopic incompleteness of the surveys used in our analysis. We show that for a robust measurement of the group velocity dispersion and group membership a first guess of the velocity dispersion is essential. We provide an accurate measurement of SFR for the bulk of the star-forming galaxies using very deep mid-infrared Spitzer MIPS and far-infrared Herschel PACS observations. For undetected IR sources, we provide a well-calibrated SFR from SED fitting.

We observe a clear evolution in the level of star formation activity in galaxy groups. The total star formation activity in high redshift groups (0.5<z<1.1) is higher with respect to the low redshift (0.15<z<0.5) sample at any mass by 0.8 ± 0.12 dex. A milder difference (0.35 ± 0.1 dex) is observed between the [0.15-0.5] redshift bin and the groups at $z \sim 0$. This evolution seems to be faster for more massive halos ($\mathrm{M}_{200} > 3 \times 10^{13} M_{\odot}$) than the one observed in the whole galaxy population. The HOD and the total stellar mass-M_{200} relations are consistent with a linear relation in any redshift bin in the M_{200} range considered in our analysis. We do not observe any evolution in the HOD since $z \sim 1.1$. Similarly we do not observe any evolution in the relation between the total stellar mass in groups and the total mass. The picture emerging from our findings is that massive groups of $M_{200} \sim 10^{13-14} M_{\odot}$ at z >0.5 have already accreted the same amount of mass and have

the same number of galaxies as the low redshift counterparts. This implies that the most evident evolution of the galaxy population in the most massive systems is in terms of the quenching of their star formation activity since z∼1.1.

3.1 Introduction

One of the most fundamental correlations between the properties of galaxies in the local Universe is the so-called morphology-density relation (Dressler 1980; Davis & Geller 1976). A plethora of studies utilizing multi-wavelength tracers of activity have shown that late type star-forming galaxies favour low density regimes in the local Universe (e.g. Gómez et al. 2003; Blanton et al. 2005; Hogg et al. 2004; Lewis et al. 2002). In particular, the cores of massive galaxy clusters are full of massive spheroids that are dominated by old stellar populations. A variety of physical processes might be effective in suppressing star formation and affecting the morphology of cluster and group galaxies. Two big families of such processes can be identified: (i) interactions with other cluster members and/or with the cluster potential and (ii) interactions with the hot gas that permeates massive galaxy systems. In the current standard paradigm for structure formation, dark matter collapses into halos in a bottom-up fashion: small objects form first and subsequently merge into progressively larger systems. In this context, galaxy groups are the building blocks of galaxy clusters. Galaxy groups have at any epoch a volume density orders of magnitude higher than those of massive clusters, which represents the rare and extreme specimen at the high mass end of the dark halo mass function (Jenkins et al. 2001). This is confirmed by the observational evidence that groups are the most common environment of galaxies in the present day universe, containing 50%-70% of the galaxy population (Geller & Huchra 1983; Eke et al. 2005). This naturally implies that processes taking place in the group environment can have a significant impact on the evolution of the galaxy population as a whole.

The main debate now centers on the role of galaxy "internal" versus "external" processes as driving mechanisms of the galaxy evolution, or, according to an old-fashion approach, the “nature” versus “nurture” scenario. In the current paradigm of galaxy formation the “internal” processes are mainly linked to the co-evolution of the host galaxy and its central black hole (Di Matteo, Springel & Hernquist 2005; Croton et al. 2006; Hopkins et al. 2006, Delucia et al. 2012). However, as pointed out by Delucia et al. 2012, the nature versus nurture dichotomy is an ill-posed problem. In the current paradigm of galaxy formation these physical internal and external processes are coupled with a history bias that is an integral part of the hierarchical structure formation of cosmic structure (Delucia et al. 2012, Cooper et al. 2010). Wilman et al. (2013) have demonstrated that halos in overdense regions statistically form earlier and merge more rapidly than halos in regions of lower density (Gao et al. 2004). This differential evolution leaves a trace on the observable properties of galaxies that inhabit different regions at any cosmic epoch (Delucia et al. 2012). This aspect makes the interpretation of the observational evidences even more difficult. In fact, binning galaxies according to their stellar mass does not suffice to disentangle the role of nature and nurture. For instance, two galaxies of identical mass at some cosmic epoch can end up having different stellar masses if one of them falls on to a cluster and the other remains in a region of average density. An important attempt to investigate from the observational point of view the inter-relationships between stellar mass, star-formation rate and environment comes from Peng et al. (2010) in the SDSS, zCOSMOS surveys. This study shows that a) two distinct processes, mass (internal) quenching and environment (external) quenching are both operating since z∼1, b) environment-quenching occurs as large-scale structure develops and is more effective on satellite galaxies, c) mass-quenching is more efficient for central and generally more massive galaxies. The limit of this analysis is mainly in the definition of the environment that relies on the local galaxy density, which is only a poor proxy of the DM halo mass.

In the last decade a lot of effort has been devoted to the study of high redshift groups to investigate the possibility of a differential evolution of group galaxies with respect to field galaxies. A big step forward was done thanks to the advent of very deep multiwavelength surveys conducted on several blank fields, such as the Great Observatories Origin Deep Survey -South and -North (GOODS-S and GOODS-N, respectively), the Extended Chandra Deep Field South (ECDFS), the Cosmic Evolution Survey (COSMOS) and the All-wavelength Extended Groth strip International Survey (AEGIS). Those surveys combine deep photometric (from the X-rays to the far-infrared wavelengths) and spectroscopic (down to $i_{AB} \sim 24$ mag and b $\sim$ 25 mag) observations over relatively large areas to lead, for the first time, to the construction of statistically significant samples of groups up to to high redshift (z∼1.3-1.6, e.g. Finoguenov et al. 2010 and Bielby et al. 2010). In this context, the main outcome of these surveys is that group galaxies show a much faster evolution with respect to the field galaxies. For instance, the formation of the galaxy red sequence, which leads to the local dichotomy between red and blue galaxies, happens earlier in groups than in the field especially at high stellar masses (Iovino et al. 2010; Kovač et al. 2010b; Cooper et al. 2007; Wilman et al. 2009; Wilman & Erwin 2012). It seems also that group galaxies undergo a substantial morphological transformation. Indeed, groups at z∼1 host a transient population of "red spirals" which is not observed in the field (Jeltema et al. 2007; Tran et al. 2008; Balogh et al. 2009; Wolf et al. 2009; Mei et al. 2012).

Most analyses so far have concentrated on comparisons of the star-forming properties of the group galaxy population as a whole with those of field galaxies. However, it is also important to assess the dependence (if any) of the star-forming properties of group galaxies on their system global properties, such as the mass, velocity dispersion and X-ray luminosity of the groups at different epochs to understand if and how the evolution of the star formation activity depends on these variables. A way of looking at the evolution of the SF activity in galaxy systems is to consider global quantities such as the total star formation rate, that is the sum of the SFRs of all the galaxies in a system (see e.g. Popesso et al. 2007) or the fraction of star-forming galaxies in a system (see e.g. Poggianti et al. 2006). Understanding how the relation between these global quantities and the group properties changes with time can teach us how the evolution of galaxies depends on the environment where they live. For this purpose we create the largest homogeneously X-ray selected sample of groups at $0.15 < z < 1$ by using the deepest available X-ray surveys conducted with *Chandra* and $XMM - Newton$ on the ECDFS, CDFN, COSMOS and EGS regions. In addition, we use the latest and deepest available *Spitzer* MIPS and *Herschel* PACS (Photoconducting Array Camera and Spectrometer, poglitsch et al. 2010) mid and far infrared surveys, respectively, conducted on the same blank fields to retrieve an accurate measure of the star formation rate of individual group galaxies. This is the first of a series of papers analyzing the relation between SF activity and galaxy environment defined as the membership of a galaxy to a massive dark matter halo. In this paper we carefully describe the catalog and present a calibration of all the relevant quantities involved in our analysis. We use this unprecedented dataset to study the evolution of the relation between the total SFR in galaxy groups at $0.15 < z < 1$ with the group global properties, mainly the total halo mass, and to the stellar mass content of the groups and Halo Occupation Distribution (HOD) to understand how the group galaxy population evolves though cosmic times.

The paper is organized as follows. In Sect. 2 we describe our dataset. In Sect. 3 we describe how all relevant quantities are estimated. In Sect. 4 we describe our results and in Sect. 5 we discuss them and draw our conclusions. We adopt a Chabrier (2003) initial mass function (IMF), $H_0 = 71$ km s^{-1} Mpc^{-1}, $\Omega_m = 0.3$, $\Omega_\Lambda = 0.7$ throughout this paper.

3.2 The dataset

The aim of this work is to analyse the evolution of the star formation activity in galaxy groups. For this purpose, we build a dataset which combines wide area surveys with good X-ray coverage, deep photometry, and high spectroscopic coverage. Galaxy clusters and groups are permeated by a hot intracluster medium radiating optically diffuse thermal emission in the X-ray band. Under the condition of hydrostatic equilibrium, the gas temperature and density are directly related to halo mass. A tight relation (rms 0.15 dex) exists also between the cluster dynamical mass and the X-ray luminosity (L_X, Pratt et al. 2007; Rykoff et al. 2008). A similar scaling relation, though with a larger scatter, holds also in the galaxy group mass regime (Sun 2012, rms 0.3 dex). Thus, the X-ray selection is the best way to select galaxy groups and clusters and to avoid incorrect galaxy group identifications due to projection effects associated with optical selection techniques. In addition, deep and accurate multi-wavelength catalogues are necessary in order to identify the group membership and to study the properties of the group galaxy population. Thus, we combine X-ray selected group catalogues and photometric and spectroscopic galaxy catalogues of four major blank field surveys: AEGIS field, COSMOS, the ECDFS and the CDFN. Throughout our analysis we use spectroscopic redshifts to define the group membership and the multiwavelength photometric information for studying the galaxy properties. For calibration purposes we will also make use of photometric redshifts. In the following section we describe the multiwavelength dataset of each field.

3.2.1 The blank fields

AEGIS

The All-Wavelength Extended Groth Strip International Survey (AEGIS) brings together deep imaging data from X-ray to radio wavelengths and optical spectroscopy over a large area (0.5-1 deg^2; Davis et al. 2007). This survey includes: *Chandra*/ACIS X-ray (0.5-10 keV; Laird et al. 2009), GALEX ultraviolet (1200-2500 $\AA$), CFHT/MegaCam Legacy Survey optical (3600-9000 $\AA$), CFHT/CFH12K optical (4500-9000 $\AA$; Coil et al. 2004), Hubble Space Telescope/ACS optical (4400-8500 $\AA$; Lotz et al. 2008), Palomar/WIRC near-infrared (1.2-2.2 μm;Bundy et al. 2006), Spitzer/IRAC mid-infrared (3.6, 4.5, 5.8, 8 μm; Barmby et al. 2008), Herschel far-infrared (100, 160 μm), VLA radio continuum (6-20cm; Willner et al. 2012) and a large spectroscopic dataset.

In particular, the X-ray data come from sensitive *Chandra* and $XMM-Newton$ observations of this field which lead to one of the largest X-ray selected samples of galaxy groups catalog to date (Erfanianfar et al., 2013). The total X-ray exposure time with *Chandra* in this field is about 3.4 Ms with a nominal exposure of 800 ks in three central fields. The $XMM-Newton$ observations in the southern part of this field have an exposure of 100 ks. The spectroscopic information is taken from different spectroscopic surveys performed in this field. The AEGIS field, as part of the Extended Groth Strip (EGS) field, has been targeted with the DEEP2 galaxy redshift survey (Davis et al. 2003; Newman et al. 2012) and it is the only field that has been a subject of extensive spectroscopic follow-up data in DEEP3 (Cooper et al. 2011, 2012). In the DEEP2 fields EGS is the only field which is not color selected, so it gives us a nearly complete sample with redshift. In addition to DEEP2 and DEEP3, EGS is located in Sloan Digital Sky Survey coverage so we have additional spectra for low-redshift galaxies. We also used redshifts of spectroscopic galaxies obtained in follow-up observations of the DEEP2 sample with the Hectospec spectrograph on the Multiple Mirror Telescope (MMT; Coil et al. 2009).

Furthermore, the EGS field is located at the center of the third wide field of the Canada-France-Hawaii Telescope Legacy Survey (CFHTLS-Wide3, W3) which is imaged in u^*, g', r', i' and z' filters down to i'=24.5 with photometric data for 366,190 galaxies (Brimioulle et al. 2008). The EGS field also contains the CFHTLS Deep 3 field, which covers 1 deg^2 with $ugriz$ imaging to depths ranging from 25.0 in z to 27 in g. For this work, we have used the T0006 release of the CHTLS Deep data. The CFHTLS Deep field also contains near-infrared coverage in the JHK bands via the WIRCam Deep Survey (WIRDS - Bielby et al. 2012). This covers 0.4 deg^2 of the D3 field and provides deep imaging to $\sim$ 24.5 (AB) in the three NIR bands. Photometric redshifts in the region covered by the NIR data were determined using the `Le Phare` code as described in Bielby et al. (2012).

COSMOS

The Cosmological Evolution survey (COSMOS) is the largest survey ever made using the Hubble Space Telescope (HST). With its 2 square degrees of coverage, COSMOS enables the sampling of the large scale structure of the universe, and reduces cosmic variance

(Scoville et al. 2007). In particular COSMOS guarantees full spectral coverage, with X-ray (*Chandra* & $XMM-Newton$), UV (GALEX), optical (SUBARU), near-infrared (CFHT), mid-infrared (Spitzer), Herschel far-infrared (100, 160 μm), sub-millimetric (MAMBO) and radio (VLA) imaging. Furthermore, the X−ray information provided by the 1.5 Ms exposure with $XMM - Newton$ (53 pointings on the whole field, 50 ksec each, Hasinger et al. 2007) and the additional 1.8 Ms exposure with *Chandra* in the central square degree (Elvis et al., 2009) enable robust detections of galaxy groups out to $z \sim 1.2$ (Finoguenov et al., 2007; George et al., 2011, 2013).

COSMOS has been targeted by many spectroscopic programs at different telescopes and has a broad spectral coverage. The spectroscopic follow up is still continuing and so far includes: the zCOSMOS survey at VLT/VIMOS (Lilly et al., 2007, 2009), GEEC2 survey with the GMOS spectrograph on the GEMINI telescope (Balogh et al., 2011; Mok et al., 2013), Magellan/IMACS (Trump et al., 2007) and MMT (Prescott et al., 2006) campaigns, observations at Keck/DEIMOS (PIs: Scoville, Capak, Salvato, Sanders, Kartaltepe) and FLWO/FAST (Wright, Drake & Civano, 2010).

The COSMOS photometric catalog (Capak et al., 2007; Capak, 2009) contains multi-wavelength photometric information for $\sim 2 \times 10^6$ galaxies over the entire field. The position of galaxies has been extracted from the deep i-band imaging (Taniguchi et al., 2007). A limit of 80% completeness is achieved at $i_{\rm AB}$ =26.5. The optical catalog of Capak et al. (2007); Capak (2009) includes 31 bands (2 bands from the Galaxy Evolution Explorer (GALEX), 6 broad bands from the SuprimeCam/Subaru camera, 2 broad bands from MEGACAM at CFHT, 14 medium and narrow bands from SuprimeCam/Subaru, J band from the WFCAM/UKIRT camera, H and K band from the WIRCAM/CFHT camera, and the 4 IRAC/Spitzer channels). In particular, We take the catalogue provided by Ilbert et al. (2009) and Ilbert et al. (2010). They cross-match the S-COSMOS Sanders et al. (2007) 3.6 μm selected catalogue with the multi-wavelength catalogue (Capak et al., 2007; Capak, 2009) and calculate photo-z, stellar masses and SFR in a consistent way by using the `Le Phare` code(Ilbert et al., 2009, 2010).

ECDFS

ECDFS is observed broadly from X-ray to radio wavelengths and centred on one of the most well-studied extragalactic fields in the sky (e.g. Giavalisco et al. 2004; Rix et al. 2004; Lehmer et al. 2005; Quadri et al. 2007; Miller et al. 2008; Padovani et al. 2009; Cardamone et al. 2010; Xue et al. 2011; Damen et al. 2011). The smaller Chandra Deep Field South (CDFS, $\alpha = 03h32m25s$, $\delta = -27^o49^m58^s$), in the central part of ECDFS, is currently the deepest X-ray survey with *Chandra* (4Ms) and $XMM - Newton$ (3Ms) programs.

The redshift assemblage in the ECDFS and the smaller CDFS and GOODS-S regions is achieved by complementing the spectroscopic redshifts contained in the Cardamone et al. (2010) catalog with all new publicly available spectroscopic redshifts, such as the one of Silverman et al. (2010) and the Arizona CDFS Environment Survey (ACES, Cooper et al. 2012). We clean the new catalogue of redshift duplications for the same source by matching the Cardamone et al. (2010) catalog with the Cooper et al. (2012) and the Silverman et al.

(2010) catalog within 1 arcsec and by keeping the most accurate z_{spec} entry (smaller error and/or higher quality flag) in case of multiple entries (see Ziparo et al. 2013 for a more detailed discussion). We also include the very high quality redshifts of the GMASS survey (Cimatti et al. 2008) using the same procedure. The total number of secure redshifts in the sample is 5080 out of 7277 total, unique targets.

We use the multi-wavelength photometric data from the catalogue of Cardamone et al. (2010). It includes a total of 10 ground-based broad bands (U, $U38$, B, V, R, I, z, J, H, K), 4 IRAC bands (3.6 μm, 4.5 μm, 5.8 μm, 8.0 μm), and 18 medium-band imaging ($IA427$, $IA445$, $IA464$, $IA484$, $IA505$, $IA527$, $IA550$, $IA574$, $IA598$, $IA624$, $IA651$, $IA679$, $IA709$, $IA738$, $IA767$, $IA797$, $IA856$). The catalogue includes multi-wavelength SEDs and photometric redshifts for $\sim$ 80000 galaxies down to $R_{AB} \sim 27$.

CDFN

The Chandra Deep Field North (CDFN) survey is one of the deepest 0.5-8.0 keV surveys ever made. The Chandra survey is comprised of two partially overlapping $\sim$1 Ms ACIS-I exposures covering a total of 448 sq. arcmin, of which $\approx$160 sq. arcmin has 1.7-1.9 Ms of exposure. In addition, there is 150 ks of good XMM-Newton exposure. The GOODS-North field within the CDFN centers at RA= $12^h36^m55^s$, Dec.= $+62°14^m15^s$ (J2000) and has become one of the most well-studied extragalactic fields in the sky with existing observations among the deepest at a broad range of wavelengths (e.g., Alexander et al. 2003; Morrison et al. 2010; Cooper et al. 2011; Elbaz et al. 2011). GOODS-N covers an area of approximately 10×16 arcmin^2 (Giavalisco et al., 2004).

We use the multi-wavelength catalogue of GOODS-N built by Berta et al. (2010), who adopted the Grazian et al. (2006) approach for the PSF matching. The catalogue includes ACS *bviz* (Giavalisco et al. 2004), Flamingos JHK, and Spitzer IRAC data. Moreover, MIPS 24 μm (Magnelli et al. 2009) and deep U, Ks (Barger, Cowie & Wang 2008). The catalog is also complemented by the spectroscopic redshift compilation of Barger, Cowie & Wang (2008).

3.2.2 X-ray Analysis

All the blank fields considered in our analysis are observed extensively in the X-ray with $Chandra$ and $XMM-Newton$. Firstly, we remove point sources in both of the $Chandra$ and $XMM-Newton$ images following the procedure explained in Finoguenov et al. (2009). Then the residual images were coadded, taking into account the different sensitivity of each instrument. The "residual" image, free of point sources, is then used to identify extended emission. Groups and clusters are selected as extended emission with at least 4σ significance with respect to the background (see Finoguenov et al. (2009) for further details regarding the precise definition of background and detection significance level). A redshift to each systems on the basis of spectroscopic redshifts, when available, or otherwise photometric redshift is assigned. The X-ray luminosity L_X is estimated within r_{500}[1] after taking into account the possible missed flux through the use of the beta-model. The total masses M_{200}, within r_{200}, are estimated based on the measured L_X and its errors, using the scaling relation from weak lensing calibration of Leauthaud et al. (2010). The intrinsic scatter for mass in this relation is 20% (Leauthaud et al., 2010; Allevato et al., 2012) which is larger than a formal statistical error associated with the measurement of L_X.

The X-ray group catalogs derived with this approach comprise 52 detections in AEGIS (Erfanianfar et al. 2013), 277 detections in the COSMOS field (George et al. 2011), 50 detections in the ECDFS (Finoguenov et al. in prep.) and 27 detection in CDFN. We present the full CDFN X-ray group catalog in the Appendix. In the following section we describe how we select a subsample of "secure" groups and how we associate them to the respective galaxy population.

Group Identification

To associate the respective galaxy population to any X-ray extended emission and to define properly the group redshift we follow the same procedure described in Erfanianfar et al. (2013) and performed on the AEGIS X-ray dataset. We extend here this procedure to all the other fields described in the previous section. In brief, we estimate the galaxy over-density along the line of sight in the region of each X-ray extended emission following the red sequence technique (Finn et al. 2010). Additionally we screen for the existence of an over-density of red galaxies in the 3rd dimension using the spectroscopic redshift distribution of the X-ray extended source.

As described in Erfanianfar et al. (2013), we assigned to each X-ray extended source a flag that describes the quality of the identification. We define the following flags:

- flag=1 indicates a confident redshift assignment, significant X-ray emission, and a well-determined center of red galaxies with respect to X-ray emission center
- flag=2 indicates that the centering has a large uncertainty ($\sim 15''$)
- flag=3 indicates no secure spectroscopic confirmation but good centering
- flag=4 or more depending on the survey indicates that we have uncertain redshifts due to the lack of spectroscopic objects and red galaxies, and also a large uncertainty in centering or unreliable cases for which we could not identify any redshift.

For the purpose of this work we consider only X-ray extended emission with a secure redshift definition with flag 1 or 2. Out of the initial 406 X-ray group candidates in the four considered fields, we identify 244 secure groups. The secure redshift estimate is used to refine the initial X-ray luminosity of the groups and, thus, the mass M_{200} with the scaling relation of Leauthaud et al. (2010) as described in the previous paragraph. The final step

---

[1] r_Δ (where $\Delta = 500, 200$) is the radius at which the density of a cluster is equal to Δ times the critical density of the universe (ρ_c) and M_Δ is defined as $M_\Delta = (4\pi/3)\Delta\rho_c r_\Delta^3$.

of the analysis is the identification of the group galaxy members via dynamical analysis as described below.

Group Membership

In order to properly define the galaxy membership of each group, we identify among our 244 secure groups those which are relatively isolated. Indeed, the presence of a close companion may bias the estimate of the velocity dispersion of the group and, thus, also the galaxy membership definition which relies on this quantity. This procedure leads to a subsample of 211 clean isolated groups. We follow the procedure described in Erfanianfar et al. (2013) to estimate the group velocity dispersion and the galaxy membership definition. The procedure is iterative and it needs a first guess of the velocity dispersion to define the redshift interval around the group redshift to determine the initial galaxy membership. We derive the first guess of the velocity dispersion from the group's X-ray luminosity L_X by using the relation of Leauthaud et al. 2010. This velocity dispersion provides the intrinsic velocity dispersion ($\sigma(v)_{intr}$-which can be achieved by subtracting the errors of the redshift measurements in quadrature from the rest frame velocity dispersion) of the group. We estimate, then, the observed velocity dispersion by considering the redshift of the group (z_{group}) and the errors of the redshift in our spectroscopic samples, $\langle\Delta(v)\rangle^2$ according to these relations:

$$\sigma(v)^2_{rest} = \sigma(v)^2_{intr} + \langle\Delta(v)\rangle^2 \tag{3.1}$$

$$\sigma(v)_{obs} = \sigma(v)_{rest} \times (1 + z_{group}) \tag{3.2}$$

We consider as initial group members all galaxies within $|z - z_{group}| < \delta(z)_{max}$ where $\delta(z)_{max} = 2\frac{\sigma(v)_{obs}}{c}$ and within virial radii (r_{200}) from the X-ray center. We recompute the observed velocity dispersion of the groups, $\sigma(v)_{obs}$ using the "gapper" estimator method which gives more accurate measurements of velocity dispersion for small size groups (Beers, Flynn & Gebhardt 1990; Wilman et al. 2005) in comparison to the usual formula for standard deviation (see Erfanianfar et al. 2013 for more details). The observed velocity dispersion is estimated according to:

$$\sigma(v)_{obs} = 1.135c \times \frac{\sqrt{\pi}}{N(N-1)} \sum_{i=1}^{n-1} \omega_i g_i \tag{3.3}$$

where $w_i = i(N - i)$, $g_i = z_{i+1} - z_i$ and N is the total number of spectroscopic members. In this way we measure the velocity dispersion using the line-of-sight velocity gaps where the velocities have been sorted into ascending order. The factor 1.135 corrects for the 2σ clipping of the Gaussian velocity distribution. We iterate the entire process until we obtain a stable membership solution. We then calculate errors for our velocity dispersions using the Jackknife technique (Efron 1982). The procedure can be considered reliable for groups with at least 10 galaxy members. The 10 galaxy members threshold is reached for

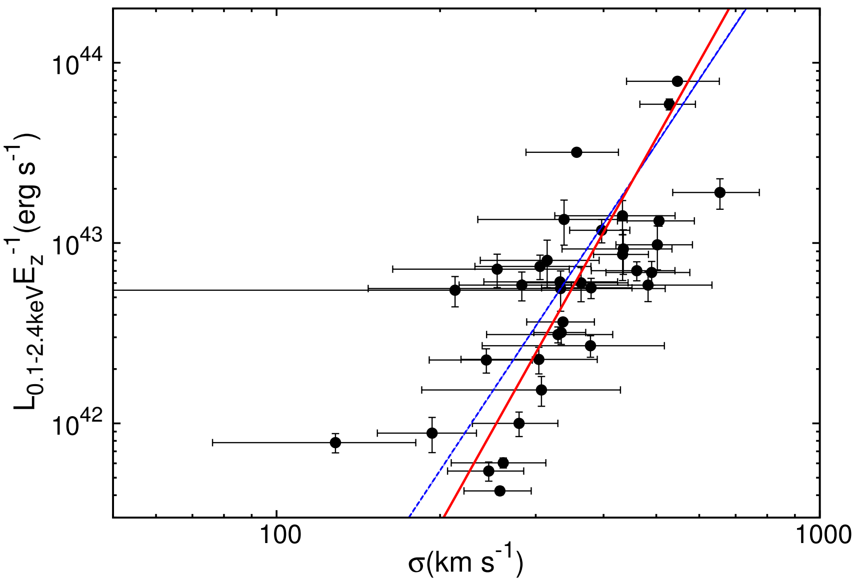

Figure 3.1: $L_X - \sigma$ relation for X-ray groups. The dashed blue line show our expectation for $L_X - \sigma$ relation from scaling relations (Leauthaud et al. 2010) and the solid red line is our bisector fit to data.

36 groups out of 211. For the groups with less than 10 members but still more than 5 members within r_{200}, we base the velocity dispersion estimate on M_{200} and the relation between σ and r_{200} as in Carlberg, Yee & Ellingson (1997). This leads to a sample of 111 groups out of 211. Figure 3.1 shows the $L_x - \sigma$ relation for X-ray groups with more than 10 spectroscopic members, where σ is estimated via dynamical analysis. The solid red line shows the power-law fit to the relation. The bisector procedure is used for this fit (Akritas & Bershady 1996). We also plot the $L_x - \sigma$ relation (dashed blue line) expected from scaling relations obtained for a sample of groups with similar luminosities in the $0 < z < 1$ redshift range in COSMOS (Leauthaud et al. 2010). The consistency between two relations ensures that the estimate of the velocity dispersion derived from the X-ray luminosity and the one calculated via dynamical analysis are in good agreement.

Once we have the estimate of the velocity dispersion of each group, we define as group members all galaxies within $2 \times r_{200}$ in the angular direction and $\pm 3 \times (\sigma/c) \times (1 + z_{group})$ in the line of sight direction in order to consider also the infalling regions of the groups. When a member galaxy is associated to more than one group, we consider it as a member of the group for which the distance to the galaxy is lowest in units of virial radii.

3.2.3 Infrared data

For all considered fields we use the deepest available *Spitzer* MIPS 24 μm and PACS 100 and 160 μm datasets. For COSMOS these are coming from the public Spitzer 24 μm (Le Floc'h et al., 2009; Sanders et al., 2007) and PEP PACS 100 and 160 μm data

(Lutz et al. 2011). Both *Spitzer* MIPS 24 μm and PEP source catalogues are obtained by extracting sources using NIR priors as described in Magnelli et al. (2009). In short, IRAC and MIPS 24 μm source positions are used to detect and extract MIPS and PACS sources, respectively, at 24, 100 and 160 μm. This is feasible since extremely deep IRAC and MIPS 24 μm observations are available for the COSMOS field (Scoville et al. 2007). The source extraction is based on a PSF-fitting technique, presented in detail in Magnelli et al. (2009). The association between 24 μm and PACS sources with their optical counterparts, taken from the optical catalog of Capak et al. (2007) is done via a maximum likelihood method (see Lutz et al., 2011, for details).

The same approach is used also for the AEGIS field, where we use the *Spitzer* MIPS 24 and PEP PACS 100 and 160 μm catalogs produced by the PEP team (see Magnelli et al. 2009).

In the CDFS and GOODS regions the deepest available MIR and FIR data are provided by the *Spitzer* MIPS 24 μm Fidel Program (Magnelli et al. 2009) and by the combination of the PACS PEP (Lutz et al. 2011) and GOODS-Herschel (Elbaz et al. 2011) surveys at 70, 100 and 160 μm. The GOODS Herschel survey covers a smaller central portion of the entire GOODS-S and GOODS-N regions. Recently the PEP and the GOODS-H teams combined the two sets of PACS observations to obtain the deepest ever available PACS maps (Magnelli et al. 2013) of both fields. The more extended CDFS area has been observed in the PEP survey as well, yet having a higher flux limit. As for the COSMOS catalogs, the 24 μm and PACS sources are associated to their optical counterparts via a maximum likelihood method (see Lutz et al., 2011, for details).

For all galaxies identified as galaxy group members, we use the MIPS and PACS data to accurately estimate the IR bolometric luminosity and, thus, the SFR. We compute the IR luminosities integrating the SED templates from Elbaz et al. (2011) in the range 8-1000 μm. The PACS (70, 100 and 160 μm) fluxes, when available, together with the 24 μm fluxes are used to find the best fit templates among the main sequence (MS) and starburst (SB, Elbaz et al. 2011) templates. When only the 24 μm flux is available for undetected PACS sources, we rely only on this single point and we use the MS template for extrapolating the L_{IR}. Indeed, Ziparo et al. (2013) show that the MS template turns out to be the best fit template in the majority of the cases with common PACS and 24 μm detection. Ziparo et al. (2013) show also that by using only 24 μm data and the MS template there could be a slight underestimation (10%) only above $z \sim 1.7$ or $L_{IR}^{24} > 10^{11.7}$ $L_{\odot}$. In larger fields such as COSMOS and ECDFS there is a larger probability to find rare strong star-forming off-sequence galaxies at $L_{IR}^{24} > 10^{11.7}$ $L_{\odot}$ even at low redshift. However, those sources should be captured by the Herschel observations given the very high luminosity threshold. Thus, it would not be a problem in getting a proper estimate of the L_{IR} from the best fit templates also for these rare cases. The SFR for these sources is then estimated via the Kennicutt (1998) relation and then corrected from Salpeter IMF to Chabrier IMF for consistency with SFR_{SED} and stellar mass.

Stellar masses and star formation rate from SED fitting

Due to the flux limits of the MIPS and PACS catalogs in the four considered blank fields, the IR catalogs are sampling only the Main Sequence region and can not provide a SFR estimate for galaxies below the Main Sequence or in the region of quiescence. For a complete census of the star formation activity of the group galaxies, we need, however, an estimate of the SFR of all group members. For this reason, we complement the SFR estimates derived from IR data (SFR_{IR}), as described in the previous section, with an alternative estimate of the SFR. SFR based either on SED fitting technique (SFR_{SED}) or on rest-frame UV observations (SFR_{UV}) are both reliable candidates. According to Ziparo et al. (2013), the scatter of the SFR_{UV}-SFR_{IR} relation is always bigger (at every redshift) with respect to the SFR_{SED}-SFR_{IR} calibration. So, we use SFR_{SED} as an alternative estimate of the SFR. Thus, for all galaxies undetected in MIPS and PACS maps, we use the SFR_{SED} taken from the following catalogs:

- in AEGIS, SFR estimated with FAST (Kriek et al., 2009) taken from Wuyts et al. (2011)
- in COSMOS, SFR estimated with `Le Phare` taken from Ilbert et al. (2010)
- in ECDFS, SFR estimated with `Le Phare`, from Ziparo et al. (2013)
- in CDFN, SFR estimated with FAST (Kriek et al., 2009) taken from Wuyts et al. (2011)

The same catalogs provide also an estimate of the galaxy stellar mass. All SFR_{SED} and stellar mass estimates are in Chabier IMF.

Ziparo et al. (2013) point out that, in general, the stellar masses and SFR_{SED} derived from Wuyts et al. (2011), Ilbert et al. (2010) and Ziparo et al. (2013) are all in agreement when compared on a common galaxy subsample. According to Ziparo et al. (2013), the scatter around the 1 to 1 relation is of the order of 0.6 dex. Indeed, previous studies (Papovich, Dickinson & Ferguson, 2001; Shapley et al., 2001, 2005; Santini et al., 2009) already demonstrate that, while stellar masses are rather well determined (within a factor of 2) by very different methods, the SED fitting procedure does not strongly constrain star formation histories at high redshifts, where the uncertainties become larger due to the SFR–age–metallicity degeneracies. This degeneracy leads to the confusion of young, obscured star-forming galaxies with more massive, old, more quiescent galaxies. Wuyts et al. (2011) confirm the SFR_{SED} provides a quite good estimate of the SFR for moderately star-forming galaxies and fails to provide a good estimate for very obscured objects.

Indeed, if we examine the scatter of the $SFR_{SED} - SFR_{IR}$ relation we clearly see a degeneracy with the stellar mass, as shown in the left column panels of Fig. 3.2. This degeneracy is stronger than the one due to the redshift, as shown in Wuyts et al. (2011), though the two aspects are related via selection effects (only massive star-forming galaxies are generally have spectroscopic redshifts at high redshift). The mass dependence of the scatter is different from field to field and depends on the method used for the SED fitting.

This is probably due to two aspects. First, any blank field is characterized by a different dataset in terms of multiwavelength coverage (number and type of broad band filters) and, thus, by a different sampling of the galaxy SED. Second, different recipes, thus different star formation histories, and different fitting techniques are used for estimating the stellar masses and the SFR_{SED}. This also explains why there is such a large scatter in the SFR_{SED} derived with different methods.

The result of this exercise shows that we can not use the $SFR_{SED} - SFR_{IR}$ relation observed in one of the fields to calibrate the SFR_{SED} of the other fields or obtained with a different method. Thus, we use the following approach. In order to correct a posteriori for the stellar mass bias in the SFR_{SED}, we fit the plane $SFR_{IR} - SFR_{SED} - Mass$, separately for each field. The best fit relation is listed below for AEGIS and CDFN (same fitting procedure):

$$SFR_{IR} = -6.16 + 0.59 \times SFR_{SED} + 0.66 \times M_* \tag{3.4}$$

for COSMOS:

$$SFR_{IR} = -4.54 + 0.61 \times SFR_{SED} + 0.49 \times M_* \tag{3.5}$$

and for ECDFS and GOODS-S:

$$SFR_{IR} = -4.56 + 0.63 \times SFR_{SED} + 0.49 \times M_* \tag{3.6}$$

Once this calibration is used to correct the SFR_{SED} with the additional information of the stellar mass, the scatter around the $SFR_{SED} - SFR_{IR}$ relation decreases to 0.21 dex, 0.23 dex and 0.12 dex in comparison to SFR_{IR} for galaxies with more than $10^{10} M_{\odot}$ in AEGIS, COSMOS, and ECDFS, respectively, as shown in central column panels of Fig. 3.2. The values of the scatter are still 0.34, 0.42 and 0.44 in AEGIS, COSMOS, and ECDFS, respectively, when the whole mass range is considered.

We adopt this calibration to correct a posteriori the SFR_{SED} estimates for all IR undetected galaxies above $log(SFR) > -0.5$. We think that this calibration is applicable in the SFR range considered here to IR undetected galaxies for the following reasons. Elbaz et al. (2011) show that the IR SED of star-forming galaxies are not evolving with redshift and that, instead, there is a much stronger dependence on the location of galaxies with respect to the galaxy Main Sequence. In addition, Buat et al. (2009), by using Spitzer MIPS data, also show that the dust attenuation expressed in terms of $log(L_{IR}/L_{UV})$ as a function of the $log(L_{IR} + L_{UV})$, which is proportional to the SFR, seems to be redshift independent (Fig. 2 of Buat et al. 2009) in particular between redshift 0 and 1 as considered in this work. The same work also shows that $log(L_{IR}/L_{UV})$ as a function of the rest-frame K-band (L_K) luminosity, which is a proxy for the stellar mass, does not show any redshift dependence. This was recently confirmed also by Berta et al. (2013) with the most recent *Herschel* PEP and Hermes data. Thus, the substantial lack of evolution of IR and rest-frame UV properties of galaxies of a given mass and SFR, would suggest that the low redshift IR detected galaxies that populate the low star formation regime of Fig. 3.2 can be used to calibrate the SFR_{SED} of IR undetected galaxies in the same SFR regime at higher redshift.

We point out that in the COSMOS field, as shown in the central panels of Fig. 3.2, our calibration does not consistently move all galaxies to the 1 to 1 line (middle panel). High star-forming galaxies still show a slightly too low SFR_{SED} with respect to the IR measure. This is probably due to the fact, that in the case of the Ilbert et al. (2010) SED fitting results, a plane in log-log space is not the best analytical form and, thus, it does not provide the best representation of the $SFR_{IR} - SFR_{SED} - Mass$ relation. However, we still improve the agreement within SFR_{SED} and SFR_{IR} by more than a factor of two even in this field.

3.2.4 The final galaxy group and group galaxy samples

The aim of our analysis is to study how the star formation activity in group-sized halos depends on the global properties of the systems. In order to do that, we would need to sample the complete group galaxy population in stellar mass and SFR. However, since the group members are spectroscopically selected, we need to consider how the spectroscopic selection function drives our galaxy selection and, thus, how it can affect our results.

The mean spectroscopic completeness of the ECDFS and the CDFN group in the IRAC 3.6 μm is the same as the one shown in Fig. 1 of Ziparo et al. (2013), which use ECDFS dataset. The AEGIS field has the same level of spectroscopic completeness as the CDFN. We point out that the use of the full zCOSMOS and the GEEC2 spectroscopic sample increases the level of completeness in the COSMOS field by 20% in the mean and in the group regions with respect to Ziparo et al. (2013).

Since we need to define a group galaxy population which is complete in stellar mass and SFR, we check also how the spectroscopic completeness in the irac band translates into a completeness in mass and SFR. For ECDFS and CFDN this is already done in Ziparo et al. (2013). For the new datasets of AEGIS and COSMOS we follow the same approach of the mentioned work. This is done separately in two redshift bins ($0.15 < z < 0.5$ and $0.5 < z < 1.1$). The reference catalogs used to estimate this completeness are the photometric catalogs described in Section 3.2.3. All those photometric catalogs are IRAC selected at 3.6 or 4.5 μm and should ensure photometric completeness down to at least $m_{AB}(3.6\mu m) \sim 23$. From these catalogs we extract, for each field, the photometric redshift, the stellar mass and the SFR information derived from the SED fitting technique, after replacing the SFR_{SED} with SFR_{IR}, where available, and after correcting SFR_{SED} with the calibration presented in Section 3.2.3. Given the high accuracy of the photometric redshifts of Cardamone et al. (2010), Wuyts et al. (2011) and Ilbert et al. (2010), we assume the photometric redshifts, and the physical properties based on those, to be correct. We, then, estimate the completeness per stellar mass and SFR bins, respectively, as the ratio between the number of galaxies with spectroscopic redshift and the total number of galaxies in that bin. This procedure allows us to determine how the spectroscopic selection, based on the photometric information (e.g. colour, magnitude cuts, etc.), affects the choice of galaxies as spectroscopic targets according to their physical properties. As expected and shown also in Ziparo et al. (2013), the spectroscopic selection function, tends in general to select the most massive and most star-forming systems.

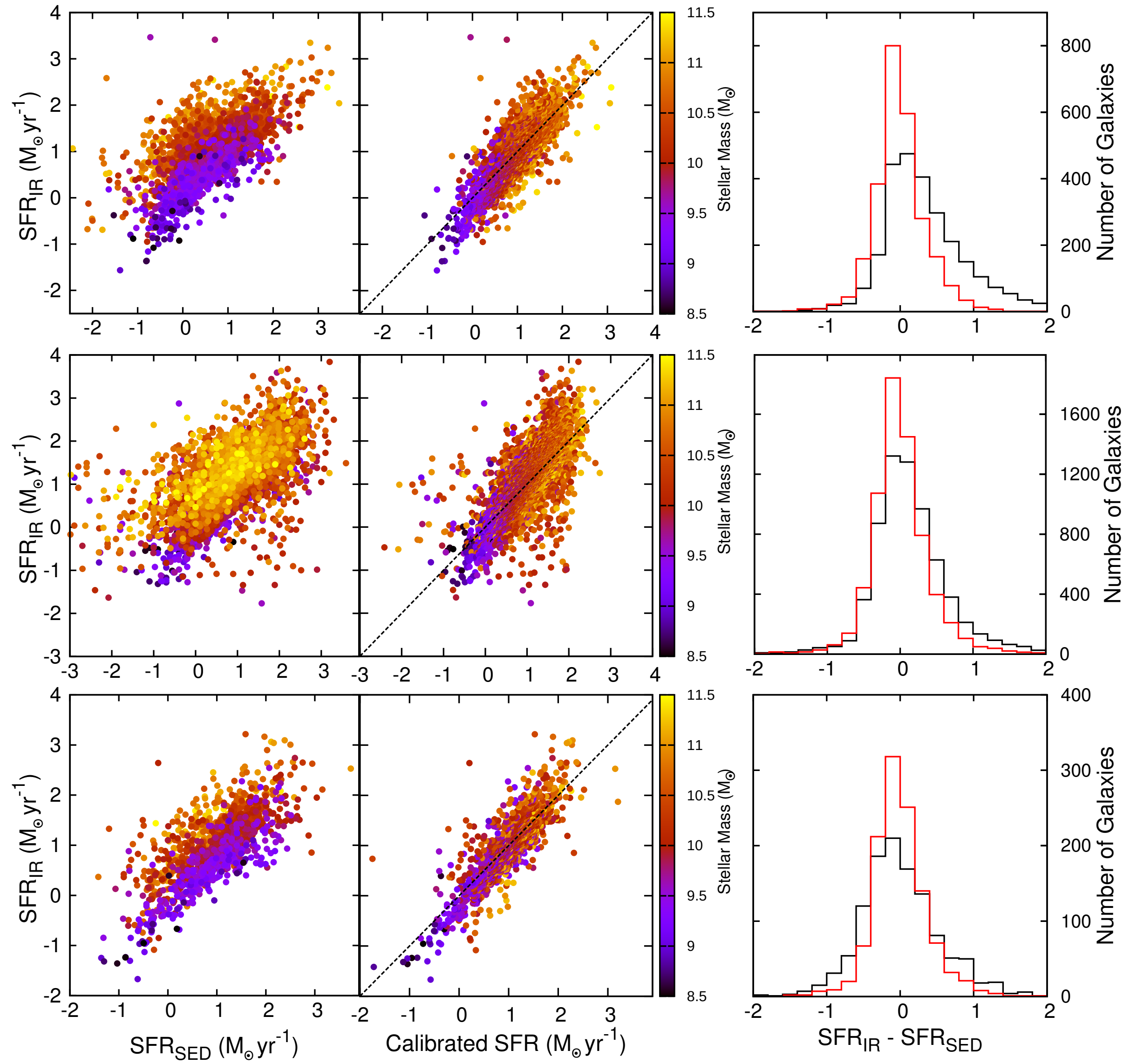

Figure 3.2: The left panels show SFR_{IR} vs. SFR_{SED} before re-calibration for EGS, COSMOS and GOODS-S from top to bottom respectively. The middle panels show corresponding SFR_{IR} vs.re-calibrated SFR_{SED}. The dashed line is one to one relation. The right panels are the histogram of corresponding $SFR_{IR} - SFR_{SED}$. The black and red histograms show before (black) and after (red) re-calibration.

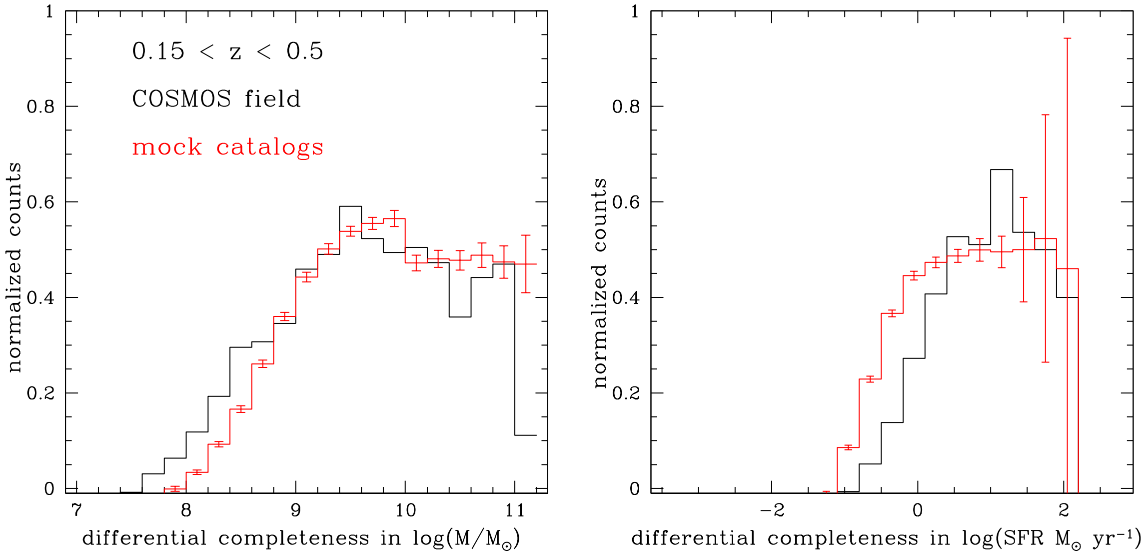

Figure 3.3: *Left panel*: spectroscopic completeness per stellar mass bin in the low redshift sample (black histogram) and in the simulated “incomplete” mock catalog (red line) in the same redshift range. *Right panel*: spectroscopic completeness per SFR bin for the low redshift sample (black histogram) and in the simulated “incomplete” mock catalog (red line).

Given the completeness level in stellar mass and SFR shown in Fig. 3.3, it is clear that we can not define a galaxy sample which is, at the same time, complete in stellar mass and SFR. Indeed, while in any bin of stellar mass, the most star-forming galaxies are preferentially selected, the most massive galaxies are preferentially observed at any given SFR. Thus, we follow the following approach. We fix the stellar mass threshold to a value of 10^{10} $M_{\odot}$, which guarantees a minimum spectroscopic completeness (40%) for our analysis. We impose that this minimum completeness level above the stellar mass threshold must be reached in the region of the group. This completeness in mass is estimated as follows. We consider a cylinder along the line of sight of the group with a radius of twice r_{200} from the X-ray center and half width in redshift equal to $5\times\sigma_{\Delta z/(1+z)}$, where $\sigma_{\Delta z/(1+z)}$ is the error of the photometric redshifts in each survey. This width is set to be much larger than the photometric redshift uncertainty and still small enough to sample the group region. The completeness is the ratio of the number of galaxies with spectroscopic redshift to the number of galaxies with spectroscopic or photometric redshift within this cylinder, with stellar mass above the given mass threshold. We perform the same analysis with different values of the cylinder half width (up to $10\times\sigma_{\Delta z/(1+z)}$) and we obtain consistent measures of the completeness in mass.

This additional condition is fulfilled for almost all groups in the AEGIS, ECDFS, CDFN due to a very high and spatially homogeneous spectroscopic completeness. However, the 40 % threshold is hardly reached in many of the COSMOS group regions. The requirements

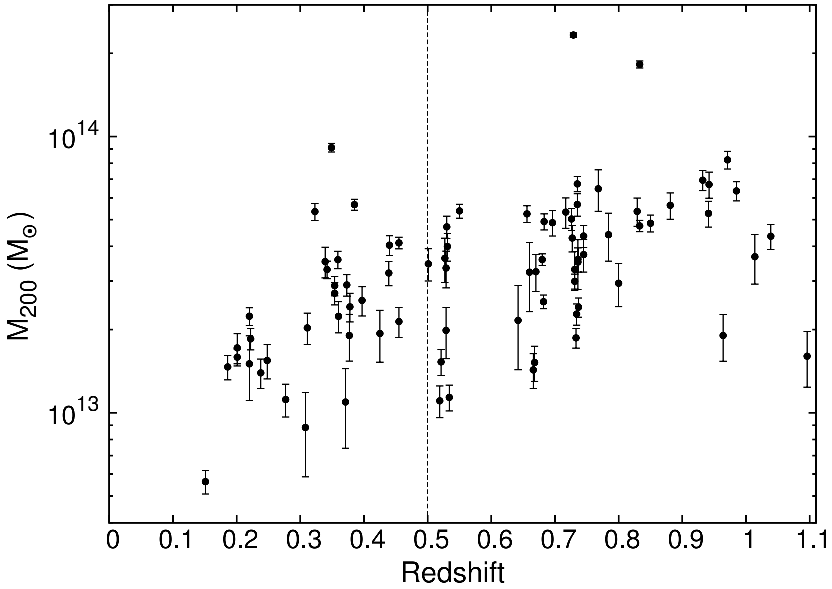

Figure 3.4: M_{200} vs. redshift for the final sample of galaxy groups in our analysis. The vertical dashed line separates low-z and high-z sample.

is mainly fulfilled by the groups in the zCOSMOS region and by the GEEC2 groups.

To deal with the spectroscopic incompleteness in SFR, we analyse the possible biases induced by the spectroscopic selection function using mock catalogs. Our approach is explained in Section 3.3.

The final group sample is shown in Figure 3.4. The sample comprises 83 galaxy groups in the redshift range $0.15 < z < 1.1$. In order to study the evolution of the relation between the SF activity in groups and the system global properties, we divide the sample in two subsamples at 0.15<z<0.5 (31 galaxy groups) and z>0.5 (52 galaxy groups). For 29 of 83 galaxy groups we have velocity dispersion from dynamical analysis and for the rest of them from X-ray properties. 50 of galaxy groups have Flag=1 and the remanining 33 have Flag=2.

3.2.5 The reference nearby group sample

Our group sample does not cover the local Universe. Indeed, we apply a cut at $z = 0.15$ in order to sample the same cosmic time epoch in the two redshift bins ($\sim$ 3 Gyrs) considered in our analysis. In order to follow the evolution of the group galaxy population down to $z \sim 0$, we complement our sample with a reference sample of nearby groups. Unfortunately, an X-ray selected sample of nearby groups in the same mass range of our sample with the same information as our groups, does not exist. Most of the X-ray selected samples available in the literature have a quite complicated selection function. In addition we need also a complete , spectroscopically confirmed, membership of any system and auxiliary information of the group galaxy stellar mass and star formation activity. Thus, we choose

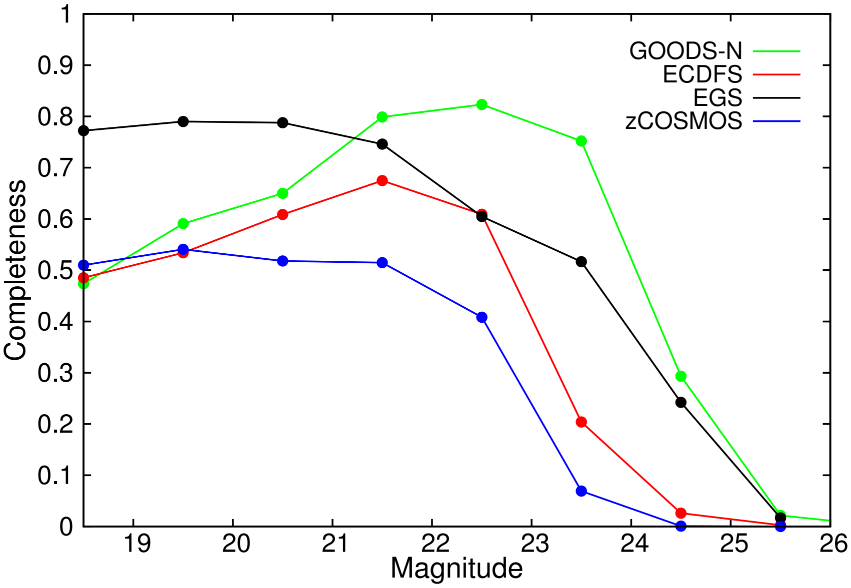

Figure 3.5: Spectroscopic completeness for different fields in R-band magnitude. We use v-band magnitude for GOODS-N.

as a reference sample an optically-selected sample of nearby groups drawn from the SDSS and with a well studied and clean selection function. The group catalog and its general properties are discussed in Yang et al. (2007). The catalog is drawn from the clean NYU-VAGC DR4 galaxy catalog (Blanton et al. 2005), which is a subsample of the SDSS DR4 galaxy spectroscopic catalog. The group selection is based on the halo-based group finder of Yang et al. (2005), that is optimized for grouping galaxies that reside in the same dark matter halo. The performance of this group finder is extensively tested using mock galaxy redshift surveys constructed from the conditional luminosity function model (Yang, Mo & van den Bosch 2003; van den Bosch, Yang & Mo 2003; Yang et al. 2004). The Yang et al. (2007) group catalog provides for each system the group membership and an estimate of the halo mass (M_{200}) (see Yang et al. 2007 for a detailed discussion). In order to study the SF activity of nearby groups, we complement the group galaxy catalog of Yang et al. (2007) with the stellar masses and the SFR based on SDSS $H\alpha$ emission estimated by Brinchmann et al. (2004). These quantities are corrected from aperture to total and to the same IMF used in our work. We also apply the same stellar mass cut ($M_* > 10^{10}$) and completeness level (> 40%) in the nearby group sample for consistency.

3.2.6 The Millennnium mock catalogs

In order to estimate the errors involved in our analysis and check for possible biases due to the spectroscopic incompleteness, we follow the same approach used in Ziparo et al. (2013) based on the mock catalogs provided by the Millennium Simulation (Springel et al., 2005). The Millennium simulation follows the hierarchical growth of dark matter structures from redshift z = 127 to the present (Springel et al., 2005). Out of several mock catalogues created from the Millennium simulation, we choose to use those of Kitzbichler & White (2007) based on the semi-analytical model of Delucia et al. 2006. The simulation assumes the concordance ΛCDM cosmology and follows the trajectories of $21603^3 \sim 1.0078 \times 10^{10}$ particles in a periodic box 500 Mpc h^{-1} on a side. Kitzbichler & White (2007) make mock observations of the artificial Universe by positioning a virtual observer at $z \sim 0$ and finding the galaxies which lie on a backward light-cone. The backward light-cone is defined as the set of all light-like worldlines intersecting the position of the observer at redshift zero. We select as information from each catalogue the Johnson photometric band magnitudes available (R_J , I_J and K_J), the redshift, the stellar mass and the star formation rate of each galaxy with a cut at $I_J < 26$ to limit the data volume to the galaxy population of interest. In order to simulate the spectroscopic selection function of the surveys used in this work, we choose one of the available photometric bands (R_J) and extract randomly in each magnitude bin a percentage of galaxies consistent with the percentage of systems with spectroscopic redshift in the same magnitude bin observed in each of our surveys. We do this separately for each survey, since each field shows a different spectroscopic selection function as shown in Fig. 3.5. We follow this procedure to extract randomly 25 catalogs for each survey from different light- cones. The "incomplete" mock catalogues, produced in this way, tend to reproduce, to a level that we consider sufficient to our needs, the selection of massive and highly star-forming galaxies observed in the real galaxy samples, as already shown in Ziparo et al. (2013).

We note that the galaxy mock catalogs of the Millennium simulation fail in reproducing the correct distribution of star-forming galaxies in the SFR-stellar mass plane, as already shown in Elbaz et al. (2007) at higher redshift ($z \sim 1$), although they provide a rather good representation of the local Universe. This is caused by the difficulty of the semi-analytical models of predicting the observed evolution of the galaxy stellar mass function and the cosmic star formation history of our Universe (Kitzbichler & White, 2007; Guo et al., 2010). We stress here that this does not produce a problem for our approach. Indeed, we aim to understand the bias induced by selection function like the spectroscopic selection function of our dataset by using the Millennium galaxy mock catalogues. In other words, we only need to extract mock catalogues randomly to reproduce the same bias in selecting, on average, the same percentage of most star-forming and most massive galaxies of the parent sample. By comparing the results obtained in the biased randomly extracted mock catalogues and the unbiased parent catalogue, we estimate the bias of our analysis. Since in both biased and unbiased mock catalogues the underestimation of the SFR or the stellar mass of high redshift galaxies exists, it does not affect the result of this comparative analysis. We also stress that the aim of this analysis is only to provide a way to interpret our results in terms of possible biases introduced by the spectroscopic selection function not to provide correction factors for our observational results.

3.3 Estimate of Total M$_*$, Total SFR and Halo occupation Distribution of galaxy groups

In this section we describe our method for estimating the total stellar mass (ΣM$_*$), the total star formation rate (ΣSFR) and the Halo Occupation Distribution of the galaxy groups in our sample. As explained in Section 3.2.4, we impose a stellar mass cut at $M_* > 10^{10} M_\odot$ since below this limit the spectroscopic completeness is rather low in all considered fields (see left panel of Fig. 3.3). The total stellar mass and star formation rate of each system are estimated as the sum of all group galaxy members stellar mass and SFR, respectively, with mass above the given limit. The halo occupation distribution of each group is defined by the number of galaxies with stellar mass above $M_* > 10^{10} M_\odot$. We correct for spectroscopic incompleteness by dividing each quantity by the spectroscopic completeness estimated as explained in Section 3.2.4. In order to check if there are biases in our estimates due to the spectroscopic selection function or to our method, and to calculate the uncertainties of each quantity, we use the galaxy mock catalogs described in Section 3.2.6. For this purpose we extract from the original Kitzbichler & White (2007) Mock catalog a sample of galaxy groups in the same mass and redshift range of the observed sample. We base our selection on the dark matter halo virial mass which, according to Delucia et al. 2006, is consistent with the mass calculated within r_{200}, as in the observed group sample. The members of the groups are identified by the same Friends of Friends (FoF) identification number, defined according to the FoF algorithm described in Delucia et al. 2006. We assume that the group galaxy members identified by the FoF algorithm, which takes into account also the real 3D spatial distribution of galaxies, are the correct ("true") group members. The "true" velocity dispersion, Σ SFR, Σ M$_*$ and N are, thus, the one based on this membership.

We apply, then, our method for calculating the membership, the velocity dispersion, total M$_*$, total SFR and halo occupation distribution on the "incomplete" mock catalogs described in Section 3.2.6, which include also the effect of the different spectroscopic selection functions. For each group we assume the coordinates of the central galaxy (the identification of central and satellite galaxies is provided in the mock catalog) as group center coordinates. These estimates are based on the 2D projected galaxy distribution and redshift information as in the real dataset. In this way we take into account both projection and incompleteness effects. These quantities provide the "observed" velocity dispersion, Σ SFR, Σ M$_*$ and N.

3.3.1 Reliability of group membership and velocity dispersion estimate

In order to check if our method is able to recover efficiently the membership of each group, we compare the completeness and the contamination of the membership obtained in our analysis with the original group membership identified by the FoF algorithm of the mock catalog. The completeness is estimated by computing the fraction of "true" members identified by our method. The contamination is estimated by calculating the fraction of interlopers (galaxy identified as group members by our method but not in the original mock catalog). Fig. 3.6 shows the completeness level (top panel) and the contamination level (bottom panel) of our group membership. The dashed histograms in both panels show the completeness and contamination levels obtained if we considered all members without any stellar mass cut. The completeness level is quite high ($> 90\%$) but on average 35% of the members are interlopers. If we apply a mass cut of $10^{10} M_\odot$, the completeness level reaches almost in all cases 100% with a much lower contamination fraction (solid histograms). It is clear that our method is much more robust in identifying rather massive galaxy members, which are likely more clustered in the phase space, than low mass galaxies. The red and blue histograms indicate the cases in which the velocity dispersion first guess is estimated from the mock catalog M_{200} without and with error, respectively (see below). After performing the same recovery test on the "incomplete" mock catalog, we check that the completeness level is driven by the mean simulated completeness of the sample, while the contamination level remains at the same values.

We estimate the "observed" velocity dispersion on the basis of this membership to take into account the effect of spectroscopic incompleteness. We measure the "observed" σ as in the real dataset. In other words, we base the velocity dispersion estimate on M_{200} and the relation between σ and r$_{200}$ as in Carlberg, Yee & Ellingson (1997) for groups with less than 10 members and on the dynamical analysis for groups with more than 10 galaxies. We consider also that our first guess for the velocity dispersion is affected by the uncertainty in the M_{200} in the observed dataset, which is retrieved via $L_X - M_{200}$ correlation. To take this into account we add a random error to the M_{200} of the group provided by the mock catalog. The scatter of the $L_X - M_{200}$ relation is qouted about 20% in the group mass regime based on the estimattion via stacking analysis (Leauthaud et al. 2010; Allevato et al. 2012). However, to be conservative, we use the $L_X - T_x$ relation and scatter reported in Sun (2011) to estimate a scatter in the $L_X - M_{200}$ relation. We use a value of 0.3 dex in our exercise. The green histogram of Fig. 3.7 shows the residual distribution between the "true" and "observed" velocity dispersion. The two values are in rather good agreement with a scatter of 0.1 dex. The main source of scatter is given by the spectroscopic incompleteness. Indeed, if we perform the same test by using the original "complete" mock catalog, the scatter decreases to 0.06 dex (blue histogram) and it is due to projection effects. The uncertainty in the first guess of the velocity dispersion does not affect significantly the final estimate. Indeed, without including this source of error the scatter decreases only to 0.09 dex (red histogram).

As shown in Fig. 3.7, the peak of the residual distribution is not zero but it shows that we tend to underestimate the true velocity dispersion by $\sim$20%. This shows that the Carlberg, Yee & Ellingson (1997) relation (used for estimating the first guess, in general, and the velocity dispersion for systems with less than 10 members, in particular) is not itself a source of scatter but it could cause a bias in the estimation of velocity dispersion.

We also point out that using the estimate of M_{200} for deriving the velocity dispersion first guess is a fundamental ingredient of our analysis. Indeed, if we use a constant value for the first guess, as usually done in the literature, we find that the scatter in the relation between "true" and "observed" velocity dispersion increased significantly as shown in Fig.

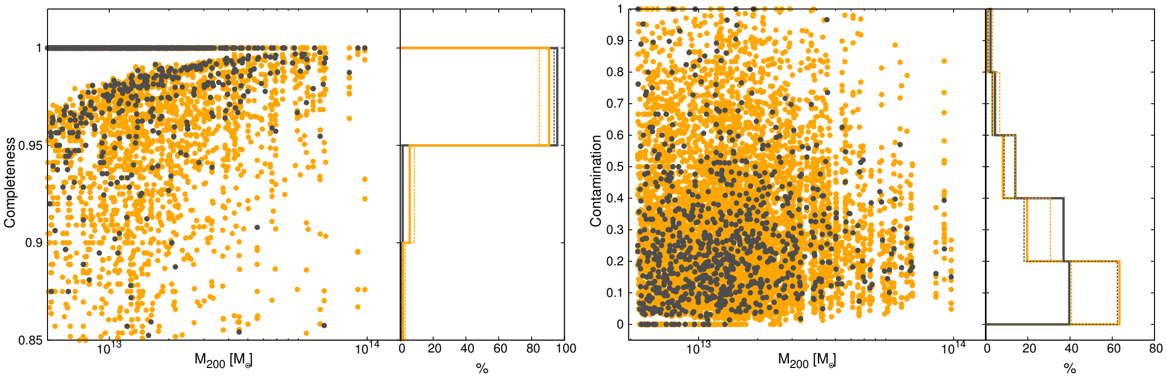

Figure 3.6: Completeness and contamination level of the member galaxies using the gapper estimator method with initial condition from M_{200} (grey points) and M_{200} with error (orange points) in the mock catalog. The right panels show corresponding histograms. The solid lines in the histograms show galaxies with $M_* > 10^{10} M_\odot$ and the dashed histograms are related to the whole sample.

3.8 (orange points) and there is no good correlation between the two quantities.

3.3.2 Reliability of Total M_* , Total SFR and HOD

As for the "observed" velocity dispersion, we also estimate the "observed" total stellar mass, total star formation rate and halo occupation distribution by applying our method to the "incomplete" mock catalogs to include the effect of projection and spectroscopic incompleteness. Each estimate is obtained after applying our stellar mass cut at $M_* > 10^{10} M_\odot$. We also apply the correction for incompleteness as described in Section 3.2.4. Figure 3.9 shows the comparison of the "true" and "observed" quantities. We find a rather good agreement between the two values in all cases. However, we notice a large scatter (0.3 dex) between the "true" and "observed" total SFR and a smaller scatter for "true" versus "observed" total M_* (0.17 dex) and HOD (0.15 dex). This different behavior of the scatter is due to two aspects. On average, the galaxies contaminating the group membership are field galaxies, likely less massive, due to mass segregation, and more star-forming than group galaxies. This is true in particular for the Millennium Simulation mock catalogs that are affected by an overabundance of red and dead galaxies in groups due to the satellite overquenching problem described in Weinmann et al. (2009). The result of this overquenching is that the level of the star formation in group galaxies is suppressed with respect to less crowded environments. Thus, in the case of groups with a low number of galaxies, the presence of even one contaminant with a high star formation rate can highly alter the total level of star formation activity. On the other hand, group galaxies tend to be rather massive and the addition of one or few field galaxies of average mass does not much affect the total M_* of the system. Thus, the uncertainty turns out to be much larger in the total SFR than in the total M_* or the HOD. Since in the local Universe we do not observe such a high abundance of red and dead satellite in groups as in the mocks

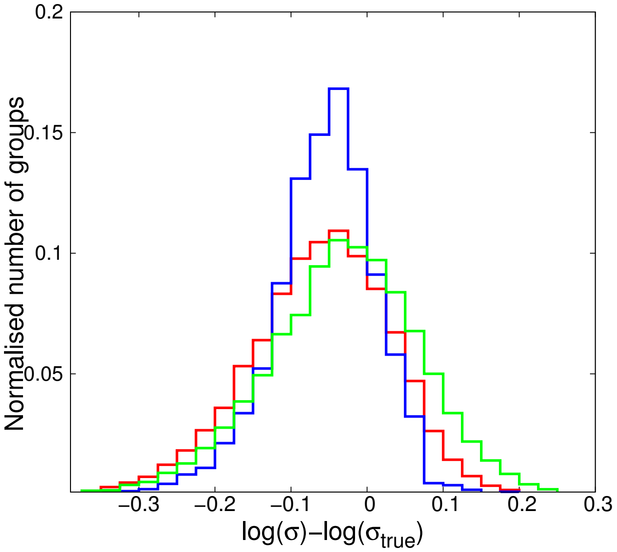

Figure 3.7: Distribution of the residuals of the logarithm of the "true" and "observed" velocity dispersion. The blue histogram shows the distribution of the residuals obtained from the original mock catalogs. The red histogram shows the distribution obtained if we take into account the error on M_{200} derived from L_X as done in the real dataset. The green histogram show the same diagram but with the "observed" velocity dispersion estimated on the basis of the "incomplete" mock catalog.

(Weinmann et al. 2009), it is likely that the uncertainty from the total SFR estimated in the Millennium Simulation mock catalogs is overestimating the actual uncertainty.

The low level contamination (see previous section) also explains why in some cases we observed a slightly larger number of galaxies in groups with respect to the "true" value.

3.4 Results

In this section we analyse several relations. First we study the correlation between the total SFR in groups versus the group global properties such as L_X, σ_v and M$_{200}$. Since L_X and σ_v are the only independent measurments and they also exhibit a relation with a tight scatter (Fig.3.1), we discuss in particular only the $\Sigma(SFR) - M_{200}$ relation to relate the evolution of the star formation activity of the group population to the total DM halo mass. However, all the relations derived are listed in Table 3.2. As previously mentioned, we divide our sample in two "low"and "high"redshift bins ($0.15 < z < 0.5$ and $0.5 < z < 1.1$). The two redshift bins are defined in order to have enough statistics and to sample a comparable fraction of the age of the Universe ($\sim$ 3 Gyr) at different epochs. However, we must take into account that the two bins are rather wide and a significant evolution in terms of stellar population can occur in galaxies in such a large amount of time. Thus, to check that the correlations observed in our analysis are not driven by the different evolutionary state of

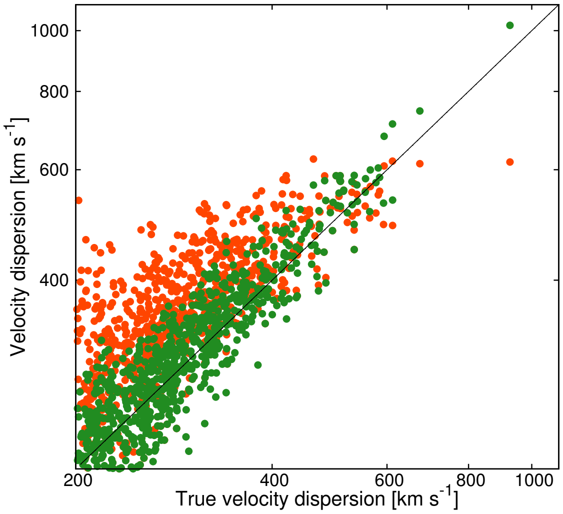

Figure 3.8: Velocity dispersion from gapper estimator vs. true velocity dispersion for mock groups. The orange points show the choice of constant initial velocity dispersion and the green one is based on the initial velocity dispersion computed from M_{200}

the galaxy population among the group sample of each redshift bin, we verify that there is no correlation between either the ΣSFR or ΣM_* or the number of galaxies per DM mass ($N(M_{200})$) with the galaxy group redshift. In the low redshift bin, a Spearman test confirms that in none of the considered cases there is a significant correlation, while there is a rather poor correlation between the total mass M_{200} and the group redshift as already visible in Fig. 3.4. Thus, at least in the low redshift bin, the different evolutionary state of the galaxy population of groups can be an additional source of scatter in the analyzed relations but it does not affect the slope of the relation.

However, at high redshift we observe a quite significant correlation between each quantity and the redshift. These correlations are induced by the strong correlation between M_{200} and the group redshift as visible in Fig. 3.4 at $z > 0.5$. This correlation is due to the X-ray selection that tends to select higher mass systems at high redshift. In order to take this selection effect into account we select a subsample of the high redshift groups in the redshift range $0.5 < z < 0.8$. This subsample comprises 38 systems and it does not show any correlation between M_{200}, $\Sigma(SFR)$ or M_* or HOD with the group redshift. We use this subsample to check whether the observed correlations between the aforementioned quantities and their slopes are driven by a redshift dependence.

We perform the analysis of each correlation by estimating the quantities within r_{200} and $2 \times r_{200}$. The results obtained within r_{200} are consistent with the corresponding results in $2 \times r_{200}$. We present in this section the results obtained within $2 \times r_{200}$ since this is the case with the best statistics.

Table 3.1: The results of the fitted line to log(N) vs. log(M_{200})

relation	z	Intercept	Slope	Spearman ρ	Spearman P
log(M_{200})-log(Σ SFR)	0.15-0.5	$-7.68^{\pm 2.32}$	$0.68^{\pm 0.17}$	0.3	0.02
log(M_{200})-log(Σ SFR)	0.5-1.1	$-11.32^{\pm 1.52}$	$1.00^{\pm 0.11}$	0.44	4e-6
log(L_X)-log(Σ SFR)	0.15-0.5	$-14.35^{\pm 5.9}$	$0.37^{\pm 0.14}$	0.29	0.02
log(L_X)-log(Σ SFR)	0.5-1.1	$-23.22^{\pm 3.9}$	$0.59^{\pm 0.09}$	0.47	3e-7
log(σ)-log(Σ SFR)	0.15-0.5	$-1.32^{\pm 1.69}$	$1.12^{\pm 0.5}$	0.26	0.02
log(σ)-log(Σ SFR)	0.5-1.1	$-2.60^{\pm 1.00}$	$1.93^{\pm 0.4}$	0.4	6e-5
log(M_{200})-log(Σ M_*)	0.15-0.5	$-1.82^{\pm 3.23}$	$1.02^{\pm 0.24}$	0.5	2e-4
log(M_{200})-log(Σ M_*)	0.5-1.1	$-1.52^{\pm 3.67}$	$0.99^{\pm 0.25}$	0.4	1e-5
log(L_X)-log(Σ M_*)	0.15-0.5	$-14.36^{\pm 4.53}$	$0.62^{\pm 0.09}$	0.52	8e-5
log(L_X)-log(Σ M_*)	0.5-1.1	$-11.63^{\pm 4.5}$	$0.55^{\pm 0.11}$	0.38	7e-5
log(σ)-log(Σ M_*)	0.15-0.5	$7.09^{\pm 0.93}$	$1.95^{\pm 0.38}$	0.47	1e-4
log(σ)-log(Σ M_*)	0.5-1.1	$6.88^{\pm 1.06}$	$2.02^{\pm 0.42}$	0.37	8e-5
log(M_{200})-log(N)	0.15-0.5	$-8.04^{\pm 1.98}$	$0.67^{\pm 0.14}$	0.5	1e-4
log(M_{200})-log(N)	0.5-1.1	$-10.87^{\pm 1.52}$	$0.90^{\pm 0.11}$	0.57	1e-8
log(L_X)-log(N)	0.15-0.5	$-17.13^{\pm 3.65}$	$0.43^{\pm 0.08}$	0.5	5e-4
log(L_X)-log(N)	0.5-1.1	$-21.39^{\pm 2.9}$	$0.52^{\pm 0.06}$	0.51	0
log(σ)-log(N)	0.15-0.5	$-2.27^{\pm 0.73}$	$1.34^{\pm 0.31}$	0.44	1e-4
log(σ)-log(N)	0.5-1.1	$-3.39^{\pm 0.75}$	$1.81^{\pm 0.3}$	0.43	1e-6
log(M_{200})-SF fraction	0.15-0.5	$1.97^{\pm 4.08}$	$-0.11^{\pm 0.3}$	-0.25	0.35
log(M_{200})-SF fraction	0.5-1.1	$6.94^{\pm 1.9}$	$-0.45^{\pm 0.13}$	-0.49	0.002
log(L_X)-SF fraction	0.15-0.5	$2.40^{\pm 8.02}$	$-0.045^{\pm 0.18}$	-0.251	0.34
log(L_X)-SF fraction	0.5-1.1	$13.3^{\pm 3.54}$	$-0.29^{\pm 0.08}$	-0.5	0.001
log(σ)-SF fraction	0.15-0.5	$1.31^{\pm 1.0}$	$-0.33^{\pm 0.41}$	-0.25	0.34
log(σ)-SF fraction	0.5-1.1	$2.94^{\pm 0.66}$	$-0.87^{\pm 0.26}$	-0.41	0.0097

Table 3.2: The table present all the best fit results of the ordinary least squares regression method performed on the low and high galaxy group sample. The first column indicates the considered $x - y$ relation. The second column indicates the redshift bin. The third and fourth columns indicate the intercept and the slope, respectively, of the best fit so that $y = slope * x + intercept$. The fifth column indicates the Spearman correlation coefficient and the sixth column indicate the value of the probability of the null hypothesis of no correlation among the considered quantities.

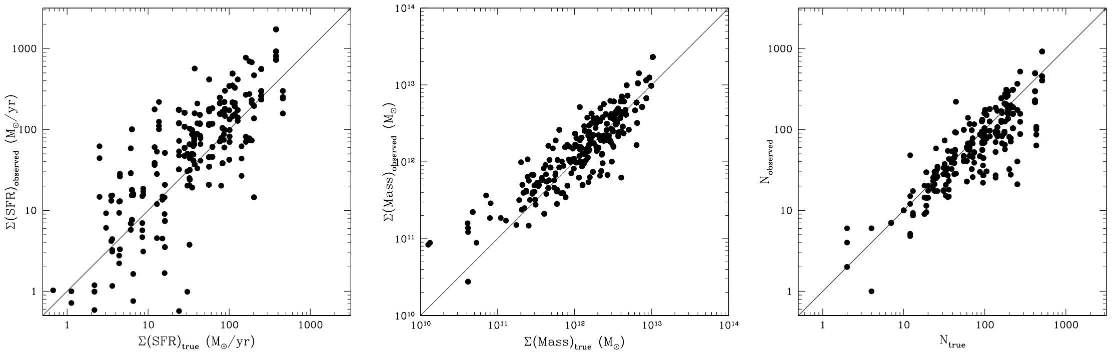

Figure 3.9: From left to right, "True" values of total SFR, total stellar masses and halo occupation number of the groups vs. our estimates in the "incomplete catalogs" with the same level of spectroscopic incompleteness of the surveys used in this work.

3.4.1 Σ SFR, Σ M_* vs M_{200} and HOD

The upper panel of Fig. 3.10 shows the ΣSFR-M_{200} relation in the low (blue points) and high (red points) redshift bins. A Spearman correlation test shows a much more significant positive correlation in the high-z sample and a very mild correlation in the low-z one (see Table 3.2).

We first investigate the possibility that the lack of a significant correlation in the low redshift bin could be due to the low number statistics. Indeed, the low redshift bin contains 31 galaxy groups. This relatively low number together with the scatter due to the differences in the age of the stellar population of the group galaxies in such a wide redshift bin ($\sim$ 3Gyrs), could prevent us from observing a correlation. To check this possibility we use as a reference sample of nearby groups the optically-selected group sample of Yang et al. (2007) drawn from the SDSS. We select in particular a subsample of groups at $z < 0.085$. This is done because the SDSS spectroscopic sample is complete at masses $> 10^{10} M_\odot$ below this redshift limit (see Peng et al. 2010). As shown in the left panel of Fig. 3.11, the total SFR and total mass of the nearby groups are strongly correlated. We do not see, however, a simple linear correlation in the log-log space but a double slope, flatter ($\Sigma SFR \propto M_{200}^{0.56\pm0.01}$) at $M_{200} < 10^{13} M_\odot$ and steeper ($\Sigma SFR \propto M_{200}^{0.89\pm0.03}$) at $M_{200} > 10^{13} M_\odot$. As explained by Yang, Mo & van den Bosch (2008) the break at the low-mass end can be explained by the Halo Occupation Statistics. Indeed, we observe the same sharp break in the HOD of the Yang et al. (2007) subsample at $N(M > 10^{10} M_\odot) \sim 1$ (central panel of Fig. 3.11). This break indicates that, on average, below $M_{200} \sim 10^{13} M_\odot$ only the central galaxy has a mass above $M > 10^{10} M_\odot$ and satellites have lower masses. The existence of a significant correlation between ΣSFR and M_{200} in the nearby groups and in the more populated high redshift group sample would suggest that we should likely observe a correlation also in the low redshift bin. Thus, to check if the low number statistics and the scatter are hiding such a correlation, we perform the following test. We extract randomly 5000 times the same number of objects as in the intermediate redshift sample from the Yang et al.

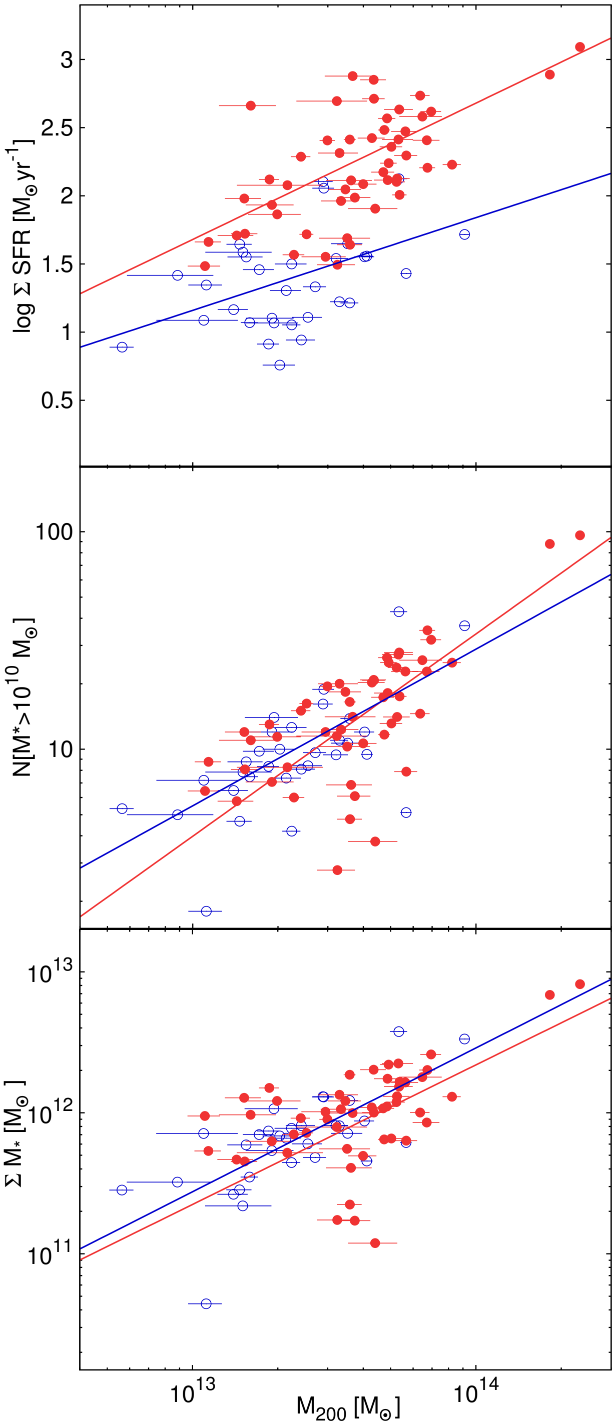

Figure 3.10: Σ SFR- (upper panel), HOD- (middle panel) and Σ M_*- (bottom panel) M_{200} relations for memebr galaxies with $M_* > 10^{10}$ $M_\odot$ in the low-z sample (0.15<z<0.5, in blue) and the high-z groups (0.5<z<1.1, in red). The blue and red lines show the best-fitting using the ordinary least squares regression method presented by Akritas & Bershady (1996). The total star formation activity in high-z groups is higher with respect to the low-z sample at any mass by 0.8 ± 0.12 dex. The HOD- and Σ M_*- M_{200} are consistent with a linear relation in both redshift bins with no evolution since z∼1.1.

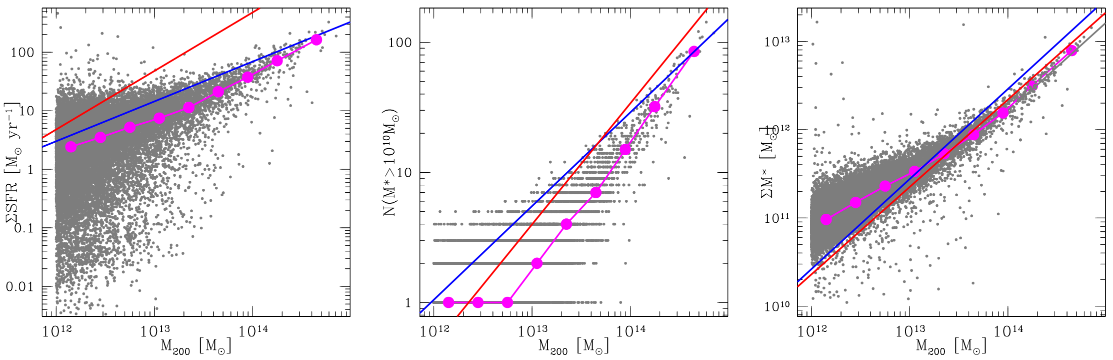

Figure 3.11: Σ SFR- (left panel), HOD- (middle panel) and Σ M_*- (right panel) M_{200} relations for a subsample of Yang et al. (2007) optically selected catalog at $z < 0.085$ (grey points). The magenta points connected by the solid line shows the median per bin of M_{200} in the Yang et al. (2007) subsample. The blue solid lines show the best fit relation of our low-z sample and the red solid lines show the best fit relation of our high-z group sample. The Σ SFR and total mass of the nearby groups are strongly correlated. We do not see, however, a simple linear correlation in the log-log space but a double slope, flatter ($\Sigma SFR \propto M_{200}^{0.56\pm0.01}$) at $M_{200} < 10^{13} M_\odot$ and steeper ($\Sigma SFR \propto M_{200}^{0.89\pm0.03}$) at $M_{200} > 10^{13} M_\odot$.

(2007) subsample in the same mass range. We perform for each extraction the Spearman test between ΣSFR and M_{200}. In 65% of the cases we observe a correlation between the two quantities of the same significance as in our low redshift sample. Thus, we conclude that the mild correlation observed in our low redshift group sample is due to low number statistics in addition to the scatter due to the width of the redshift bin.

To further check if the positive correlation between M_{200} and the redshift of the groups in the high redshift bin can induce the positive correlation observed between ΣSFR and M_{200}, we consider the subsample of the high-z groups, described above, at $0.5 < z < 0.8$. We perform the Spearman test and the ordinary least squares regression method (Akritas & Bershady 1996) in the log-log space of ΣSFR and M_{200} for such subsample and we find a correlation significance and slope to be perfectly consistent (within 1σ) with the results obtained with the whole high redshift sample. The effect of the addition of the remaining $z > 0.8$ groups is only to increase the scatter of the relation by 17%. Thus, we conclude that the positive correlation is not induced by a redshift bias in our group sample and that the positive correlation of the ΣSFR-M_{200} relation is real.

By comparing the ΣSFR-M_{200} relation at different redshifts, we see a clear evolution in the level of star formation activity. Indeed, the total star formation activity in high redshift groups is higher with respect to the low redshift sample. By dividing the two samples in several M_{200} bins, we estimate a mean difference of 0.8 ± 0.1 dex between high and low redshift groups. A milder difference (0.35 ± 0.1 dex) is observed between the [0.15-0.5] redshift bin and the groups at $z < 0.085$ of Yang et al. (2007). In order to check if this evolution is happening faster in the group galaxy population than the field population, we

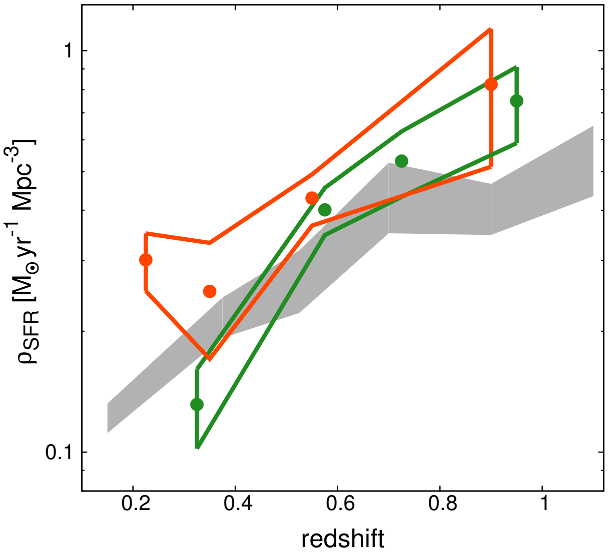

Figure 3.12: Redshift evolution of comoving SFR density for group galaxies with $M_{200} < 3 \times 10^{13}$ (orange points) with its corresponding uncertainty (orange lines) and group galaxies with $M_{200} > 3 \times 10^{13}$ (green points) with its corresponding uncertainty (green lines). The orange and green points in the figure show the average SFR density per redshift bin. The grey shaded region shows the comoving SFR density of Gruppioni et al. (2013) for the global galaxy population with the same mass cut as in this work.

estimate the SFR density in each group region by dividing the ΣSFR by the comoving volume contained within r_{200}. We compare the SFR density as a function of redshift with the global relation obtained by Gruppioni et al. (2013), based on PACS data, for galaxies with mass above $M* > 10^{10} M_\odot$. We confirm the result of Popesso et al. (2012) that, above $z \sim 0.3$ the star formation activity per unit of volume is higher in the groups with respect to the global relation (grey shaded region in Fig. 3.12), with a slightly higher value in the lower mass groups ($M_{200} < 3 \times 10^{13}$, orange contour) with respect to the more massive halos ($M_{200} > 3 \times 10^{13}$, green contour). In addition, as discussed above, the SFR density of the more massive halos is declining faster than the global relation. Since the whole galaxy population should be dominated by lower mass halos, $M_{200} \sim 10^{12-12.5} M_\odot$ according to the predicted dark matter halo mass function (e.g. Jenkins et al. 2001; Tinker et al. 2008) and to the estimate of Eke et al. (2005), this would imply that the level of SF activity is declining more rapidly since $z \sim 1$ in the more massive halos than in the more common lower mass halos. This confirms a "halo downsizing" effect as discussed in Popesso et al. (2012). We also point out that the result does not change if we do not calibrate SFR_{SED} (see §3.2.3). The effect of this calibration is just to slightly reduce the scatter of the relation.

The central and bottom panels of Fig. 3.10 show the HOD and the Σ M_*-M_{200} relations in the two redshift bins. In these cases we see a very tight relation in both samples as confirmed by a Spearman test at 99% confidence level (see Table 3.2). This is not surprising. Indeed, while the stellar mass function of the galaxy population, and of the group galaxy population in particular, is not evolving significantly since redshift $\sim$1 as shown in Ilbert et al. (2010) and Giodini et al. (2012), respectively, the SF activity of the Universe is dropping down by an order of magnitude in the same time window (see e.g. Magnelli et al. 2013 for the whole galaxy population, Popesso et al. 2012 for groups and clusters in particular). As a consequence the spread in ΣSFR is much higher than the spread of ΣM_*. Thus, we see a strong correlation between Σ M_* and M_{200} and only a mild correlation between ΣSFR and M_{200}.

The HOD is consistent with a linear relation in the high redshift bin and marginally consistent with it (within 2.5 σ, see Table 3.2) in the low redshift bin. This is probably due to a bias induced by our selection of groups with more than 5 members, needed to properly define the group redshift and membership. Indeed, this cut makes more likely that we favor the selection of rich groups for a given mass, in particular among the low mass groups. Since the mean M_{200} of the low redshift sample is a factor of two lower than the mean mass of the high redshift sample, this bias is more significant in the low redshift sample at low masses, leading to a sub-linear HOD. Indeed, the HOD obtained using the Yang et al. (2007) group subsample at $z < 0.085$ and with the same stellar mass cut is highly consistent with a linear relation for halos with masses $M_{200} > 10^{13} M_\odot$ as discussed above (see central panel of Fig. 3.11). As for the ΣSFR-M_{200} relation, also the Σ M_*-M_{200} relation shows a double slope, $\Sigma M_* \propto M_{200}^{0.61\pm0.002}$ at $M_{200} < 10^{13} M_\odot$ and $\Sigma M_* \propto M_{200}^{1.00\pm0.07}$ at $M_{200} > 10^{13} M_\odot$. Since the Yang et al. (2007) groups with masses below $M_{200} < 10^{13} M_\odot$ typically contain only the central galaxy, the relation below this limit shows actually the mean relation between the central galaxy stellar mass and the halo mass. We should note that different fitting methods on our sample lead to perfectly consistent results.

We point out that, according to Popesso et al. (2007), groups exhibit a much flatter radial density profile with respect to more massive systems. Thus, the correction for projection effects for groups should be higher than for more massive systems. However, our sample covers a much lower and narrower mass range with respect to the one of Popesso et al. (2007) and we do not know accurately the radial density profile of our group sample. We point out that the correction is of the order of 20-15% and it would not change significantly our results given the relatively large error on the slope of the relation. We also notice that the slope of the observed relation is consistent with the one observed in galaxy clusters at much higher masses (Marinoni & Hudson 2002; Pisani, Ramella & Geller 2003; Lin, Mohr & Stanford 2004; Popesso et al. 2007).

We do not observe any evolution in the HOD since $z \sim 1.1$. Similarly we do not observe evolution in the relation between the total stellar mass in groups and the total mass, in agreement with the results of Giodini et al. (2012) (see bottom panel of Fig. 3.10 and right panel of Fig. 3.11).

The picture emerging from Fig. 3.10 and 3.11 is that massive groups of $M_{200} \sim 10^{13-14} M_\odot$ at z >0.5 have already accreted the same amount of mass and have the same number of galaxies as the low redshift counterparts. Indeed, these massive halos are not predicted to increase their total mass by a large factor. Stewart et al. (2008) show that 35% (80%) of the halos with mass $\sim 10^{13} M_\odot$ ($\sim 10^{14} M_\odot$) increase their mass by 30% (10%)

through a merger event in the last 10 Gyr. Thus, the same is true for their stellar mass and number of galaxies. This implies that the most evident evolution of the galaxy population of the most massive systems is in terms of the quenching of their star formation activity. This also implies that the group galaxy population should progressively move from high to low specific star formation rate from $z \sim 1$ to $z \sim 0$ and move away from the Main Sequence more rapidly than galaxies in lower mass halos, in agreement with the result of Ziparo et al. (2014).

3.4.2 Fraction of MS galaxies vs. M_{200} and velocity dispersion

Often the level of star formation activity in groups and clusters is estimated through the fraction of star-forming galaxies. In order to compare with previous results, we analyze in this section the evolution of the fraction of star-forming galaxies as a function of the group halo mass. We define the star-forming galaxies as the ones lying on the Main Sequence (Elbaz et al. 2007). In order to identify the main sequence at different redshifts, we extrapolate the MS relation at the mean redshift of each redshift bin by interpolating the MS relation of Peng et al. (2010), Noeske et al. (2007b) and Elbaz et al. (2007). According to these works the scatter of the relation is ~ 0.3 dex. Figure 3.13 illustrates the distribution of the residual $\Delta(SFR) = SFR_{MS} - SFR_{observed}$, where SFR_{MS} is the SFR given by the MS relation at a given mass and $SFR_{observed}$ is the observed SFR of a galaxy at that mass. The distribution shows a well known bimodal distribution with the Gaussian representing the MS location with peak around 0 residual, and a tail of quiescent/low star-forming galaxies at high positive values of Δ SFR. This distribution is reminiscent of the bimodal behavior of the U-R galaxy color distribution observed by Strateva et al. (2001) in the SDSS galaxy sample. At all redshifts, the value Δ SFR = 1 turns out to be the best separation for MS galaxies. It is also consistent with 3σ of main sequence uncertainty. The fraction of star-forming galaxies is, then, defined as the ratio between the number of SF galaxies with $M_* > 10^{10} M_\odot$ and the total number of galaxies with $M_* > 10^{10} M_\odot$. We do not find any correlation in the low redshift bin with the halo mass (see Table 3.2). This is confirmed also by a lack of correlation in the Yang et al. (2007) group subsample at $z < 0.085$. We observe a significant anti-correlation with the halo mass in the high redshift bin, as confirmed by a Spearman test (see Fig. 3.14). Fig. 3.15 shows the relation between fraction of star-forming galaxies and velocity dispersion for the galaxy groups with more than 10 spectroscopic members for which we have a reasonable estimate of the galaxy velocity dispersion. The magenta line in Fig. 3.15, is the upper envelope of Poggianti et al. (2006) for the EDisCS clusters and groups at z=0.4-0.8. Even in this case, high mass systems seem to be already evolved at z$\sim$1 by showing a fraction of star-forming galaxies consistent with the low redshift counterparts at $z < 0.085$, where we measure a mean constant fraction of SF galaxies of 0.28 ± 0.5.

Given the almost linear relation between the ΣSFR and M_{200} in the high-z sample, this implies that most of the contribution to the total SFR of the most massive systems ($M_{200} \sim 10^{14} M_\odot$) is given by few but highly star-forming galaxies, while in lower mass systems ($M_{200} \sim 10^{13} M_\odot$) it is given by more star-forming galaxies of average activity.

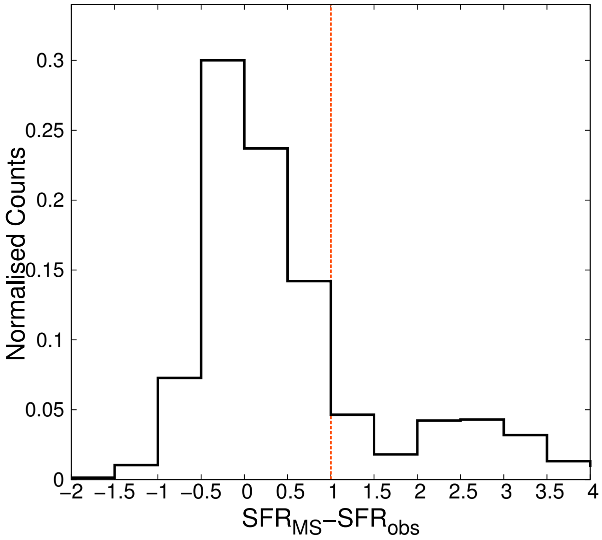

Figure 3.13: Normalized distribution of differences between Main Sequence SFR and observed SFR of member galaxies (Δ SFR). The orange vertical line shows our limit for separation MS member galaxies.

Thus, this would still indicate a faster evolution in the more massive systems in terms of star formation activity with respect to lower mass groups.

3.4.3 Comparison with the mock catalog

To compare our results with theory, we look at the results based on the mock catalog of the Millennium Simulation as described in Sect. 3.2.6. We analyze the same relations studied in our work by extracting from the mock catalog a sample of groups in the same mass range and redshift range adopted in our study. The quantities Σ M_*, Σ SFR and number of galaxies per halo mass are calculated by following the same criteria used for the real dataset. In addition, we also estimate the properties of the groups at $1<z<2$ to completely follow the evolutionary trends of galaxies up to $z \sim 2$. Fig. 3.16 shows the predictions of the same relations presented in Fig. 3.10. The top panel of the figure shows the total SFR of the mock groups as a function of their halo masses. As already known, the semi-analytical models of the Millennium simulation underpredict the level of star formation activity of the galaxy population and, in particular, of the group and cluster galaxies. Indeed, even the level of activity of the high redshift groups is well below the level of the low redshift groups of our sample (dotted blue line in the plot). This class of models assumes that, when galaxies are accreted onto a more massive system, the associated hot gas reservoir is stripped instantaneously. This, in addition to the AGN feedback, induces a very rapid decline of the star formation histories of satellite galaxies, and contributes to create an excess of red and passive galaxies with respect to the observations (e.g. Wang et al. 2007). More recent high resolution simulations do not help in improving the results (Weinmann,

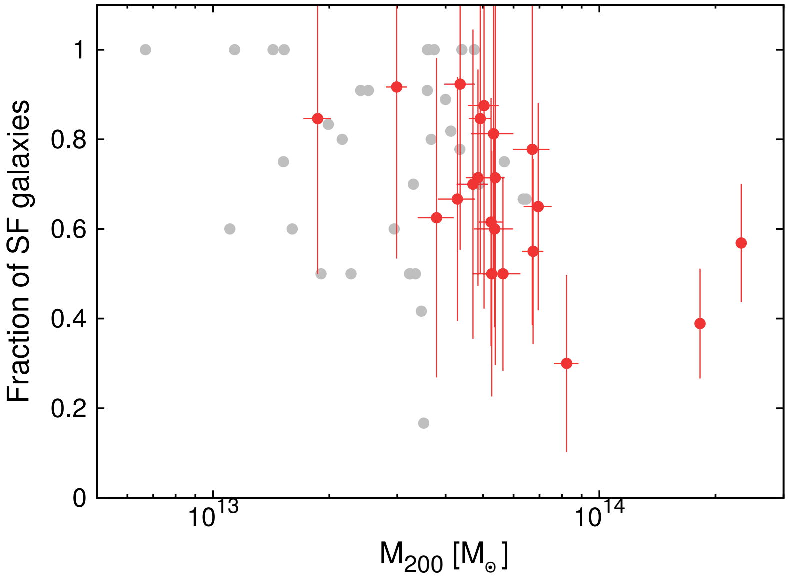

Figure 3.14: Fraction of star-forming galaxies as a function of halo mass for the high-z sample with more than 10 members (red points) and less than 10 members (in grey). Spearman test confirms a significant anticorrelation for the high-z sample but no correlation for low-z one.

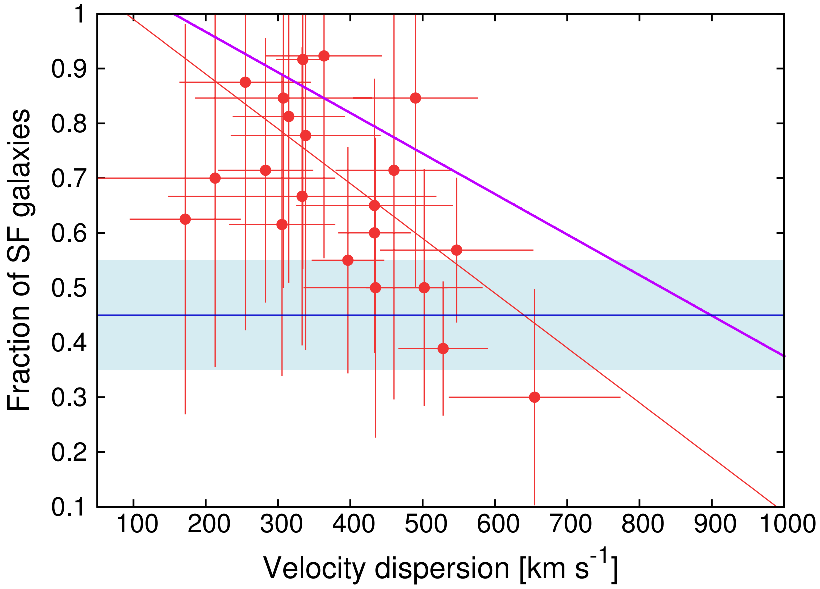

Figure 3.15: Fraction of star-forming galaxies vs. velocity dispersion for groups in the high-z sample with more than 10 spectroscopic members. The magenta line is the upper envelope of Poggianti et al. (2006) for the EDisCS clusters and groups at z=0.4-0.8. The horizontal blue line and the shaded blue area show the median fraction of star-forming galaxies and its corresponding one sigma error in low-z groups.

Neistein & Dekel 2011; Guo et al. 2011). This is known as the "overquenching problem" for satellites galaxies. Over 95% of the cluster and group galaxies within the virial radius in the local simulated Universe are passive (Guo et al. 2011), at odds with observations (e.g. Weinmann et al. 2006; Kimm et al. 2009; Liu et al. 2010; Hansen et al. 2009; Popesso et al. 2005). Indeed, as Fig. 3.17 shows, galaxies in mock groups reside under the main sequence in any redshift bin, indicating that the evolution even in group galaxies is happening at $z > 2$. This is at odds with our results since in the previous section we have shown that in the low mass groups most of the galaxies above $10^{10} M_{\odot}$ are Main Sequence galaxies.

We do not observe any evolution in the HOD (central panel of Fig. 3.16), which is consistent also quantitatively with the HOD observed in our group sample. In the same way we do not observe any evolution in the Σ $\mathrm{M}_{*} - M_{200}$ relation but we also observe a quantitative discrepancy with respect to observations. Indeed, at any redshift the total stellar mass in groups is underpredicted with respect to the observed one. This is understandable given the much lower star formation rate of the simulated group galaxies with respect to the observations, which limits the galaxy stellar mass growth.

3.5 Summary and conclusion

In this paper we provide an analysis of the evolution of the total star formation activity, total stellar mass and HOD by using one of the largest X-ray selected samples of galaxy groups with secure spectroscopic identification on the major deep field surveys (ECDF, CDFN, COSMOS, AEGIS) up to z∼1.1. We first check the robustness of our method in determining the group velocity dispersion and membership extensively usingn mock catalogs and check the possible biases induced by the spectroscopic incompleteness of the surveys used in our analysis. We show that for a robust measurement of the group velocity dispersion and group membership definition even a poor first guess of the velocity dispersion derived from the X-ray luminosity is essential for a reliable result. We compare our results with the one based on an optically-selected sample of groups at $z < 0.085$ in order to fully follow the evolution of the galaxy population in groups to the local Universe. We list below our main results:

- We observe a clear evolution in the level of star formation activity in galaxy groups. Indeed, the total star formation activity in high redshift groups (0.5 < z <1.1) is higher with respect to the low redshift sample (0.15 < z <0.5) at any mass by almost 0.8 ± 0.1 dex. A milder difference (0.35 ± 0.1 dex) is observed between the [0.15-0.5] redshift bin and the groups at $z < 0.085$. This evolution seems to be much faster than the one observed in the whole galaxy population (Gruppioni et al. 2013), dominated by lower mass halos ($M_{200} \sim 10^{12-12.5} M_{\odot}$, Jenkins et al. 2001; Tinker et al. 2008; Eke et al. 2005). This would imply that the level of SF activity is declining more rapidly since $z \sim 1.1$ in the more massive halos than in the more common lower mass halos, confirming a "halo downsizing" effect as discussed by Popesso et al. (2012).

- The HOD and the total stellar mass-M_{200} relation are consistent with a linear relation

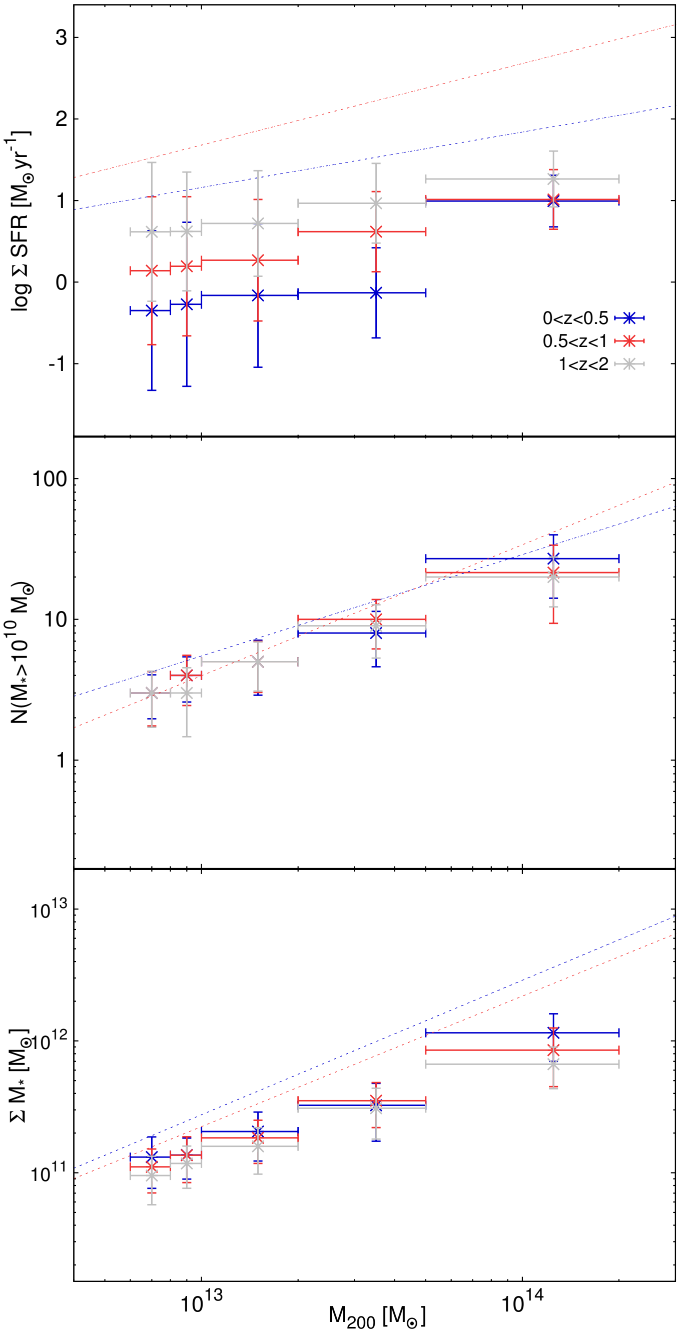

Figure 3.16: Σ SFR- (upper panel), HOD- (middle panel) and Σ M_*- (bottom panel) M_{200} relations for the groups with 0<z<0.5 (in red) and 0.5<z<1 (in blue) and with 1<z<2 (in grey) for the mock catalog. The dashed lines show the results based on the observations.

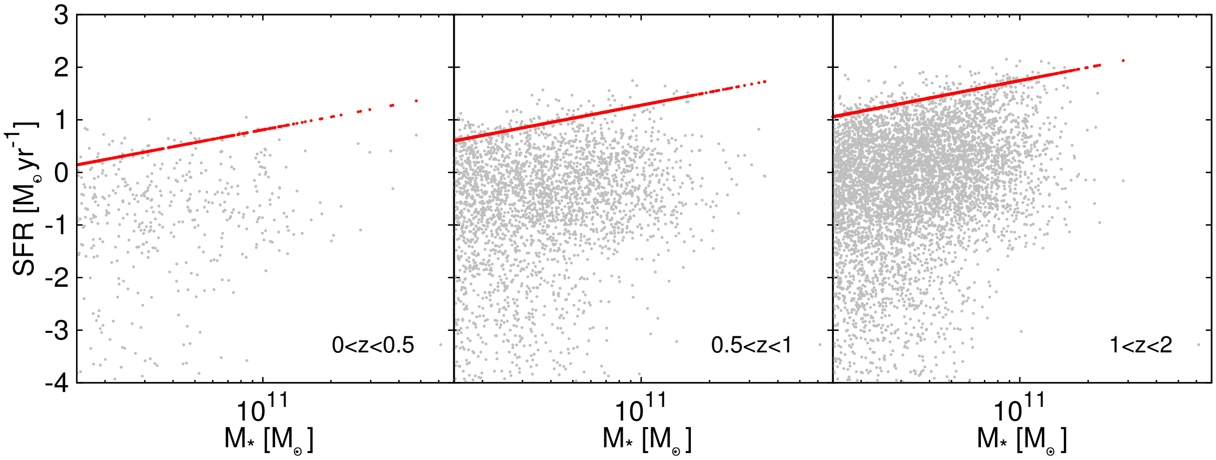

Figure 3.17: SFR as a function of stellar mass for the member galaxies in the mock catalog. The red points show the position of the main sequence for the lowest redshift (z= 0, 0.5 and 1 from left to right, respectively) in each bin.

in all redshift bins in the M_{200} range considered in our analysis. We do not observe any evolution in the HOD since $z \sim 1.1$. Similarly we do not observe evolution in the relation between the total stellar mass in groups and the total mass, in agreement with the results of Giodini et al. (2012). The picture emerging from our findings is that massive groups at $M_{200} \sim 10^{13-14} M_{\odot}$ have already accreted the same amount of mass and have the same number of galaxies as the low redshift counterparts, as predicted by Stewart et al. (2008). This implies that the most evident evolution of the galaxy population of the most massive systems acts in terms of quenching their galaxy star formation activity. This also implies that the group galaxy population should progressively move from high to low specific star formation rates from $z \sim 1$ to $z \sim 0$ and rapidly move away from the Main Sequence since $z \sim 1$ consistent with the recent results of Ziparo et al. (2013) based on a similar dataset.

- The analysis of the evolution of the fraction of SF galaxies as a function of halo mass or velocity dispersion shows that high mass systems seem to be already evolved at z∼1 by showing a fraction of star-forming galaxies consistent with the low redshift counterparts at $z < 0.085$. Given the almost linear relation between the ΣSFR and M_{200} in the high-z sample, this implies that most of the contribution to the total SFR of the most massive systems ($M_{200} \sim 10^{14} M_{\odot}$) is given by few highly star-forming galaxies, while in lower mass systems ($M_{200} \sim 10^{13} M_{\odot}$) is given by many galaxies of average activity. This would be an additional sign of a faster evolution in the more massive systems in terms of star formation activity with respect to lower mass groups. Thus, it would confirm the “halo downsizing” effect.

- The comparison of our results with the prediction of the Millennium Simulation semi-analytical model confirms the known problem of the models. We confirm the strong bias due to the “satellite overquenching” problem in suppressing significantly the SF activity of group galaxies (more than an order of magnitude) at any redshift with respect to observations. The HOD predicted by the simulations is remarkably in agreement with the observations. But due to the low SF activity of galaxies in massive halos, the models predict also a lower total stellar mass in groups with respect to the observed one at any redshift.

Our results support a scenario in which the quenching of SF occurs earlier in galaxies embedded in more massive halos, though we are considering a quite narrow halo mass range. This would be consistent with the results obtained by Popesso et al. (2012) in a similar redshift range but in a broader mass range, which includes also galaxy clusters. Other evidences in the literature support the differential evolution of the SF activity in massive halos with respect to the field or lower mass halos. For instance, the formation of the galaxy red sequence, which leads to the local dichotomy between red and blue galaxies, happens earlier in groups than in the field especially at high stellar masses (Iovino et al. 2010; Kovač et al. 2010b; Mok et al. 2013; Wilman et al. 2009; Wilman & Erwin 2012). Morphological transformations are in place in groups at $z<1$, leading to a transient population of “red spirals” not observed in the field (Balogh et al. 2009; Wolf et al. 2009; Mei et al. 2012). There is also evidence that at $z\sim1$ there is a flattening of the SFR-density relation (Elbaz et al. 2007; Popesso et al. 2011; Cooper et al. 2008; Ziparo et al. 2014) with respect to the local anti-correlation. Ziparo et al. (2014) find on the very same dataset that the differential evolution of the groups galaxies with respect to field is due to the fact that star-forming group galaxies are perfectly on the Main Sequence at $z\sim1$ whereas at lower redshift they are quenched, thus, dropping off the MS quicker than field galaxies towards the region of SF quiescence.

What is causing this differential evolution as a function of the halo mass? According to Peng et al. (2010) massive galaxies, as the ones considered in our sample, evolve mostly because of an internally driven process, called ’mass quenching’, caused perhaps by feedback from active galactic nuclei. But since this process is unlikely to be more efficient in quenching SF of massive galaxies in massive halos than in other environments as the stellar mass functions do not change significantly in groups with respect to field (Giodini et al. 2012), the “environmental quenching” must be the main mechanism for quenching the SF of the most massive satellites in massive halos. Which kind of process is causing this “environmental quenching” is still quite unknown. Ram-pressure stripping (Gunn & Gott 1972) and starvation (Larson, Tinsley & Caldwell, 1980) are two plausible candidates for producing this quenching. Ram-pressure stripping ”quench” star formation immediately (Abadi, Moore & Bower, 1999) as it can sweep Interstellar medium out of a galaxy. Starvation, caused by the removal of the hot gas halo reservoirs of galaxies which leads to cut of the supply of cold gas in the galaxy is also a likely candidate. Tidal galaxy-galaxy encounters or the interaction with the intra-cluster/intra-group medium can lead to the removal of galaxy hot gas reservoirs which inducing starvation. Therefore, starvation should quench SF earlier in more massive halos than in low mass halos, as we observe.

Cen (2011) propose that this differential evolution could be explained simply in terms of the current theory of gas accretion that hinges on the cold and hot two-mode accretion model (Kereš et al. 2005; Dekel & Birnboim 2006). The halo mass is the main determinant of gas accretion: large halos primarily accrete hot gas while small halos primarily accrete cold gas. The overall heating of cosmic gas due to formation of large halos (such as groups and clusters) and large-scale structure causes a progressively larger fraction of halos to inhabit regions where gas has too high entropy to cool to continue feeding the residing galaxies. The combined effect is differential in that overdense regions are heated earlier and to higher temperatures than lower density regions at any given time. Because larger halos tend to reside in more overdense regions than smaller halos, the net differential effects would naturally lead to both the standard galaxy downsizing effect and the halo downsizing effect.

The current analysis can not provide evidences in favour of one of these scenarios. Further analysis must be conducted to study the cold gas content of galaxies in halos of different masses, to distinguish between the different possibilities and identify the process responsible for the "environmental quenching".

Chapter 4

SFR-M plane

4.1 Introduction

During the past decade, there have been several efforts to find how and if the environment might affect the properties of galaxies. One way to trace the evolution of galaxies during the cosmic time is to look at their position in the SFR-Mass plane. Several studies have already shown there is a tight correlation between the SFR and the stellar masses of the bulk of the star forming galaxy population at least over the past 10 Gyr with a dispersion of ~ 0.3 dex (Noeske et al. 2007b; Elbaz et al. 2007; Daddi et al. 2007; Peng et al. 2010). The zero point of this relation evolves during the cosmic time towards higher values indicating that the level of star formation activity was much higher in the past which is consistent with the decline of the cosmic star formation rate density of galaxies since z$\sim$1 (Lilly et al. 1996; Le Floc'h et al. 2005). Quiescent galaxies are mainly located under this main sequence (MS) and in a more scattered cloud. Noeske et al. (2007b) using field galaxies in AEGIS field with quantitative HST morphologies (Gini/M20: Lotz 2007; CAS: Conselice 2003) classified < 25 %of galaxies on the MS as early types (E, S0, Sa). In agreement with this work, Wuyts et al. (2011) using statistically significant sample find evidence for a correlation between galaxy structure and stellar populations (i.e., a Hubble sequence) to be in place already three billion years after the Big Bang. In the local universe existence of such a correlation has been extensively studied by Kauffmann et al. (2003) and Brinchmann et al. (2004). The existence of the so called morphology-density relation could set, then, a link between the location of a galaxy in the SFR-stellar mass plane and the environment where the galaxy lives. Indeed, since early type galaxies mainly populate high density regions (groups and clusters) and late type galaxies are generally more isolated, the relation between the morphology and the galaxy location with respect to the MS could be translated into a relation with the environment.

According to Noeske et al. (2007b) the existence of the MS at any redshift reflects that the same set of few physical processes governs the SF activity in galaxies. If internal processes, like the mass quenching proposed by Peng et al. (2010), is mostly responsible for moving the galaxies along and across the MS, the location of a galaxy with respect to the MS should be set by its mass and should be, instead, quite independent from the environment. If, instead, the environment plays a role in affecting the SF activity of galaxies, the position of the MS should change in different environments. There is still a lack of comprehensive study of the position of galaxies relative to the MS in different environments. Peng et al. (2010) using SDSS and zCOSMOS surveys study the dependence of the location of galaxies with respect to the MS on the environment defined through the local galaxy density. They do not observe any dependence. However, they analyse the MS of only blue galaxies, thus, inducing strong selection effects. Indeed, Weinmann et al. (2006) show that among SDSS galaxies there is a strong contamination of red galaxies with high star formation rate in high density region that could be a transient population. In addition, we will also show in the next paragraph that the galaxy density field is not a good representation of the environment.

In this chapter, we intend to examine whether the position of bulk of SF galaxies depends on environment. In addition, we will analyse the dispersion of the MS in different bins of stellar mass and check whether this depends of the environment. We perform this analysis in two redshift bins to understand if there is any evolution of possible environmental dependence. This will be based on a definition of the environment based on the total mass of the host dark matter halo.

4.2 Data

For the purpose of this work, we use the dataset defined in the previous chapter. Briefly, we use a sample of member galaxies of a X-ray selected groups drawn from the ECDFS, CDFN, AEGIS and COSMOS X-ray survey. This group sample comprises 83 groups with masses ranging from $10^{12.5}$ to $10^{14.5}$ $M_{\odot}$ and in the redshift range [0.15-1.1]. The group membership is obtained via dynamical analysis. The method and its reliability for deriving group members are explained in the previous chapter. Briefly, we use all galaxy groups with flag=1 & 2 (reliable identification) in four mentioned fields. Using dynamical velocity dispersion (σ) for those with more than 10 spectroscopic members and X-ray derived velocity dispersion for other ones, we choose member galaxies inside 2 × r_{200} from X-ray center and 3σ in the line of sight direction from the group redshift. In order to follow the evolution of the position of group galaxies with respect to the MS, we divide the sample of group galaxy members in two redshift bins: one at low redshift ($0.15<z<0.5$) and one at high redshift ($0.5<z<1.1$) bins. In total we have 424 galaxies in low redshift bin and 511 galaxies in high redshift bin.

4.2.1 The local galaxy density

Most of the literature regarding the study of the role of the environment in the galaxy evolution define the environment through the local galaxy density field (e.g. Peng et al. 2010, 2012). Indeed, according to simulations, the galaxy density distribution should trace the mass density field with a *bias* that depends on the galaxy stellar mass, since massive systems tend to be more clustered while low mass objects are more uniformly distributed. However, the accuracy with which the local galaxy density field can be reconstructed has to cope with the observational limits. Indeed, most of the density estimators, such as the nearest N^{th} neighbour or the density of galaxies within a fixed volume, require accurate spectroscopic redshifts of a rather complete sample of galaxies. However, any spectroscopic survey has to cope with a selection function and with an incompleteness level. In addition, any density estimator has to cope with projection and selection effects. All this makes quite complicated, to different extent, the proper definition of the galaxy density field. To show this aspect we use the mock catalogue of Kitzbichler & White (2007) described in the previous chapter. We use different flavours of the two major density estimators mentioned above to check if the reconstructed density field can properly trace the underlying mass distribution. Namely we check how tight is the correlation between the local galaxy density around each simulated galaxy and the mass of its parent dark matter halo. Left panel of Fig. 4.1 shows the correlation between the local galaxy density field and the parent halo mass for a sample of simulated galaxies with known actual 3D position. The correlation is rather tight and it shows a large dispersion only at very low parent halo masses. The right panel of the same figure shows, instead, the relation obtained by introducing the projection effects due to the use of *ra*, *dec* and redshift information and the selection effects due to a simulated spectroscopic selection function. For this latter plot we use the incomplete catalogue extracted from the Kitzbichler & White (2007) catalogue as explained in previous chapter. The correlation still exists but, according to a Spearman test, it is statistically much less significant than the one shown in the left panel of the same figure. On average, the lowest values of the local galaxy density correspond to very low halo masses. However, there is a large number of galaxies in low mass halos with rather high values of projected density. This is probably due to the fact that such low mass halos are in region of high density like filaments around more massive halos. The same result is obtained by using all the flavours of the density estimators mentioned above. Thus, our conclusion is that the local galaxy density field can not be considered a good definition of the environment, because due to several observational limits it does not trace the underlying matter field. However, it can be used to isolate at least galaxies hosted by the lowest mass halos or the highest mass halos.

Given this conclusion, we adopt the following approach. The X-ray data used in this work allow us to create a galaxy group sample in the range of masses $10^{12.5} - 10^{14.2}$ $M_{\odot}$. Indeed, the X-ray deep surveys used here are not deep enough to let us observe lower mass groups. In order to identify the galaxy population of lower mass dark matter halos we use the properties of the galaxy density field described above. Namely, we identify the galaxy at the lowest values of the density distribution. According to the result of our simulation, this method should be able to identify galaxies of dark matter halos with mass below 10^{12} $M_{\odot}$. For this exercise we use, in particular, the galaxy density estimator that shows the lowest dispersion in the relation shown in the left panel of Fig. 4.1, since it can provide the best proxy for the underlying matter density field. The best proxy is provided by the galaxy number density of systems with a stellar mass above 10^{10} $M_{\odot}$, measured within a cilinder with radius of 0.75 Mpc and length of 1000 km/s around each galaxy. This type

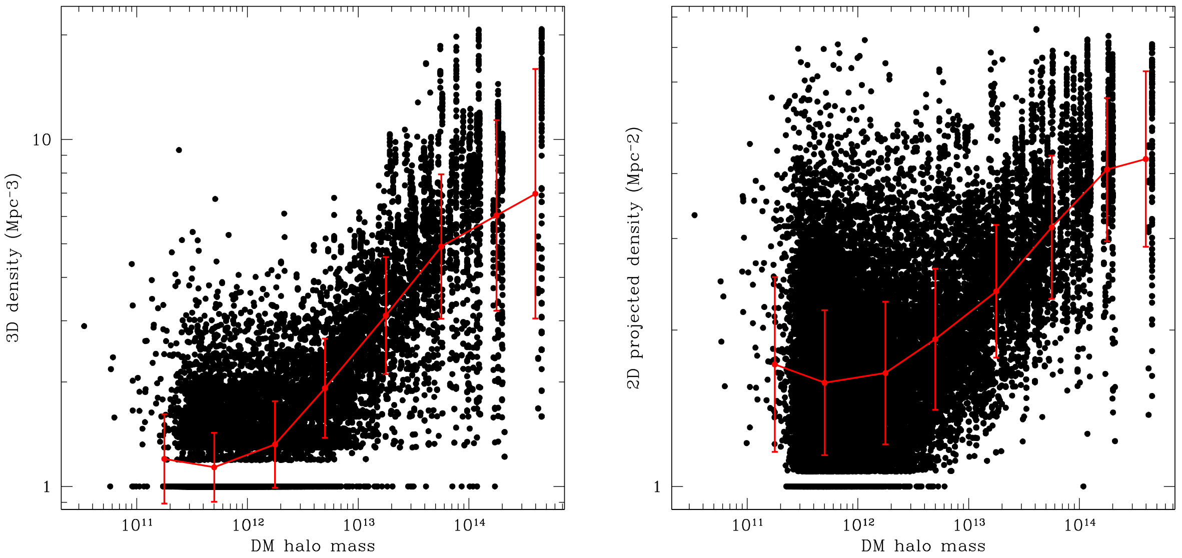

Figure 4.1: *Left panel*: The correlation between the local galaxy density field and the parent halo mass for a sample of simulated galaxies with known actual 3D position. *Right panel*: The same correlation with considering projection effects due to the use of *ra*, *dec* and redshift information and the selection effects due to a simulated spectroscopic selection function.

of density estimator takes advantage of the mass segregation observed in more massive halos (Scodeggio et al. 2009) and it is defined to sample a volume (0.75 Mpc and ±1000 km/s) quite similar to the one of a group/cluster sized halo. Indeed, the r_{200} radius varies from 0.3-0.5 Mpc for a group to 1-1.5 Mpc for a massive cluster and 1000 km/s is roughly twice the velocity dispersion of a group and quite similar to the velocity dispersion of a massive cluster. The galaxy density derived with this approach is further corrected for the spectroscopic incompleteness that would lead to an underestimation of the actual galaxy density. This correction is estimated with the same approach described in the previous chapter. Briefly, we estimate the ratio between the number of all galaxies and those with known spectroscopic redshift with mass above 10^{10} $M_{\odot}$, in a cylinder along the line of sight of the considered galaxy with radius corresponding to 0.75 Mpc at the redshift of the considered source and with $|z_{source} - z_{phot}| < 10000$ km/s, where z_{source} is the redshift of the central source and z_{phot} is the photometric redshift of the surrounding galaxies. The limit of 10000 km/s is roughly 3 times the error of the photometric redshifts (Ilbert et al. 2010). Of course z_{phot} is replaced by the spectroscopic redshift whenever this is available.

Fig. 4.2 shows the histogram of the density distribution obtained with our method for the whole galaxy population considered in this work (black histogram) and for the galaxy identified as groups spectroscopic members (red histogram). As confirmed by the simulations described above, this method is able to efficiently isolate galaxies that are not hosted by massive halos. We use this histogram to define the density cut for defining our

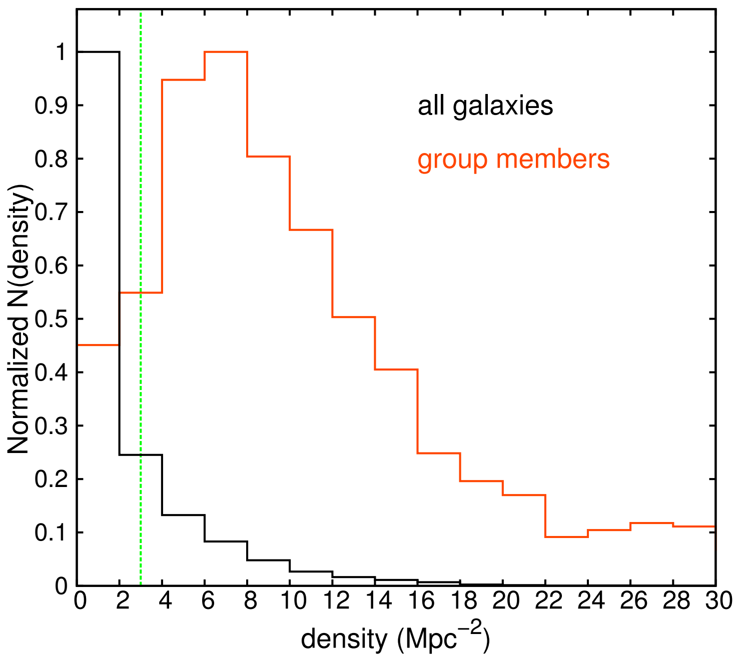

Figure 4.2: Density distribution around each galaxy with spectroscopic redshift in AEGIS, COSMOS, ECDFS and CDFN (in black) and group member galaxies in four mentioned fields (in red). The green dashed line at ρ=3 galaxies Mpc^{-2} shows the threshold to separate group from field galaxies. 73 % of all field galaxies are found at densities below this limit and 90% of all group member galaxies are above that.

“field” galaxies sample, that is galaxies that should be hosted by DM halos of masses below 10^{12} $M_\odot$ according to our simulations. The green dashed line at ρ=3 galaxies Mpc^{-2} in Fig. 4.2 shows the threshold to separate group from field galaxies. Indeed, 90% of all group member galaxies are above this limit. We do this exercise separately for the two redshift bins considered in our work. This leads to a sample of 4987 field galaxies in low redshift bin and 6063 field galaxies in high redshift bin.

Similarly to Ziparo et al. (2013) we define a third environmental class of galaxies identified by density values similar to the ones of group galaxy members but not associated to any X-ray extended emission observed in the X-ray surveys considered in this work. These galaxies have density above the ρ=3 galaxies Mpc^{-2} threshold and do not lie in the sky region defined by detected X-ray extended emissions. They likely belong to filaments, sheet like structures or to groups at lower mass with respect to the mass limit imposed by the CDFS, CDFN, AEGIS and COSMOS X-ray detection limits. We define this class of objects as “filament-like” galaxies. With this approach, we define a sample of 1246 “filament like” galaxies in low redshift bin and 2320 in high redshift bin. This additional class of objects will be used also to check whether the relative vicinity of galaxies can affect galaxy properties as suggested by Peng et al. (2010, 2012) or, instead, the membership to a massive halo is a key ingredient in the galaxy evolution.

4.3 Results

4.3.1 The non-linearity of the SF galaxy Main Sequence

In several works in the literature the Main Sequence of star forming galaxies is expressed through a linear relation with slope consistent to 1 (Elbaz et al. 2007 for 0.8<z<1.2, Noeske et al. 2007b for 0.2<z<0.7 and Peng et al. 2010 for 0.02<z<0.085). Peng et al. (2010), in particular, show that the MS of blue star forming galaxies selected from the SDSS spectroscopic catalog is linear up to very high masses and its slope and dispersion is independent from the environment. However, the selection of only blue galaxies as a way to isolate the bulk of the star forming galaxies might not be correct. Indeed, Weinmann et al. (2006) shows that 20% of the galaxies hosted by massive halos such as groups and clusters show red colors and level of star formation activity similar to the blue active galaxy population. In addition, Brinchmann et al. (2004) show that, when all galaxies are considered, the MS of the local Universe is well identified at stellar masses below $10^{10-10.5}$ $M_{\odot}$ but it breaks down at higher masses. More recently Whitaker et al. (2012) show that the deviation from a linear relation of the MS at high stellar masses is evident up to redshift ~ 2. This would be consistent also with the relatively flat slope of the MS found by Rodighiero et al. (2010) up to $z \sim 2.5$, obtained by stacking analysis in the Herschel PACS data.

In this paragraph we analyse the level of deviation of the MS from the linear relation with our dataset. This is done in the two redshift bins defined above. This will be used as a reference in the next paragraph to understand if there is any relation between this deviation or the dispersion of the MS and the environment at different stellar masses. As a starting point we need to define a reference linear relation. Since the MS is well studied in the literature (Elbaz et al. 2007 for 0.8<z<1.2, Noeske et al. 2007b for 0.2<z<0.7 and Peng et al. 2010 for 0.02<z<0.085), we interpolate existing relations to retrieve the MS in the range of redshift used in this work. We, then, define the residual of each galaxy from the MS as ΔSFR= SFR_{obs}-SFR_{MS} where the SFR_{obs} is the observed SFR and SFR_{MS} is the interpolated main sequence SFR at the stellar mass of the considered galaxies. The dark histograms of Fig. 4.3 and 4.4 show the distribution of the residuals in different stellar mass bins and in the low and high redshift bins, respectively. To check for possible biases due to our estimate of the SFR for galaxies undetected in the mid or far-infrared (see calibration of the SFR estimated via SED technique as explained in the previous paragraph), we do this exercise also with a subsample of galaxies detected in the infrared, thus, with the most reliable estimate of the SFR. This is doable because given the depth of the PACS and *Spitzer* MIPS observations in our fields, the MS is fully sampled (~80% for $\mathrm{M}_{*} > 10^{10}$) up to $z \sim 1.1$ by IR detected galaxies with the most reliable estimate of the SFR ($\sim 10\%$ uncertainty, see Magnelli et al. 2013). Thus, our estimate of the mean of SFR is not affected by the large error (~ 0.4 dex), typical of the determination of the SFR via SED fitting. The light blue and light red histograms in Fig. 4.3 and 4.4, respectively, show the residual distributions of IR detected galaxies. The light and dark histograms show a very high level of consistency. In both cases we observe that there is a well defined Gaussian

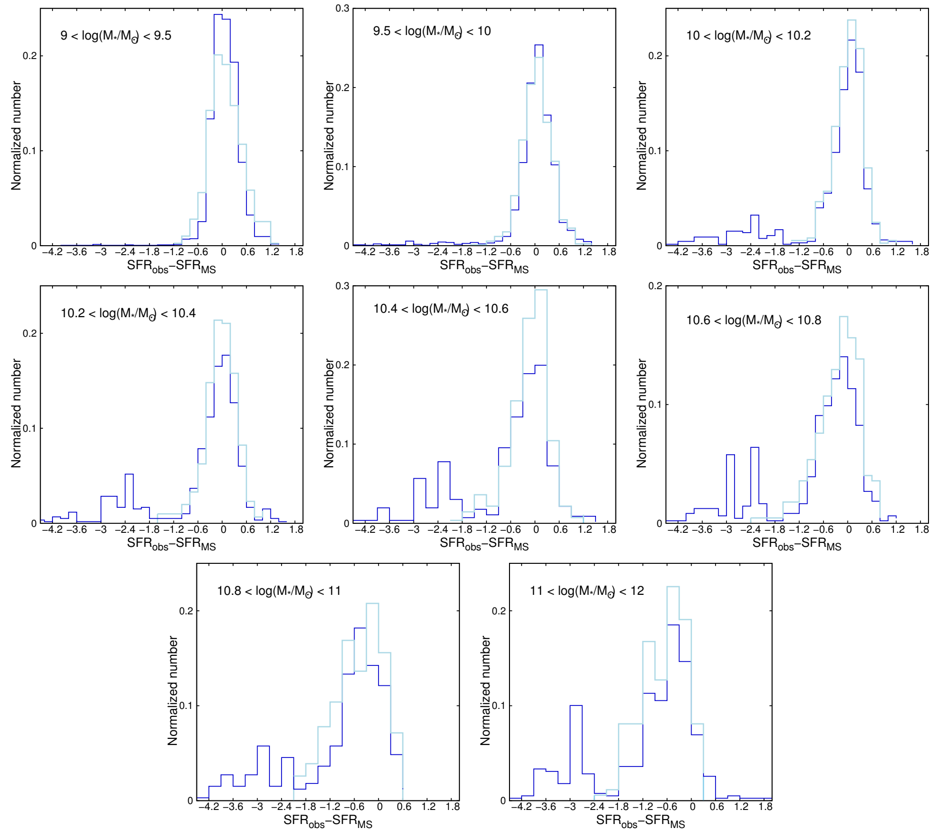

Figure 4.3: ΔSFR= SFR$_{obs}$-SFR$_{MS}$ for 0.15<z<0.5 in different stellar mass bins. The bright blue histograms show just IR detected galaxies and the dark blue histograms show galaxies with IR and SED SFR simultaneously.

distribution of the residuals around the peak of the MS at any given stellar mass bin. The location of the peak and the dispersion of the relation is highly consistent between the IR detected galaxy subsample and the whole sample. This assures that we do not have to worry about biases due to our estimate of the SFR via SED technique. Thus, to have a better statistics we use the whole galaxy sample for our analysis.

Both low-z and high-z sample clearly show a deviation from 0 (consistent with the location of the linear MS) in the peak of ΔSFR starting since $10.4 < \log(M_*/M_\odot) < 10.6$. We estimate the mean deviation from the MS by isolating the Main sequence galaxies at any mass bin as those with $|\Delta\mathrm{SFR}| < 1$ (consistent with a 3σ cut according to the values of the dispersion reported in the literature) from a first guess of the peak of the Gaussian distribution. We fit both the peak and the dispersion of the Gaussian iteratively by selecting at any iteration all galaxies with $|\Delta\mathrm{SFR}\ | < 3 \times \sigma$, where σ is the Gaussian dispersion. This is done until we reach a stable solution. Fig. 4.5 shows the mean deviation from the MS and the dispersion of the Gaussian distribution as a function the galaxy stellar mass. Above $10.4 < \log(M_*/M_\odot) < 10.6$ we observe a deviation of ~0.5 dex at 10^{11} $M_\odot$ and ~0.6-0.8 dex at $10^{11.5}$ $M_\odot$ towards the quiescence region. In addition, as shown in the

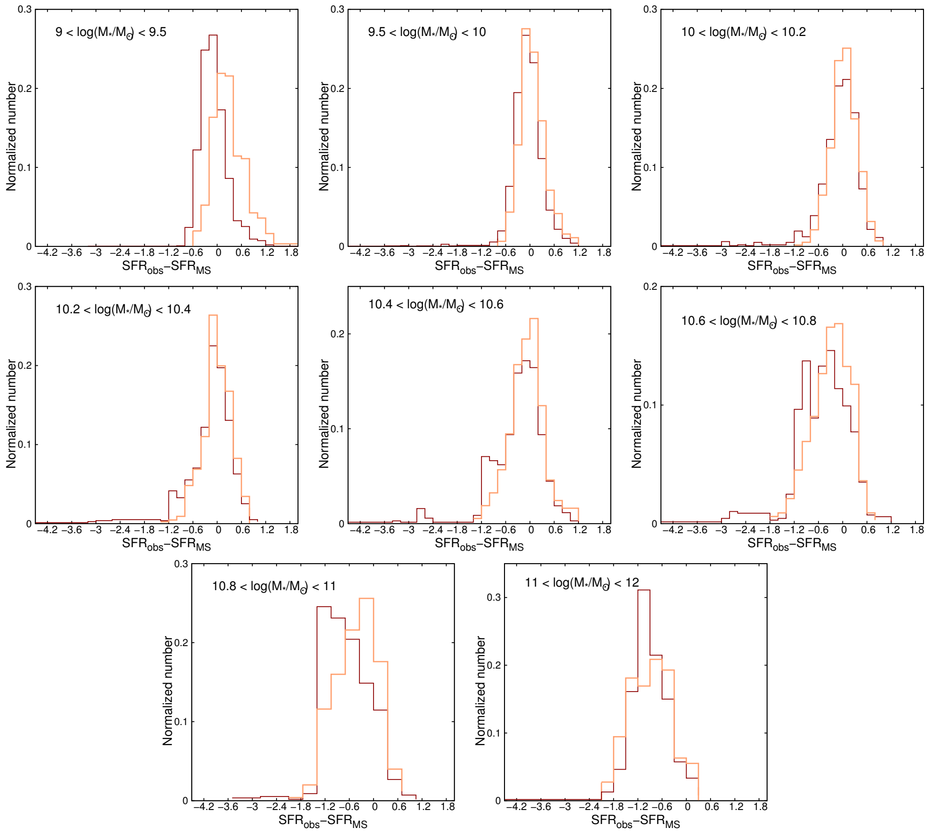

Figure 4.4: ΔSFR= SFR$_{obs}$-SFR$_{MS}$ for 0.5<z<1.1 in different stellar mass bins. The bright red histograms show just IR detected galaxies and the dark red histograms show galaxies with IR and SED SFR simultaneously.

left panel, above the same mass threshold, we observe also an increase of the dispersion around the MS location at high masses. The scatter of the MS is of 0.3-0.4 dex below $10.4 < \log(M_*/M_\odot) < 10.6$, consistent with the value reported by many of previous studies (Daddi et al. 2007; Elbaz et al. 2007; Peng et al. 2010). It increases to 0.6-0.7 dex at higher masses. In the high mass range the dispersion seems to be larger at low redshift (~ 0.7 dex) with respect to the high redshift MS (~ 0.5 dex). The final appearance of the MS estimated as explained above is shown in Fig. 4.6 in the low (left panel) and high (right panel) redshift bins.

We also fit the best relation with two different exponential laws above and below $M_* = 10^{10.4} M_\odot$. The best fit relation is reported below in the two redshift bins.

$0.15 < z < 0.5$:

$$log(SFR) = (0.97 \pm 0.004) log(M_*) - (9.15 \pm 0.04), log(M_*) < 10.4 \tag{4.1}$$

$$log(SFR) = (0.27 \pm 0.02) log(M_*) - 1.99(\pm 0.19), log(M_*) \geq 10.4 \tag{4.2}$$

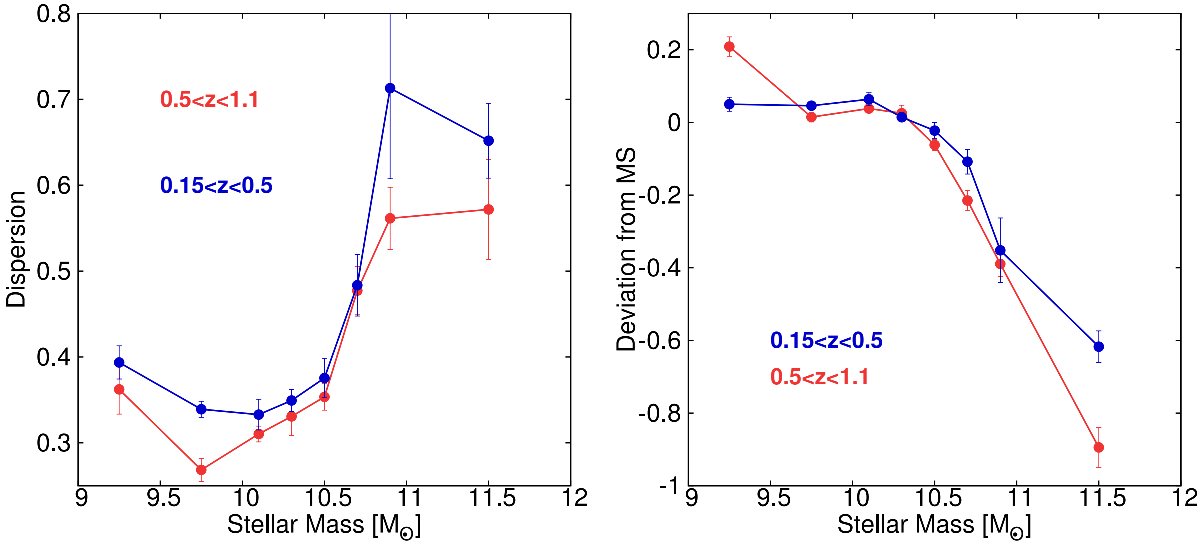

Figure 4.5: *Left panel*: dispersion around the MS location as a function of the galaxy stellar mass. *Right panel*: peak of the residual $\Delta(SFR)$ as a function of the galaxy stellar mass.

$0.5 < z < 1$:

$$log(SFR) = (1.1 \pm 0.005)log(M_*) - (10.16 \pm 0.04), log(M_*) < 10.4 \tag{4.3}$$

$$log(SFR) = (0.24 \pm 0.09)log(M_*) - (1.37 \pm 0.09), log(M_*) \geq 10.4 \tag{4.4}$$

In both cases the slope of the relation below $M_* < 10^{10.4} M_\odot$ is consistent with a linear relation consistently with the results in the literature. Above this mass limit the relation is much flatter, which is in agreement with the most recent findings of Rodighiero et al. (2010) and Whitaker et al. (2012). We use this relation to identify all MS galaxies as those within $\pm 3\sigma$ (see Fig. 4.7 and 4.8 for the new residual distribution at low and high redshift, respectively) from these best fit relations as a function of the stellar mass. This MS galaxy sample will be used in the next paragraph to study the dependence of the dispersion and location of the MS from the environment.

4.3.2 The role of the environment in the shape and dispersion of the MS

In order to check whether the slope of the MS at higher masses and the increase of its dispersion as a function of the stellar mass is environment dependent, we analyse separately the location of the MS and its dispersion in the three environmental classes defined above: field galaxies, "filament-like" galaxies and group galaxies. In order to define the MS in these three environment we perform the same exercise described above by looking for the location of the peak of the Gaussian distribution of the residual ΔSFR with respect to the best fit MS defined by the two exponential laws at low and high stellar masses.

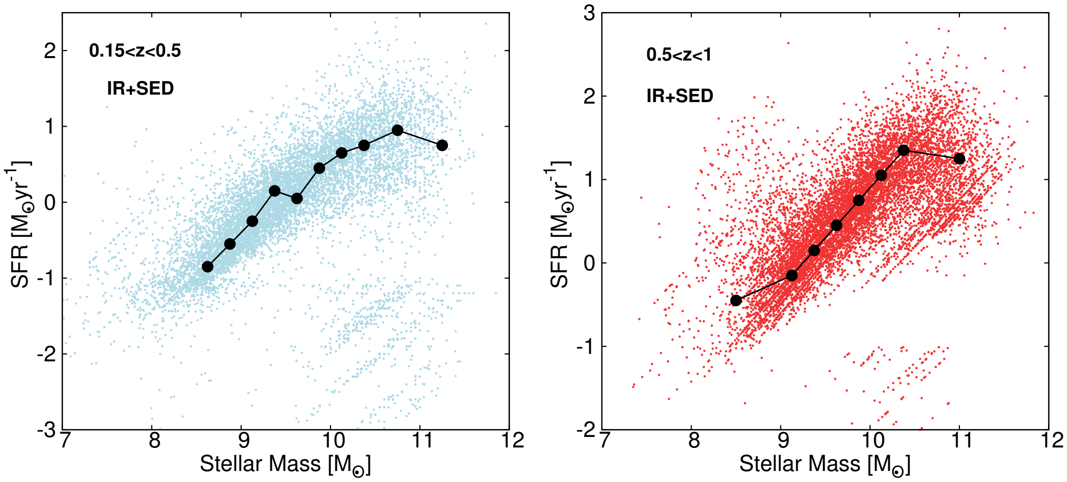

Figure 4.6: *left panel* :SFR vs. M$_*$ for galaxies in 0.15<z<0.5. The black dots show the peak of distribution of SFR in different mass bins. *right panel*: Same as left panel for galaxies in 0.5<z<1.

Fig. 4.9 shows the mean MS for field galaxies (grey connected points), "filament-like" galaxies (green connected points) and group galaxies (violet connected points) in the low redshift bin (left panel) and in the high redshift bin (right panel). These two plots are revealing the following information:

- The flattening of the MS at stellar masses above $10^{10.4-10.6}$ $M_\odot$ is clearly visible in all environments. The flattening is in place already at $z \sim 1$.
- Below the stellar mass threshold of $10^{10.4-10.6}$ $M_\odot$ the MS is the same in all three environments both at high and low redshift.
- Above this mass threshold we observe a different behaviour of MS galaxies in the three different environments. At low redshift, group galaxies show a significant departure from the mean MS and an even flatter MS. These galaxies seem to deviate from the MS at lower masses ($\sim 10^{10}$ $M_\odot$) with respect to the MS galaxies in the other environments. At higher redshifts, groups member galaxies do not deviate from the mean relation and their MS coincides with the MS of the other two environments.
- Field (isolated) and "filament-like" galaxy MS are perfectly consistent at any redshift. This shows that the relative vicinity of galaxies as expressed by the density field is not playing an important role in affecting and/or regulating the galaxy SF activity. This, in addition to the blue galaxies selection, explains why Peng et al. (2010) did not observe any difference between the MS location of galaxies at different densities.

Fig. 4.9 indicates clearly that the evolution of the star formation activity in galaxies does not simply depend on the galaxy stellar mass as suggested by Peng et al. (2010) though galaxy internal process (e.g. AGN feedback) but it must be regulated by the

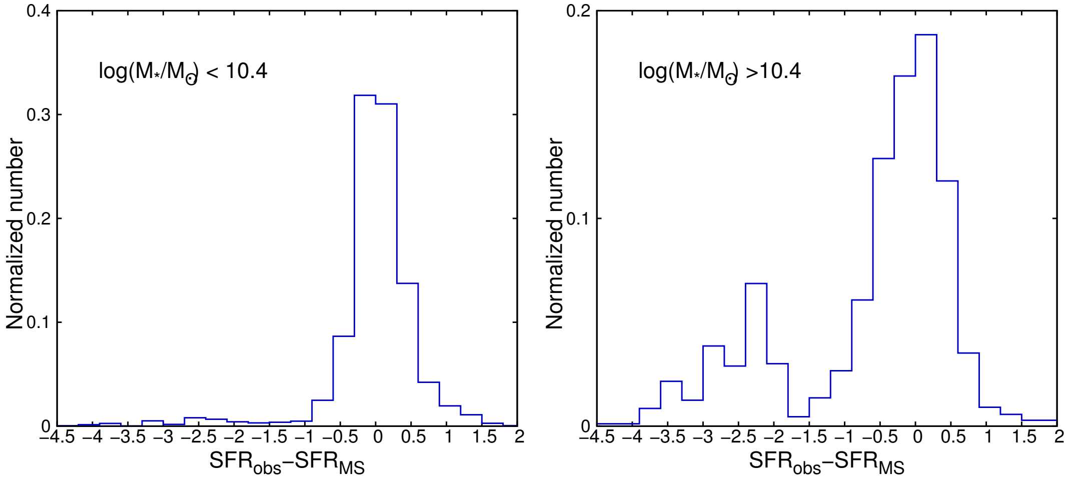

Figure 4.7: ΔSFR= SFR_{obs}-SFR_{fitMS} for 0.15<z<0.5 in two different stellar mass bins. The left and the right panel is corresponding to $\mathrm{M}_* < 10^{10.4}$ and $\mathrm{M}_* > 10^{10.4}$, respectively.

environment. In addition, our results confirm the hint provided by Ziparo et al. (2013) that group galaxies evolve in a much faster way with respect to galaxies in lower mass halos in terms of quenching of the SF activity. Thus, the membership to a massive halos and the effect of all physical processes in place in such halos are likely to be responsible for the decrease of the SF activity in groups since $z \sim 1$. Fig. 4.9 explains also the increase of the dispersion of the MS, in particular in the low redshift bin, as a function of the stellar mass shown in the left panel of Fig. 4.5. Indeed, the deviation of group galaxies towards a flatter and lower MS with respect to the mean relation has the effect of a broadening of the mean MS. Indeed, at stellar masses below $10^{10.4-10.6}$ $M_{\odot}$, where the MS of all environments coincide, the scatter is $\sim$ 0.3 dex in the mean MS and in the MS in the individual environmental classes. At higher stellar masses, the dispersion of the MS in group, field and filament-like galaxy MS is about 0.4 dex, while it is about 0.7 dex in the mean relation. At high redshift, where there is a substantial agreement of the location of the MS in all environments, the dispersion of the MS of the individual environmental classes is consistent with the dispersion of the mean relation.

4.4 Morphology

To make a step further, we investigate also the relation of morphology, SFR and environment in the SFR-stellar mass plane. This is done in order to understand if the quenching of the SFR in group galaxies is also associated to a morphological transformation. For this purpose, we use the Advanced Camera for Surveys General Catalog (ACS-GC), which is a photometric and morphological database based on publicly available data obtained with the Advanced Camera for Surveys (ACS) instrument on board of the Hubble Space Telescope (Griffith et al. 2012). This catalog contains ∼370,000 galaxies observed in the

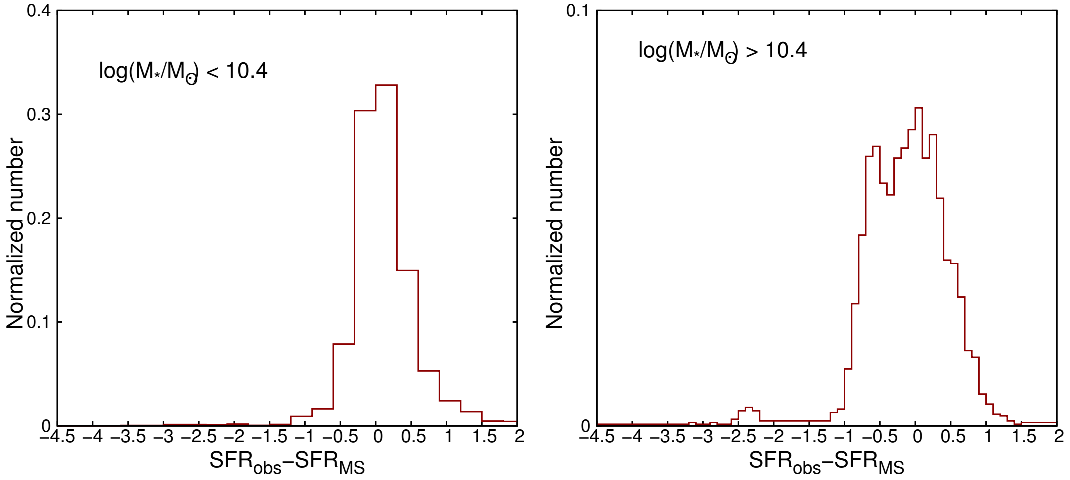

Figure 4.8: ΔSFR= SFR$_{obs}$-SFR$_{fitMS}$ for 0.5<z<1 in two different stellar mass bins. The left and the right panel is corresponding to $M_* < 10^{10.4}$ and $M_* > 10^{10.4}$, respectively.

EGS, COSMOS, GEMS and GOODS surveys. Briefly, Griffith et al. (2012) use GALFIT to measure the structural parameters of each galaxy by modelling each source with a single Sérsic profile together with a model for the sky. The Sérsic profile (Sersic, Garcia Lambas & Mosconi 1986; see Graham & Driver 2005 for the mathematical relationship) is defined as:

$$\Sigma(r) = \Sigma_e e^{-k[(r/r_e)^{1/n}-1]} \tag{4.5}$$

where r_e is the effective radius of the galaxy, Σ_e is the surface brightness at r_e, n is the Sérsic index, and k is coupled to n such that half of the total flux is always within r_e. This model is usually generalized to asymmetric cases by allowing for an axis-ratio $b/a < 1$ (that is, elliptical rather than circular isotopes). Although r_e reflects the physical size of the galaxy, n is a measure of its "concentration": the higher the Sérsic index n, the more concentrated or bulge-dominated is the galaxy. In this catalog, galaxies with Sérsic index larger than 2.5 are classified as early type and objects with n smaller than 1.5 are classified as late type (disk) galaxies. We define as "intermediate" galaxies with $1.5 < n < 2.5$.

By matching our galaxy catalogs of EGS, COSMOS and the GOODS fields with the ACS-GC catalog, we find a match for 80% of the galaxies. We use the definition of the MS given in Section 4.3.1 (eq. 4.1 and 4.2 for the low redshift bin and eq. 4.3 and 4.4 for the high redshift bin) to define MS galaxies within $\pm 3\sigma$ from the MS. We check the distribution of the Sérsic index n as a function of the environment by distinguishing field, "filament-like" and group galaxies as defined above. To check for differences among the different environmental classes, we calculate the mean and its error of the Sérsic index distribution in several mass bins. This is done to take into account the stellar mass dependence of the flattening of the MS and the differential role of the environment at different mass scales.

Fig. 4.10 shows that the Sérsic index distribution for MS galaxies is quite similar in all environmental classes both at low (left panel) and high (right panel) redshift. Indeed, the

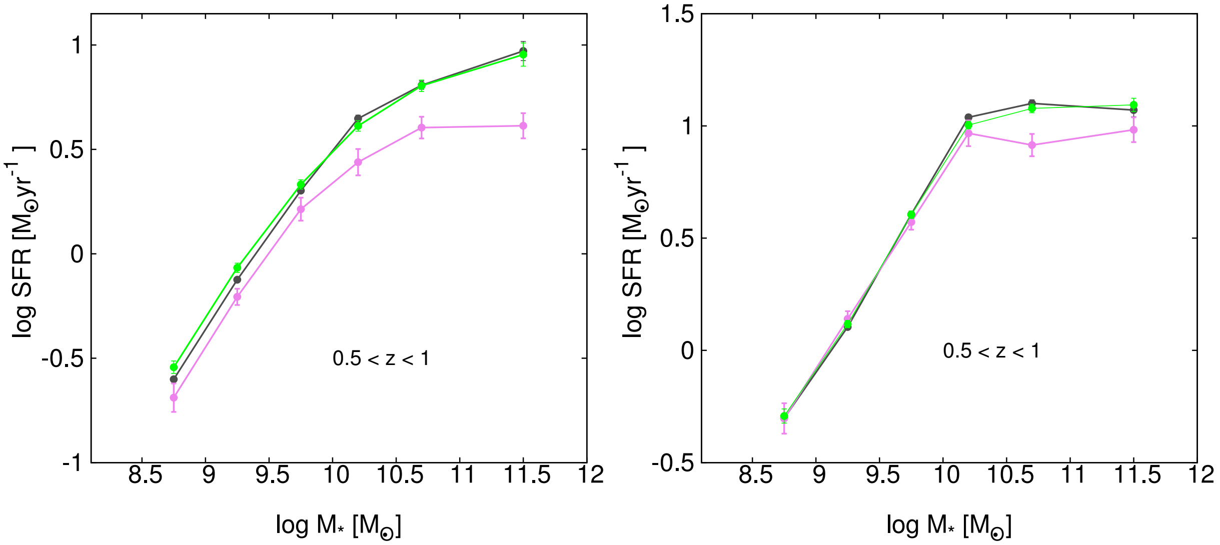

Figure 4.9: The mean of dependence of log SFR on stellar masses of MS galaxies in three different environments in the low redshift bin (left panel) and in the high redshift bin (right panel).

maximum discrepancy is of $\sim 1.5\sigma$ in the highest stellar mass bin between group and filament like galaxies in the low redshift bin. This suggests that the SF quenching observed in group galaxies in Fig. 4.9 is not associated to systematic morphological transformation. We stress that this is not at odds with the well known "morphology-density" relation. Indeed, this more general relation reflects the differential morphological type distribution of the entire galaxy population without distinction between galaxies on and off Main Sequence. In this particular analysis, we consider only MS galaxies to show that the departure of group galaxies from the MS is not related to a morphological transformation. Instead, Fig. 4.10 shows clearly a much stronger dependence of the Sérsic index distribution on the stellar mass at low and high redshift. While below $10^{10.4-10.6}\ M_{\odot}$, MS galaxies tend to be late type, above this threshold the morphological type distribution is clearly dominated by early type galaxies. This results together with Fig. 4.9 would suggest that while galaxy morphology is a stellar mass related phenomenon for MS galaxies, SF quenching is, instead, a more environment related process.

4.5 Discussion and Conclusion

To summarize, our analysis shows that:

- The Main Sequence of star forming galaxies in two redshift bins at relatively low and high redshift is not a linear relation but it shows a flattening towards higher masses ($M* > 10^{10.4-10.6}\ M_{\odot}$)
- Above this limit, the galaxy SFR has a very weak dependence on the stellar mass

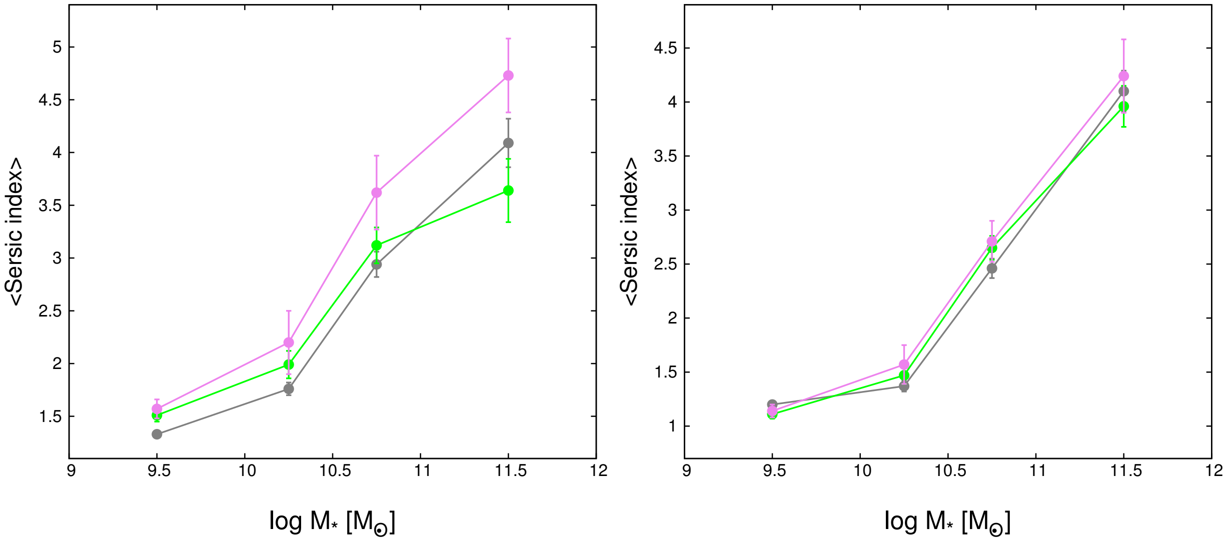

Figure 4.10: *left panel* : mean of the Sérsic index n as a function of the stellar mass in the low redshift bin in three environmental classes: groups (violet points and line), "filament-like" galaxies (green points and line) and field galaxies (grey points and line). *right panel* : same as in the left panel for the high redshift bin.

- This flattening, to a different extent, is present in all environments
- At low redshift group galaxies tend to deviate more from the mean MS towards the region of quiescence with respect to isolated and filament-like galaxies
- This environment dependent location of low redshift MS galaxies with respect to the mean MS causes the increase of the dispersion of the distribution of galaxies around the MS as a function of the stellar mass.
- At high redshift we do not find significant evidence for a differential location of galaxies with respect to the MS as a function of the environment; indeed, in this case we do not observe a significant increase of the dispersion of the distribution of galaxies around the MS as a function of the stellar mass.
- We do not find evidence for a differential distribution in the morphological type of MS galaxies in different environment. Instead we observe a much stronger dependence of the mean Sérsic index on the stellar mass.

Recently, Wuyts et al. (2011) find that across cosmic time, the typical Sérsic index of galaxies is optimally described as a function of their position relative to the the MS at the epoch of their observation. The correspondence between mass, SFR, and structure, as quantified by the Sérsic index, is equivalent to the Hubble sequence. Based on a quite similar galaxy sample (using SDSS for nearby universe and COSMOS, UDS and GOODS fields for high redshift samples), Wuyts et al. (2011) see that such a sequence already

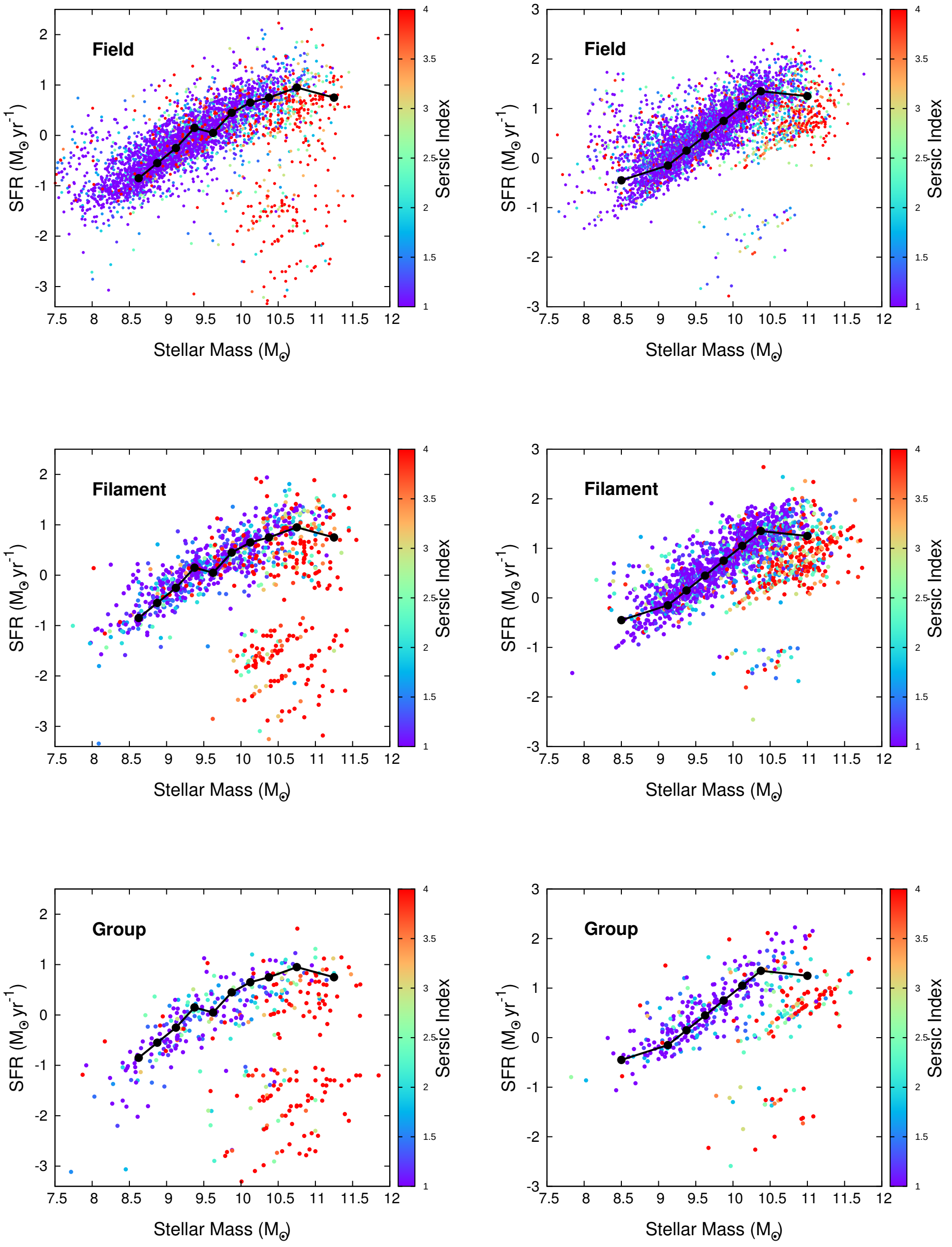

Figure 4.11: SFR-stellar mass relation for field (upper panels), filament-like (middle panels) and group (lower panels) galaxies in the low (left panels) and high (right panels) redshift bins. The color-code is according to the Sérsic index as indicated in the figures.

existed at z$\sim$2; bulge-dominated morphologies go hand in hand with a more quiescent nature. In addition, they observe that late type galaxies (Sérsic index < 1.5) follow a linear SFR-Mass relation. This is not at odds with our results. Indeed, we also observe that late type galaxies, especially among field and filament like galaxies, follow a linear relation (see Fig. 4.11). Nevertheless, they do not represent the bulk of the Main Sequence galaxy population above $10^{10.4-10.6}$ $M_{\odot}$, but only the upper envelope. This means that, while a clear morphological sequence with a linear slope and, thus, a strong stellar mass dependence, is visible in the SFR-Stellar mass plane at any mass as shown by Wuyts et al. (2011), the Main Sequence of star forming galaxies at high masses is much more poorly defined and it shows a much weaker dependence on the stellar mass ($SFR \propto M*^{0.2-0.3}$). This MS is consistent with a linear relation only in the low stellar mass range where it is dominated by late type galaxies. At high masses, late type galaxies are no longer the bulk of the MS population. There, morphological sequence and star forming galaxy sequence are no longer overlapping. Our results are, indeed, in agreement with the more recent findings of Whitaker et al. (2012), that find a flatter slope of the MS at $\sim 10^{10}$ $M_{\odot}$ due to a large percentage of red galaxies. This is also consistent with the results of Rodighiero et al. (2010) that find a rather flat MS at any redshift on the basis of Herschel PACS data. Our data indicates also that the environment does not seem to be the cause of this flattening at high masses, since the MS show the same type of shape in all environment. The effect of the environment is, instead, to increase the scatter around the MS since field and filament-like galaxies tend to occupy the upper envelope of the MS and group galaxies tend to be located in the lower envelope.

In addition, numerous previous studies of low redshift galaxies in the literature find that color and star formation rate are more strongly correlated with the environment than morphology (e.g. Kauffmann et al. 2004; Blanton et al. 2005; Christlein & Zabludoff 2005; van den Bosch et al. 2008; Weinmann et al. 2009). The implication of these studies is that the well-known correlation between morphology and environment is secondary to the correlation between environment and star formation rate. This is consistent with our findings. Indeed, we observe that among MS galaxies the distribution of the morphological type does not depend on the environment. However, at the same time group galaxies tend to be more quenched with respect to field and filament like galaxies. The distribution of the morphological type is much more related to the galaxy stellar mass than the environment.

Our results confirm the preliminary results of Ziparo et al. (2013) that group galaxies evolve in a much faster way with respect to field and filament like galaxies. Indeed, we observe a substantial quenching only at low redshift. At high redshift group galaxies are perfectly on sequence as galaxies in the other environment. This is consistent with previous study in the literature. Indeed, the environmental trends at fixed stellar mass seem to weaken at higher redshift (e.g. Poggianti et al. 2008; Tasca et al. 2009; Cucciati et al. 2010; Iovino et al. 2010; Kovač et al. 2010a). For instance, Tasca et al. (2009) and Kovač et al. (2010a) have compared the dependence of colors and morphologies on local density and in groups in the COSMOS field, finding a stronger effect on color than on morphology, similar to the low-redshift results and suggesting a longer timescale for structural transformations than for quenching star formation.

As a further step we will also include rest frame colors as additional ingredient in our analysis in order to understand whether the observed SF quenching in group galaxies is more related to a color transformation than to a morphological transformation.

Chapter 5

Conclusions

In this chapter, I summarize the main achievements of this thesis. Since large part of this PhD work is devoted to the creation of a robust method for the identification of galaxy groups and for the determination of their galaxy membership, I first describe my technical achievements and list, then, the scientific achievements derived by using this method.

5.1 Technical results: the L$_X - \sigma$ relation and its scatter

We extensively study the relation between X-ray luminosity and velocity dispersion in the group scale regime. The estimate of the velocity dispersion for the systems in the group mass range is made quite complicated and uncertain due to the low number of member galaxies inhabiting these systems. From the observational point of view, this estimate is even more difficult due to the fact that many group galaxy members lack accurate spectroscopic redshift, which is a fundamental ingredient for any dynamical analysis. In our analysis, the spectroscopic member galaxies are selected by applying different cuts: two X-ray based and optically based virial radius and two cuts along the line of sight. We examined the $L_x - \sigma$ relation for each cut and discussed the effects of them on the relation. We explored substructure in the groups by applying the Dressler-Shectman test and discussed its effect on the overestimation of velocity dispersion. We also looked at the compactness of the X-ray emission of the groups and its effect on the scaling relation. A comparison between dynamical mass and X-ray mass of the groups is also done. Finally, X-ray galaxy groups are compared with optical galaxy groups which are identified with the Voronoi-Delaunay method (VDM). Our detection of a high-z group ($z = 1.54$) illustrates that megasecond Chandra exposures are required for detecting such objects in the volume of deep fields. Our method reveals also that, in a sample of groups spanning a wide range of X-ray luminosities, the choice of a constant Δz for selecting the members along the group line of sight can cause a large scatter in $L_x - \sigma$ relation. In addition the choice of X-ray based or optically defined virial radius does not have significant effect on the scatter around

$L_x - \sigma$ relation for groups with high X-ray luminosities. Substructure in groups can inflate velocity dispersion as outliers are also included in galaxies with dynamical complexity. We do not find significant differences between the galaxy group population identified through the X-ray detection and the optically based method (VDM), as they are nearly similar in both redshift and velocity dispersion distributions.

In order to estimate the errors involved in our analysis and check for possible biases due to the spectroscopic incompleteness, we follow the same approach used in Ziparo et al. (2013) based on the mock catalogs provided by the Millennium Simulation (Springel et al., 2005). As a first test to check if our method is able to recover efficiently the membership of each group, we compare the completeness and the contamination of the membership obtained with our analysis with the original group membership identified by the FoF algorithm of the mock catalog of Kitzbichler and White (2007) drawn from the Millennium Simulation. The completeness is estimated by computing the fraction of "true" members identified by our method. The contamination is estimated by calculating the fraction of interlopers (galaxy identified as group members by our method but not in the original mock catalog). The completeness level is quite high ($> 90\%$) but on average 35% of the members are interlopers. If we apply a mass cut of $10^{10} M_\odot$, the completeness level reaches almost in all cases 100% with a much lower contamination fraction (solid histograms). It is clear that our method is much more robust in identifying rather massive galaxy members, which are likely more clustered in the phase space, than low mass galaxies.

By simulating the spectroscopic completeness of our fields in the mock catalog, we check also the effect of such selection on our measure of the group velocity dispersion. The "observed" velocity dispersion estimated with our method and the "true" velocity dispersion are in rather good agreement with a scatter of 0.1 dex. The main source of scatter is given by the spectroscopic incompleteness. We also point out that using the estimate of M_{200} for deriving the velocity dispersion first guess is a fundamental ingredient of our analysis. Indeed, if we use a constant value for the first guess, as usually done in the literature, we find that the scatter in the relation between "true" and "observed" velocity dispersion increases significantly and there is no good correlation between the two quantities.

5.2 Scientific results

5.2.1 Evolution of the relation between group total mass and global properties

In this section of the thesis we provide the analysis of the evolution of the total star formation activity, total stellar mass and HOD by using one of the largest X-ray selected sample of galaxy groups with secure spectroscopic identification on the major blank fields (ECDFS, CDFN, COSMOS, AEGIS) up to z$\sim$1.1. We compare our results with the one based on an optically selected sample of groups at $z < 0.085$ in order to fully follow the evolution of the galaxy population in groups from the local Universe. We list below the main results based on our sample:

- We observe a clear evolution in the level of star formation activity in galaxy groups. Indeed, the total star formation activity in high redshift groups (0.5<z<1.1) is higher with respect to the low redshift (0.15<z<0.5) sample at any mass by almost 0.8 ± 0.1 dex. A milder difference (0.35 ± 0.1 dex) is observed between the [0.15-0.5] redshift bin and the groups at $z < 0.085$. This evolution seems to be much faster than the one observed in the whole galaxy population (Gruppioni et al. 2013), dominated by lower mass halos ($M_{200} \sim 10^{12-12.5} M_{\odot}$, Jenkins et al. 2001; Tinker et al. 2008; Eke et al. 2005). This would imply that the level of SF activity is declining more rapidly since $z \sim 1.1$ in the more massive halos than in the more common lower mass halos, confirming a "halo downsizing" effect as discussed already in Popesso et al. (2012).

- The HOD and the total stellar mass-M_{200} relation are consistent with a linear relation in any redshift bin in the M_{200} range considered in our analysis. We do not observe any evolution in the HOD since $z \sim 1.1$. Similarly we do not observe evolution in the relation between the total stellar mass of the groups and the total mass, in agreement with the results of Giodini et al (2012). The picture emerging from our findings is that massive groups at $M_{200} \sim 10^{13-14} M_{\odot}$ have already accreted the same amount of mass and have the same number of galaxies as the low redshift counterpart, as predicted by Stewart et al. (2008). This implies that the most evident evolution of the galaxy population of the most massive systems act in terms of quenching their galaxy star formation activity. This also implies that the group galaxy population should progressively move from high to low specific star formation rate from $z \sim 1.1$ to $z \sim 0$ and rapidly move away from the Main Sequence since $z \sim 1.1$ confirming the recent results of Ziparo et al. (2014) based on a similar dataset.

- The analysis of the evolution of the fraction of SF galaxies as a function of halo mass or velocity dispersion show that high mass systems seem to be already evolved at z∼1.1 by showing a fraction of star forming galaxies consistent with the low redshift counterpart at $z < 0.085$. Given the almost linear relation between the ΣSFR and M_{200} in the high-z sample, this implies that most of the contribution to the total SFR of the most massive systems ($M_{200} \sim 10^{14} M_{\odot}$) is given by few highly star forming galaxies, while in lower mass systems ($M_{200} \sim 10^{13} M_{\odot}$) is given by many galaxies of average activity. This would be an additional sign of a faster evolution in the more massive systems in terms of star formation activity with respect to lower mass groups. Thus, it would confirm the "halo downsizing" effect.

- The comparison of our results with the prediction of the Millennium Simulation semi-analytical model confirms the known problem of the models. We confirm the strong bias due to the "satellite overquenching" problem in suppressing significantly the SF activity of group galaxies (more than one order of magnitude) at any redshift with respect to observations. The HOD predicted by the simulations is remarkably in agreement with the observations. But due to the low SF activity of galaxies in massive halos, the models predict also a lower total stellar mass in groups with respect to the observed one at any redshift.

5.2.2 SFR-Mass plane : *the location of group galaxies with respect to the Main Sequence*

During the past decade, there have been several efforts to find how and if the environment might affect the properties of galaxies. One way to trace the evolution of galaxies during the cosmic time is to look at their position in the SFR-Mass plane and, in particular, with respect to the Main Sequence of Star Forming galaxies. In several works in the literature the Main Sequence is expressed through a linear relation with slope consistent to 1 (Elbaz et al. 2007 for 0.8<z<1.2, Noeske et al. 2007b for 0.2<z<0.7 and Peng et al. 2010 for 0.02<z<0.085). Peng et al. (2010), in particular, show that the MS of blue star forming galaxies selected from the SDSS spectroscopic catalog is linear up to very high masses and its slope and dispersion is independent from the environment. However, the selection of only blue galaxies as a way to isolate the bulk of the star forming galaxies might not be correct. Indeed, Weinmann et al. 2006 shows that 20% of the galaxies hosted by massive halos such as groups and clusters show red colors and level of star formation activity similar to the blue active galaxy population.

To shed light on this relation in different environments, we used a dynamical approach to define environment. We distinguish three environmental classes. The group galaxy class is composed of galaxies identified via dynamical analysis as member of an X-ray selected group according to the method described in the previous section. We also define a sample of field galaxies and "filament-like" galaxies. This is done by using the galaxy density to find isolated galaxies (field) and galaxies in high density region but not associated to any group or more generically to an X-ray extended emission ("filament-like"). These classes of environment are used to study the location of galaxies in SFR-mass plane since $z \sim 1$ as a function of the environment. We observe a clear flattening of the main sequence at stellar masses above $\sim 10^{10.5} M_{\odot}$ in all environments. The flattening is in place already at $z \sim 1.1$. Below the stellar mass threshold of $10^{10.4-10.6}$ $M_{\odot}$ the MS is the same in all three environments both at high and low redshift. Above this mass threshold, we observe a different behavior of MS galaxies in the three different environments. At low redshift, group galaxies show a significant departure from the mean MS and an even flatter MS. These galaxies seem to deviate from the MS at lower masses ($\sim 10^{10}$ $M_{\odot}$) with respect to the MS galaxies in the other environments. At higher redshifts groups galaxies do not deviate from the mean relation and their MS coincides with the MS of the other two environments. Field (isolated) and "filament-like" galaxy MS are perfectly consistent at any redshift. This shows that the relative vicinity of galaxies as expressed by the density field is not playing an important role in affecting and/or regulating the galaxy SF activity. This, in addition to the blue galaxies selection, explains why Peng et al. (2010) did not observe any difference between the MS location of galaxies at different densities.

By matching morphological information (Sérsic profile parameters) to our galaxy catalog, we also investigated the relation of SFR, morphology and environment in the SFR-stellar mass plane . Our analysis shows that the Sérsic index distribution for MS galaxies is quite similar in all environmental classes both at low and high redshift. Indeed, the maximum discrepancy is of $\sim 1.5\sigma$ in the highest stellar mass bin between group and filament like galaxies in the low redshift bin. This suggests that the SF quenching observed in group galaxies is not associated to systematic morphological transformation. Instead, we observe clearly a much stronger dependence of the Sérsic index distribution on the stellar mass at low and high redshift. While below $10^{10.4-10.6}$ $M_{\odot}$, MS galaxies tend to be late type, above this threshold the morphological type distribution is clearly dominated by early type galaxies. Our results would suggest that while galaxy morphology is a stellar mass related phenomenon for MS galaxies, SF quenching is, instead, a more environment related process.

5.3 Discussion and conclusion

Our results support a scenario in which the quenching of SF occurs earlier in galaxies embedded in more massive halos, though we are considering a quite narrow halo mass range. This would be consistent with the results of Popesso et al. (2012) in a similar redshift range but in a broader mass range, which includes also galaxy clusters. Other evidences in the literature support the differential evolution of the SF activity in massive halos with respect to field or lower mass halos. For instance, the formation of the galaxy red sequence, which leads to the local dichotomy between red and blue galaxies, happens earlier in groups than in the field especially at high stellar masses (Iovino et al. 2010; Kovač et al. 2010b). There is also evidence that at z∼1 there is a reversal or a flattening of the SFR-density relation (Elbaz et al. 2007; Popesso et al. 2011; Ziparo et al. 2013) with respect to the local anti-correlation. Ziparo et al. (2013) find on the very same dataset that the differential evolution of the groups galaxies with respect to field is due to the fact that star forming group galaxies are perfectly on the Main Sequence at z∼1 whereas at lower redshift they are quenched, thus, dropping off the MS quicker than field galaxies towards the region of SF quiescence. However, Ziparo et al. (2013), due to the lower statistics, could analyse only the average departure of the group galaxy population from the MS. We extend this analysis to study accurately the deviation of the same population as a function of the stellar mass. Indeed, we show that group galaxies tend to occupy the lower edge of the star forming galaxy distribution across the MS above a mass threshold of $10^{10.4}M_{\odot}$. This has also the additional effect of broadening the MS toward a large dispersion in particular at low redshift. However, our data indicate also that the environment does not seem to be the cause of this flattening at high masses, since the MS show the same type of shape in all environments. At earlier epochs, MS group galaxies seem to be more in line with the distribution of star forming galaxies inhabiting other environments (field and "filament-like"). In other words, the environmental trends at fixed stellar mass seem to weaken at higher redshift, consistently with other studies (e.g. Poggianti et al. 2008; Tasca et al. 2009; Cucciati et al. 2010; Iovino et al. 2010; Kovač et al. 2010a). We point out that the departure of group star forming galaxies from the MS is a result at odds with Peng et al. (2010) who suggest the star formation activity in galaxies depends mostly on the galaxy stellar mass for massive galaxies. However, the limit of their analysis is mainly in the definition of the environment that relies on the local galaxy density, which is only a poor proxy of the DM halo mass. Indeed, we observe field (isolated) and “filament-like” galaxies MS are perfectly consistent at any redshift. As these two environments are characterized based on the relative vicinity of galaxies as expressed by the density field, it explains why Peng et al. (2010) did not observe any difference between the MS location of galaxies at different densities.

Conversely, our study of morphology among the MS galaxies in different environments clarify that the morphological type is much more related to galaxy stellar masses than star formation activity in galaxies. Indeed, recently, Wuyts et al. (2011) find that across cosmic time, the typical Sérsic index of galaxies is optimally described as a function of their positions relative to the the MS at the epoch of their observation. The correspondence between mass, SFR, and structure, as quantified by the Sérsic index, is equivalent to the Hubble sequence. Based on a quite similar galaxy sample (using SDSS for nearby universe and COSMOS, UDS and GOODS fields for high redshift samples), Wuyts et al. (2011) see that such a sequence already existed at z$\sim$2; bulge-dominated morphologies go hand in hand with a more quiescent nature. In addition, they observe that late type galaxies (Sérsic index < 1.5) follow a linear SFR-Mass relation. This is not at odds with ouer results. Indeed, we also observe that late type galaxies, especially among field and filament like galaxies, follow a linear relation. Nevertheless, they do not represent the bulk of the Main Sequence galaxy population above $10^{10.4-10.6}$ $M_{\odot}$, but only the upper envelope. This means that, while a clear morphological sequence with a linear slope and, thus, a strong stellar mass dependence, is visible in the SFR-Stellar mass plane at any mass as shown by Wuyts et al. (2011), the Main Sequence of star forming galaxies at high masses is much more poorly defined and it shows a much weaker dependence on the stellar mass ($SFR \propto M*^{0.2-0.3}$). This MS is consistent with a linear relation only in the low stellar mass range where it is dominated by late type galaxies. At high masses, late type galaxies are no longer the bulk of the MS population. There morphological sequence and star forming galaxy sequence are no longer overlapping. Our results are, indeed, in agreement with the more recent findings of Whitaker et al. (2012), that find a flatter slope of the MS at $\sim 10^{10}$ $M_{\odot}$ due to a large percentage of red galaxies. This is also consistent with the results of Rodighiero et al. (2010) that find a rather flat MS at any redshift on the basis of Herschel PACS data. Our data indicate also that the environment does not seem to be the cause of this flattening at high masses, since the MS show the same type of shape in all environment. The effect of the environment is, instead, to increase the scatter around the MS since field and filament-like galaxies tend to occupy the upper envelope of the MS and group galaxies tend to be located in the lower envelope.

We stress that our result is not at odds with the well known “morphology-density” relation. Indeed, this more general relation reflects the differential morphological type distribution of the whole galaxy population without distinction between galaxies on and off Main Sequence. In this particular analysis, we consider only MS galaxies to show that the departure of group galaxies from the MS is not related to a morphological transformation. In addition, numerous previous studies of low-redshift galaxies in the literature find that color and star formation rate are more strongly correlated with the environment than morphology (e.g. Kauffmann et al. 2004; Blanton et al. 2005; Christlein & Zabludoff 2005; van den Bosch et al. 2008; Weinmann et al. 2009). For instance, Tasca et al. (2009) and Kovač et al. (2010a) have compared the dependence of colors and morphologies on local density and in groups in the COSMOS field, finding a stronger effect on color than on morphology, similar to the low-redshift results and suggesting a longer timescale for structural transformations than for star formation quenching. The implication of these studies is that the well-known correlation between morphology and environment is secondary to the correlation between environment and star formation rate. This is consistent with our findings. Indeed, we observe that among MS galaxies the distribution of the morphological type does not depend on the environment where they reside, instead, it is much more related to the galaxy stellar masses. However, we observe a significant dependence on SF quenching of the MS group galaxies at low-redshifts. As a further step we will also include rest frame colors as additional ingredient in our analysis in order to understand whether the observed SF quenching in group galaxies is more related to a color transformation than to a morphological transformation.

What is causing this differential evolution as a function of the halo mass? According to Peng et al. (2010) massive galaxies, as the ones considered in our sample, evolve mostly because of an internally driven process, called 'mass quenching', caused perhaps by feedback from active galactic nuclei. But since this process is unlikely to be more efficient in quenching SF of massive galaxies in massive halos than in other environments, the "environmental quenching" must be the main mechanism for quenching the SF of the most massive satellites in massive halos. Which kind of process is causing this "environmental quenching" is still quite unknown. Two obvious candidates for producing this quenching, are ram-pressure stripping (Gunn & Gott 1972) and starvation (Larson, Tinsley & Caldwell, 1980). Ram-pressure stripping is a fast process (Abadi, Moore & Bower, 1999) and is effective only in galaxy systems where the gas density is high, i.e. in clusters and massive groups. Starvation, caused by the removal of the hot gas halo reservoirs of galaxies, is also a likely candidate. The removal of galaxy hot gas reservoirs inducing starvation can be caused by tidal galaxy-galaxy encounters or by the interaction with the intra-cluster/intra-group medium. Starvation should proceed more effectively in higher (galaxy or gas) density regions, hence it should quench SF earlier in more massive halos than in lower mass halos, as we observe.

However, more recently Cen (2011) propose that this differential evolution could be explained simply in terms of the current theory of gas accretion that hinges on the cold and hot two-mode accretion model (Kereš et al. 2005; Dekel & Birnboim 2006). The halo mass is the main determinant of gas accretion: large halos primarily accrete hot gas while small halos primarily accrete cold gas. The overall heating of cosmic gas due to formation of large halos (such as groups and clusters) and large-scale structures causes a progressively larger fraction of halos to inhabit regions where gas has too high entropy to cool to continue feeding the residing galaxies. The combined effect is differential in that overdense regions are heated earlier and to higher temperatures than lower density regions at any given time. Because larger halos tend to reside in more overdense regions than smaller halos, the net differential effects would naturally lead to both the standard galaxy downsizing effect and the halo downsizing effect.

Appendix A

X-ray groups of galaxies in CDFN

The catalog of X-ray groups follows the original results of Bauer et al. (2002), based on the first 1Ms Chandra data. The main difference in the catalog consist in a self-consistent use of the flux at R_{500}, larger apertures for the flux extraction. This allows us to use our calibrations of group masses, provided by COSMOS (Leauthaud et al. 2010) and ECDFS (Finoguenov et al. subm.) surveys. In column 1, 2 and 3, we provide the group identification number, RA and Dec. of the peak of X-ray emission. In Column 4, the mean of red sequence redshifts which is substituted with the median of spectroscopic redshift in case there is a spectroscopic redshift determination for the group member galaxies is given. The group flux in the 0.5–2 keV band in Column 5 with the corresponding 1σ error is listed. The rest-frame luminosity in the 0.1–2.4 keV is presented in Column 6. Column 7 gives the estimated total mass, M_{200}, computed following Leauthaud et al. (2010) and assuming a standard evolution of scaling relations: $M_{200}E_z = f(L_x E_z^{-1})$ where $E_z = (\Omega_M(1+z)^3 + \Omega_\Lambda)^{1/2}$, standard evolution of the scaling relation. The corresponding R_{200} in degrees is listed in Column 8. Column 9 lists flux significance which provides insights on the reliability of both the source detection and the identification. Column 10 presents the flag for our identification, as described in section 3.2.2. The velocity dispersion estimated from X-ray luminosities is given in column 11. The number of spectroscopic member galaxies inside $2\times R_{200}$ is given in Column 12.

Table A.1: X-ray group catalog:(1) X-ray ID; (2) RA [deg]; (3) Dec[deg]; (4) z; (5) Flux [$10^{-15} erg cm^{-2} s^{-1}$]; (6)$L_X(0.1 - 2.4 keV)[10^{42} erg/s]$; (7) $M_{200}[10^{13} M_\odot]$; (8) r_{200}[deg]; (9) Flag; (10) Flux significance; (11) Velocity dispersion from X-ray luminosities [km/s]; (12) N(z)

ID (1)	RA (2)	Dec (3)	z (4)	Flux (5)	L_X (6)	M_{200} (7)	r_{200} (8)	Flux significance (9)	Flag (10)	Velocity dispersion (11)	N(z_{spec}) (12)
2	189.45619	62.36314	0.398	1.26±0.36	1.21±0.34	2.16±0.35	0.0262	3.52	3	229	0
4	189.26089	62.35124	0.800	0.54±0.17	3.60±1.12	2.94±0.52	0.0177	3.19	1	277	9
5	188.86385	62.35366	0.652	1.91±0.57	6.32±1.89	4.69±0.79	0.0238	3.34	3	319	0
6	189.36276	62.32381	0.277	0.84±0.19	0.34±0.08	1.12±0.15	0.028	4.22	2	176	9
7	189.48284	62.25552	0.455	2.99±0.24	3.83±0.31	4.12±0.19	0.0294	12.22	1	293	14
8	189.18499	62.26416	0.850	1.38±0.17	8.92±1.07	4.85±0.34	0.0202	8.36	1	336	46
9	188.98803	62.2646	0.375	1.07±0.28	0.88±0.23	1.82±0.27	0.0259	3.78	3	214	3
10	189.07392	62.26007	1.999	0.39±0.85	36.09±7.74	4.41±0.54	0.0119	4.66	2	402	3
13	189.0872	62.18605	1.014	0.51±0.18	7.12±2.58	3.67±0.75	0.0164	2.76	1	314	20
14	189.5959	62.1628	0.914	1.24±0.32	10.77E±2.74	5.13±0.75	0.0196	3.92	3	348	0
15	189.33336	62.12823	0.943	0.76±0.17	7.80±1.71	4.13±0.52	0.0179	4.56	3	323	0
16	189.13775	62.15006	0.840	0.48±0.12	3.77±0.93	2.92±0.41	0.0171	4.05	1	279	12
17	189.04209	62.14711	1.139	0.61±0.14	11.41±2.52	4.37±0.56	0.0162	4.52	3	343	2
19	188.96164	62.12097	0.491	2.49±0.40	3.84±0.62	4.00±0.38	0.0275	6.2	3	292	0
20	189.538	62.13181	0.948	0.64±0.23	6.89±2.46	3.81±0.77	0.0174	2.8	3	314	0
21	188.86226	62.10217	0.895	1.37±0.41	11.05±3.41	5.30±0.93	0.0201	3.24	5	351	0
22	189.11361	62.10088	1.217	0.45±0.13	10.99±3.14	4.00±0.65	0.0152	3.5	3	337	1
23	189.28445	62.09072	0.956	0.69±0.17	7.46±1.88	3.97±0.57	0.0175	3.96	3	319	0
24	189.02017	62.08888	1.217	0.91±0.22	17.94±4.34	5.37±0.74	0.0167	4.13	5	375	0
25	189.22003	62.07086	0.188	4.20±0.53	0.65±0.08	1.75±0.13	0.045	7.92	3	204	0
27	189.28874	62.02523	1.640	1.20±0.27	46.55±10.55	6.73±0.88	0.0152	4.41	5	442	0
28	189.17982	62.02048	0.426	1.80±0.42	1.98±0.47	2.84±0.39	0.0273	4.22	3	254	0
30	189.08941	62.26975	0.681	0.17±0.11	0.90±0.61	1.42±0.52	0.0155	1.48	2	207	7
31	189.10007	62.25822	0.642	0.45±0.28	1.71±1.06	2.16±0.73	0.0185	1.6	2	240	10
32	189.09046	62.26367	1.241	0.19±0.08	6.75±2.73	2.93±0.66	0.0135	2.48	4	302	3
33	189.3379	62.15165	1.126	0.49±0.11	9.45±2.23	3.95±0.53	0.0158	4.24	3	330	0
34	189.53013	62.11978	0.280	1.26±0.57	0.51±0.23	1.41±0.36	0.03	2.2	5	192	0

Acknowledgement

In the last three years I had the chance to get to know many people who preciously contributed to achieve the present goal. I would like to thank my supervisor, Paul Nandra, for great support and encouragement, and for always spreading a positive, open attitude. Thanks for always being so understanding during my PhD study. I would especially like to thank my project supervisors Alexis Finoguenov and Paola Popesso. Thanks Alexis for believing in me from the first step. Thanks for offering me the possibility to be part of IMPRS and exciting scientific projects, for giving me valuable advice when needed, for encouraging new projects. Thank you for your constant presence and sponsoring. Thank you Paola for your advice in every step of my work. It is very enjoyable working with a smart person like you; thanks for being supportive. Thanks for your constant support even when you were in parental leave. Thank you very much for your patient supervision and your teachings. I hope to continue this friendly and stimulating scientific and personal collaboration.

I am indebted to many other people who contributed to this thesis either scientifically, with moral support, or just by making MPE a great place to work. Thanks to Antonis Georgakakis for being a great thesis committee member and for helpful research discussions. Thanks to Dave wilman for the useful discussion and comments. Thanks to Stijn Wuyts for the helpful advices and discussions. Thanks Mara Salvato for your precious advices. I am also indebted to Birgit Böller for going above and beyond the call duty of a secretary on more than one occasion. Special thanks to Florian Hofmann for translating the abstract in German. I would also like to thank my other collaborators around the world. Thanks Masayuki Tanaka, Andrea Biviano, Mike Lerchster, Mike Balogh and many other people who collabrate very nicely during these years.

In addition, I would like to thank those people who helped me to have a great time throughout the last three years. Thanks Alex for the good chats , the coffee breaks, and all your kind helps during these three years. I would especially like to thank Zohreh Taher, Amir Abolghassem and Yasam Taher for the great and very nice moments we had together. Thanks Mahsa for your great friendship and support. Thanks Azadeh for your long distant friendship and support. Thanks Tahmineh, Maryam for your great friendship.

And finally, my deep gratitude goes to my family for their eternal support. Thanks

to my mother and father, Azar and Faramarz, for always encouraging me to explore the science and work hard at my chosen endeavor. Thanks for your endless love and support. To my younger sister, Sepideh, for all the empathy and perspective. And Mohammad, thanks for the happiness and the serenity you gave me. Without having met you, I would not be where I am. Thank you for sharing with me the most important and beautiful moments during these years and for always being present in the difficult ones.

Bibliography

Abadi M. G., Moore B., Bower R. G., 1999, MNRAS, 308, 947

Akritas M. G., Bershady M. A., 1996, ApJ, 470, 706

Alexander D. M. et al., 2003, AJ, 126, 539

Allevato V. et al., 2012, ApJ, 758, 47

Allington-Smith J. R., Ellis R., Zirbel E. L., Oemler J. A., 1993, ApJ, 404, 521

Angulo R. E., Springel V., White S. D. M., Jenkins A., Baugh C. M., Frenk C. S., 2012, MNRAS, 426, 2046

Arnaud M., Evrard A. E., 1999, MNRAS, 305, 631

Bai L. et al., 2007, ApJ, 664, 181

Balogh M. L., Babul A., Voit G. M., McCarthy I. G., Jones L. R., Lewis G. F., Ebeling H., 2006, MNRAS, 366, 624

Balogh M. L. et al., 2009, MNRAS, 398, 754

Balogh M. L. et al., 2011, MNRAS, 412, 2303

Balogh M. L., Navarro J. F., Morris S. L., 2000, ApJ, 540, 113

Barger A. J., Cowie L. L., Wang W.-H., 2008, ApJ, 689, 687

Barmby P., Huang J.-S., Ashby M. L. N., Eisenhardt P. R. M., Fazio G. G., Willner S. P., Wright E. L., 2008, ApJS, 177, 431

Barnes J., 1985, MNRAS, 215, 517

Bartelmann M., Schneider P., 2001, Physis Reports, 340, 291

Bauer F. E. et al., 2002, AJ, 123, 1163

Baugh C. M., 2006, Reports on Progress in Physics, 69, 3101

Baugh C. M., Cole S., Frenk C. S., Lacey C. G., 1998, ApJ, 498, 504

Beers T. C., Flynn K., Gebhardt K., 1990, AJ, 100, 32

Benson B. A., Church S. E., Ade P. A. R., Bock J. J., Ganga K. M., Henson C. N., Thompson K. L., 2004, ApJ, 617, 829

Berta S. et al., 2013, A&A, 551, A100

Berta S. et al., 2010, A&A, 518, L30

Berta S. et al., 2011, A&A, 532, A49

Bielby R. et al., 2012, A&A, 545, A23

Bielby R. M. et al., 2010, A&A, 523, A66

Binney J., Tremaine S., 1987, Galactic dynamics

Blanton M. R. et al., 2005, AJ, 129, 2562

Böhringer H. et al., 2000, ApJS, 129, 435

Borne K. D., Bushouse H., Lucas R. A., Colina L., 2000, ApJ, 529, L77

Brimioulle F., Lerchster M., Seitz S., Bender R., Snigula J., 2008, ArXiv e-prints

Brinchmann J., Charlot S., White S. D. M., Tremonti C., Kauffmann G., Heckman T., Brinkmann J., 2004, MNRAS, 351, 1151

Buat V., Takeuchi T. T., Burgarella D., Giovannoli E., Murata K. L., 2009, A&A, 507, 693

Bundy K. et al., 2006, ApJ, 651, 120

Butcher H., Oemler J. A., 1978, ApJ, 219, 18

Butcher H., Oemler J. A., 1984, ApJ, 285, 426

Caldwell N., Rose J. A., Sharples R. M., Ellis R. S., Bower R. G., 1993, AJ, 106, 473

Capak P. et al., 2007, ApJS, 172, 99

Capak P. L., 2009, in American Astronomical Society Meeting Abstracts, Vol. 214, American Astronomical Society Meeting Abstracts #214, p. #200.06

Caputi K. I. et al., 2009, ApJ, 691, 91

Caputi K. I. et al., 2007, ApJ, 660, 97

Cardamone C. N. et al., 2010, ApJS, 189, 270

Carlberg R. G., Yee H. K. C., Ellingson E., 1997, ApJ, 478, 462

Carlberg R. G. et al., 1999, Royal Society of London Philosophical Transactions Series A, 357, 167

Carlstrom J. E., Holder G. P., Reese E. D., 2002, ARA&A, 40, 643

Cen R., 2011, ApJ, 741, 99

Chabrier G., 2003, PASP, 115, 763

Chandrasekhar S., 1943, ApJ, 97, 255

Charlot S., Bruzual A. G., 1991, ApJ, 367, 126

Christlein D., Zabludoff A. I., 2005, ApJ, 621, 201

Cimatti A. et al., 2008, A&A, 482, 21

Coil A. L. et al., 2009, ApJ, 701, 1484

Coil A. L., Newman J. A., Kaiser N., Davis M., Ma C.-P., Kocevski D. D., Koo D. C., 2004, ApJ, 617, 765

Cole S., 1991, ApJ, 367, 45

Colless M. et al., 2001, MNRAS, 328, 1039

Connelly J. L. et al., 2012, ApJ, 756, 139

Conselice C. J., 2003, ApJS, 147, 1

Cooper M. C. et al., 2011, ApJS, 193, 14

Cooper M. C. et al., 2012, MNRAS, 419, 3018

Cooper M. C. et al., 2007, MNRAS, 376, 1445

Cooper M. C. et al., 2008, MNRAS, 383, 1058

Croton D. J. et al., 2006, MNRAS, 365, 11

Cucciati O. et al., 2010, A&A, 524, A2

Daddi E. et al., 2007, ApJ, 670, 156

Damen M. et al., 2011, ApJ, 727, 1

Dariush A., Khosroshahi H. G., Ponman T. J., Pearce F., Raychaudhury S., Hartley W., 2007, MNRAS, 382, 433

Davis M. et al., 2003, in Society of Photo-Optical Instrumentation Engineers (SPIE) Conference Series, Vol. 4834, Society of Photo-Optical Instrumentation Engineers (SPIE) Conference Series, Guhathakurta P., ed., pp. 161–172

Davis M., Geller M. J., 1976, ApJ, 208, 13

Davis M. et al., 2007, ApJ, 660, L1

De Lucia G., Blaizot J., 2007, MNRAS, 375, 2

De Lucia G., Springel V., White S. D. M., Croton D., Kauffmann G., 2006, MNRAS, 366, 499

De Lucia G., Weinmann S., Poggianti B. M., Aragón-Salamanca A., Zaritsky D., 2012, MNRAS, 423, 1277

Dekel A., Birnboim Y., 2006, MNRAS, 368, 2

Di Matteo T., Springel V., Hernquist L., 2005, Nat, 433, 604

Diaferio A., Geller M. J., 1997, ApJ, 481, 633

Diaferio A., Geller M. J., Ramella M., 1994, AJ, 107, 868

Diaferio A., Geller M. J., Ramella M., 1995, AJ, 109, 2293

Díaz-Giménez E., Mamon G. A., Pacheco M., Mendes de Oliveira C., Alonso M. V., 2012, MNRAS, 426, 296

Dressler A., 1980, ApJ, 236, 351

Dressler A., Shectman S. A., 1988, AJ, 95, 985

Efron B., 1982, The Jackknife, the Bootstrap and other resampling plans

Eigenthaler P., Zeilinger W. W., 2009, Astronomische Nachrichten, 330, 978

Einasto J. et al., 2003a, A&A, 410, 425

Einasto J., Hütsi G., Einasto M., Saar E., Tucker D. L., Müller V., Heinämäki P., Allam S. S., 2003b, A&A, 405, 425

Eisenhardt P. R. M. et al., 2008, ApJ, 684, 905

Eke V. R., Baugh C. M., Cole S., Frenk C. S., King H. M., Peacock J. A., 2005, MNRAS, 362, 1233

Eke V. R. et al., 2004, MNRAS, 348, 866

El-Zant A. A., Hoffman Y., Primack J., Combes F., Shlosman I., 2004, ApJ, 607, L75

Elbaz D. et al., 2007, A&A, 468, 33

Elbaz D. et al., 2011, A&A, 533, A119

Elvis M. et al., 2009, ApJS, 184, 158

Erfanianfar G. et al., 2013, ApJ, 765, 117

Faber S. M. et al., 2003, in Society of Photo-Optical Instrumentation Engineers (SPIE) Conference Series, Vol. 4841, Instrument Design and Performance for Optical/Infrared Ground-based Telescopes, Iye M., Moorwood A. F. M., eds., pp. 1657–1669

Farouki R., Shapiro S. L., 1981, ApJ, 243, 32

Feruglio C. et al., 2010, ApJ, 721, 607

Finn R. A. et al., 2010, ApJ, 720, 87

Finoguenov A. et al., 2009, ApJ, 704, 564

Finoguenov A. et al., 2007, ApJS, 172, 182

Finoguenov A. et al., 2010, MNRAS, 403, 2063

Forman W., Jones C., 1982, ARA&A, 20, 547

Frederic J. J., 1995, ApJS, 97, 259

Gao L., White S. D. M., Jenkins A., Stoehr F., Springel V., 2004, MNRAS, 355, 819

Gavazzi G., Boselli A., Pedotti P., Gallazzi A., Carrasco L., 2002, A&A, 396, 449

Geller M. J., Huchra J. P., 1983, ApJS, 52, 61

George M. R. et al., 2011, ApJ, 742, 125

George M. R., Ma C.-P., Bundy K., Leauthaud A., Tinker J., Wechsler R. H., Finoguenov A., Vulcani B., 2013, ApJ, 770, 113

Gerke B. F. et al., 2012, ApJ, 751, 50

Gerke B. F. et al., 2005, ApJ, 625, 6

Gerke B. F. et al., 2007, MNRAS, 376, 1425

Giacconi R. et al., 2002, ApJS, 139, 369

Giavalisco M. et al., 2004, ApJ, 600, L93

Gilbank D. G., Gladders M. D., Yee H. K. C., Hsieh B. C., 2011, AJ, 141, 94

Giodini S. et al., 2012, A&A, 538, A104

Girardi M., Mezzetti M., 2001, ApJ, 548, 79

Gladders M. D., Yee H. K. C., 2005, ApJS, 157, 1

Gnedin O. Y., 2003, ApJ, 582, 141

Gómez P. L. et al., 2003, ApJ, 584, 210

Goto T. et al., 2003, PASJ, 55, 739

Governato F., Tozzi P., Cavaliere A., 1996, ApJ, 458, 18

Graham A. W., Driver S. P., 2005, PASA, 22, 118

Grazian A. et al., 2006, A&A, 449, 951

Griffith R. L. et al., 2012, ApJS, 200, 9

Gruppioni C. et al., 2013, MNRAS, 432, 23

Gunn J. E., 1977, ApJ, 218, 592

Gunn J. E., Gott I. J. R., 1972, ApJ, 176, 1

Guo Q. et al., 2011, MNRAS, 413, 101

Guo Q., White S., Li C., Boylan-Kolchin M., 2010, MNRAS, 404, 1111

Guth A. H., 1981, Phys. Rev. D, 23, 347

Hansen S. M., Sheldon E. S., Wechsler R. H., Koester B. P., 2009, ApJ, 699, 1333

Hasinger G. et al., 2007, ApJS, 172, 29

Hausman M. A., Ostriker J. P., 1978, ApJ, 224, 320

Helsdon S. F., Ponman T. J., 2000, MNRAS, 319, 933

Hickox R. C., Markevitch M., 2006, ApJ, 645, 95

Hickson P., 1982, ApJ, 255, 382

Hickson P., 1997, ARA&A, 35, 357

Hoekstra H., Bartelmann M., Dahle H., Israel H., Limousin M., Meneghetti M., 2013, Space Science Reviews, 177, 75

Hoekstra H., Franx M., Kuijken K., Squires G., 1998, ApJ, 504, 636

Hoekstra H., Jain B., 2008, Annual Review of Nuclear and Particle Science, 58, 99

Hogg D. W. et al., 2004, ApJ, 601, L29

Hopkins P. F., Hernquist L., Cox T. J., Di Matteo T., Robertson B., Springel V., 2006, ApJS, 163, 1

Huchra J. P., Geller M. J., 1982, ApJ, 257, 423

Ilbert O. et al., 2009, ApJ, 690, 1236

Ilbert O. et al., 2010, ApJ, 709, 644

Iovino A. et al., 2010, A&A, 509, A40

Jansen R. A., Franx M., Fabricant D., 2001, ApJ, 551, 825

Jeltema T. E. et al., 2009, MNRAS, 399, 715

Jeltema T. E., Mulchaey J. S., Lubin L. M., Fassnacht C. D., 2007, ApJ, 658, 865

Jenkins A., Frenk C. S., White S. D. M., Colberg J. M., Cole S., Evrard A. E., Couchman H. M. P., Yoshida N., 2001, MNRAS, 321, 372

Jones L. R., Ponman T. J., Forbes D. A., 2000, MNRAS, 312, 139

Jones L. R., Ponman T. J., Horton A., Babul A., Ebeling H., Burke D. J., 2003, MNRAS, 343, 627

Kaiser N., Squires G., 1993, ApJ, 404, 441

Kang X., Jing Y. P., Mo H. J., Börner G., 2005, ApJ, 631, 21

Kauffmann G., 1995, MNRAS, 274, 153

Kauffmann G. et al., 2003, MNRAS, 341, 54

Kauffmann G., White S. D. M., Heckman T. M., Ménard B., Brinchmann J., Charlot S., Tremonti C., Brinkmann J., 2004, MNRAS, 353, 713

Kennicutt J. R. C., 1998, ARA&A, 36, 189

Kennicutt R. C., Evans N. J., 2012, ARA&A, 50, 531

Kepner J., Fan X., Bahcall N., Gunn J., Lupton R., Xu G., 1999, ApJ, 517, 78

Kereš D., Katz N., Weinberg D. H., Davé R., 2005, MNRAS, 363, 2

Kewley L. J., Geller M. J., Jansen R. A., 2004, AJ, 127, 2002

Khosroshahi H. G., Ponman T. J., Jones L. R., 2007, MNRAS, 377, 595

Kimm T. et al., 2009, MNRAS, 394, 1131

Kitzbichler M. G., White S. D. M., 2007, MNRAS, 376, 2

Knobel C. et al., 2012, ApJ, 753, 121

Knobel C. et al., 2009, ApJ, 697, 1842

Koester B. P. et al., 2007, ApJ, 660, 239

Kovač K. et al., 2010a, ApJ, 718, 86

Kovač K. et al., 2010b, ApJ, 718, 86

Kriek M., van Dokkum P. G., Labbé I., Franx M., Illingworth G. D., Marchesini D., Quadri R. F., 2009, ApJ, 700, 221

Kroupa P., 2001, MNRAS, 322, 231

Lacey C., Silk J., 1991, ApJ, 381, 14

Laird E. S. et al., 2009, ApJS, 180, 102

LaRoque S. J. et al., 2003, ApJ, 583, 559

Larson R. B., Tinsley B. M., 1978, ApJ, 219, 46

Larson R. B., Tinsley B. M., Caldwell C. N., 1980, ApJ, 237, 692

Lavery R. J., Henry J. P., 1986, ApJ, 304, L5

Lavery R. J., Henry J. P., 1988, ApJ, 330, 596

Le Floc'h E. et al., 2009, ApJ, 703, 222

Le Floc'h E. et al., 2005, ApJ, 632, 169

Leauthaud A. et al., 2010, ApJ, 709, 97

Lehmer B. D. et al., 2005, ApJS, 161, 21

Lewis I. et al., 2002, MNRAS, 334, 673

Lilly S. J. et al., 2009, ApJS, 184, 218

Lilly S. J., Le Fevre O., Hammer F., Crampton D., 1996, ApJ, 460, L1

Lilly S. J. et al., 2007, ApJS, 172, 70

Lin Y.-T., Mohr J. J., Stanford S. A., 2004, ApJ, 610, 745

Liu L., Yang X., Mo H. J., van den Bosch F. C., Springel V., 2010, ApJ, 712, 734

Lotz J. M., 2007, in Astronomical Society of the Pacific Conference Series, Vol. 380, Deepest Astronomical Surveys, Afonso J., Ferguson H. C., Mobasher B., Norris R., eds., p. 467

Lotz J. M. et al., 2008, ApJ, 672, 177

Lucatello S., Gratton R. G., Beers T. C., Carretta E., 2005, ApJ, 625, 833

Lutz D. et al., 2011, A&A, 532, A90

Lynden-Bell D., 1967, MNRAS, 136, 101

Madau P., Ferguson H. C., Dickinson M. E., Giavalisco M., Steidel C. C., Fruchter A., 1996, MNRAS, 283, 1388

Magnelli B., Elbaz D., Chary R. R., Dickinson M., Le Borgne D., Frayer D. T., Willmer C. N. A., 2009, A&A, 496, 57

Magnelli B. et al., 2013, A&A, 553, A132

Mahdavi A., Geller M. J., Böhringer H., Kurtz M. J., Ramella M., 1999, ApJ, 518, 69

Mamon G. A., 1986, ApJ, 307, 426

Mamon G. A., 1987, ApJ, 321, 622

Maraston C., Strömbäck G., Thomas D., Wake D. A., Nichol R. C., 2009, MNRAS, 394, L107

Marcillac D., Rigby J. R., Rieke G. H., Kelly D. M., 2007, ApJ, 654, 825

Margoniner V. E., de Carvalho R. R., Gal R. R., Djorgovski S. G., 2001, ApJ, 548, L143

Marinoni C., Hudson M. J., 2002, ApJ, 569, 101

Martin D. C. et al., 2005, ApJ, 619, L1

Massey R. et al., 2007, MNRAS, 376, 13

Materne J., 1978, A&A, 63, 401

Mei S. et al., 2012, ApJ, 754, 141

Mellier Y., 1999, ARA&A, 37, 127

Miller C. J. et al., 2005, AJ, 130, 968

Miller N. A., Fomalont E. B., Kellermann K. I., Mainieri V., Norman C., Padovani P., Rosati P., Tozzi P., 2008, ApJS, 179, 114

Miyazaki S., Hamana T., Ellis R. S., Kashikawa N., Massey R. J., Taylor J., Refregier A., 2007, ApJ, 669, 714

Mo H., van den Bosch F. C., White S., 2010, Galaxy Formation and Evolution

Mok A. et al., 2013, MNRAS, 431, 1090

Moore B., Katz N., Lake G., Dressler A., Oemler A., 1996, Nat, 379, 613

Morrison G. E., Owen F. N., Dickinson M., Ivison R. J., Ibar E., 2010, ApJS, 188, 178

Moss C., Whittle M., 1993, ApJ, 407, L17

Moustakas J., Kennicutt J. R. C., Tremonti C. A., 2006, ApJ, 642, 775

Mulchaey J. S., 2000, ARA&A, 38, 289

Mulchaey J. S., Zabludoff A. I., 1998, ApJ, 496, 73

Mulchaey J. S., Zabludoff A. I., 1999, ApJ, 514, 133

Newman J. A. et al., 2012, ArXiv e-prints

Nichol R. C., 2004, Clusters of Galaxies: Probes of Cosmological Structure and Galaxy Evolution, 24

Noeske K. G. et al., 2007a, ApJ, 660, L47

Noeske K. G. et al., 2007b, ApJ, 660, L43

Nolthenius R., White S. D. M., 1987, MNRAS, 225, 505

Osmond J. P. F., Ponman T. J., 2004, MNRAS, 350, 1511

O'Sullivan E., Ponman T. J., 2004, MNRAS, 354, 935

O'Sullivan E., Ponman T. J., Collins R. S., 2003, MNRAS, 340, 1375

Padovani P., Mainieri V., Tozzi P., Kellermann K. I., Fomalont E. B., Miller N., Rosati P., Shaver P., 2009, ApJ, 694, 235

Papovich C., Dickinson M., Ferguson H. C., 2001, ApJ, 559, 620

Peacock J. A., 1999, Cosmological Physics

Peebles P. J. E., 1980, The large-scale structure of the universe

Peng Y. et al., 2010, ApJ, 721, 193

Peng Y., Lilly S. J., Renzini A., Carollo M., 2012, ApJ, 757, 4

Pérez-González P. G. et al., 2005, ApJ, 630, 82

Pierre M., Clerc N., Maughan B., Pacaud F., Papovich C., Willmer C. N. A., 2012, A&A, 540, A4

Pilbratt G. L. et al., 2010, A&A, 518, L1

Pipino A., Fan X. L., Matteucci F., Calura F., Silva L., Granato G., Maiolino R., 2011, A&A, 525, A61

Pisani A., Ramella M., Geller M. J., 2003, AJ, 126, 1677

Poggianti B. M. et al., 2008, ApJ, 684, 888

Poggianti B. M., Smail I., Dressler A., Couch W. J., Barger A. J., Butcher H., Ellis R. S., Oemler J. A., 1999, ApJ, 518, 576

Poggianti B. M. et al., 2006, ApJ, 642, 188

Poglitsch A. et al., 2010, A&A, 518, L2

Ponman T. J., Allan D. J., Jones L. R., Merrifield M., McHardy I. M., Lehto H. J., Luppino G. A., 1994, Nat, 369, 462

Ponman T. J., Cannon D. B., Navarro J. F., 1999, Nat, 397, 135

Ponman T. J., Sanderson A. J. R., Finoguenov A., 2003, MNRAS, 343, 331

Popesso P. et al., 2012, A&A, 537, A58

Popesso P., Biviano A., Romaniello M., Böhringer H., 2007, A&A, 461, 411

Popesso P., Böhringer H., Romaniello M., Voges W., 2005, A&A, 433, 415

Popesso P. et al., 2011, A&A, 532, A145

Postman M., Geller M. J., 1984, ApJ, 281, 95

Pratt G. W., Böhringer H., Croston J. H., Arnaud M., Borgani S., Finoguenov A., Temple R. F., 2007, A&A, 461, 71

Prescott M. K. M., Impey C. D., Cool R. J., Scoville N. Z., 2006, ApJ, 644, 100

Quadri R. et al., 2007, AJ, 134, 1103

Rakos K. D., Schombert J. M., 1995, ApJ, 439, 47

Reddy N. A., Steidel C. C., Pettini M., Adelberger K. L., Shapley A. E., Erb D. K., Dickinson M., 2008, ApJS, 175, 48

Ricciardelli E., Franceschini A., 2010, A&A, 518, A14

Richstone D. O., 1976, ApJ, 204, 642

Rix H.-W. et al., 2004, ApJS, 152, 163

Rodighiero G. et al., 2010, A&A, 518, L25

Rykoff E. S. et al., 2008, MNRAS, 387, L28

Sanders D. B. et al., 2007, ApJS, 172, 86

Santini P. et al., 2009, A&A, 504, 751

Santos W. A., Mendes de Oliveira C., Sodré J. L., 2007, AJ, 134, 1551

Schmidt M., 1959, ApJ, 129, 243

Scodeggio M. et al., 2009, A&A, 501, 21

Scoville N. et al., 2007, ApJS, 172, 1

Sersic J. L., Garcia Lambas D., Mosconi M. B., 1986, RMxAA, 12, 132

Shapley A. E., Steidel C. C., Adelberger K. L., Dickinson M., Giavalisco M., Pettini M., 2001, ApJ, 562, 95

Shapley A. E., Steidel C. C., Erb D. K., Reddy N. A., Adelberger K. L., Pettini M., Barmby P., Huang J., 2005, ApJ, 626, 698

Silverman J. D. et al., 2010, ApJS, 191, 124

Soifer B. T., Helou G., Werner M., 2008, ARA&A, 46, 201

Somerville R. S., Hopkins P. F., Cox T. J., Robertson B. E., Hernquist L., 2008, MNRAS, 391, 481

Spitzer J. L., Baade W., 1951, ApJ, 113, 413

Springel V., Frenk C. S., White S. D. M., 2006, Nat, 440, 1137

Springel V., Hernquist L., 2003, MNRAS, 339, 312

Springel V. et al., 2005, Nat, 435, 629

Stanford S. A. et al., 2006, ApJ, 646, L13

Stewart K. R., Bullock J. S., Wechsler R. H., Maller A. H., Zentner A. R., 2008, ApJ, 683, 597

Stoughton C. et al., 2002, AJ, 123, 485

Strateva I. et al., 2001, AJ, 122, 1861

Sun M., 2012, New Journal of Physics, 14, 045004

Sunyaev R. A., Zeldovich Y. B., 1972, Comments on Astrophysics and Space Physics, 4, 173

Tanaka M., Finoguenov A., Ueda Y., 2010, ApJ, 716, L152

Taniguchi Y. et al., 2007, ApJS, 172, 9

Tasca L. A. M. et al., 2009, A&A, 503, 379

Tinker J., Kravtsov A. V., Klypin A., Abazajian K., Warren M., Yepes G., Gottlöber S., Holz D. E., 2008, ApJ, 688, 709

Toomre A., Toomre J., 1972, ApJ, 178, 623

Tran K.-V. H., Moustakas J., Gonzalez A. H., Bai L., Zaritsky D., Kautsch S. J., 2008, ApJ, 683, L17

Trump J. R. et al., 2007, ApJS, 172, 383

Tucker D. L. et al., 2000, ApJS, 130, 237

Tully R. B., 1980, ApJ, 237, 390

Tully R. B., 1987, ApJ, 321, 280

Tumlinson J., 2007a, ApJ, 665, 1361

Tumlinson J., 2007b, ApJ, 664, L63

Turner E. L., Gott I. J. R., 1976, ApJS, 32, 409

Tyson J. A., Wenk R. A., Valdes F., 1990, ApJ, 349, L1

van den Bosch F. C., Aquino D., Yang X., Mo H. J., Pasquali A., McIntosh D. H., Weinmann S. M., Kang X., 2008, MNRAS, 387, 79

van den Bosch F. C., Yang X., Mo H. J., 2003, MNRAS, 340, 771 van Dokkum P. G., 2008, ApJ, 674, 29

van Dokkum P. G., Conroy C., 2010, Nat, 468, 940

Vikhlinin A. et al., 2009, ApJ, 692, 1033

Vikhlinin A., McNamara B. R., Hornstrup A., Quintana H., Forman W., Jones C., Way M., 1999, ApJ, 520, L1

Voit G. M., 2005, Reviews of Modern Physics, 77, 207

von Benda-Beckmann A. M., D'Onghia E., Gottlöber S., Hoeft M., Khalatyan A., Klypin A., Müller V., 2008, MNRAS, 386, 2345

Wang L., Li C., Kauffmann G., De Lucia G., 2007, MNRAS, 377, 1419

Weinmann S. M., Kauffmann G., van den Bosch F. C., Pasquali A., McIntosh D. H., Mo H., Yang X., Guo Y., 2009, MNRAS, 394, 1213

Weinmann S. M., Neistein E., Dekel A., 2011, MNRAS, 417, 2737

Weinmann S. M., van den Bosch F. C., Yang X., Mo H. J., 2006, MNRAS, 366, 2

Werner M. W. et al., 2004, ApJS, 154, 1

Whitaker K. E., van Dokkum P. G., Brammer G., Franx M., 2012, ApJ, 754, L29

White M., Kochanek C. S., 2002, ApJ, 574, 24

White S. D. M., Frenk C. S., 1991, ApJ, 379, 52

White S. D. M., Rees M. J., 1978, MNRAS, 183, 341

Willner S. P. et al., 2012, ApJ, 756, 72

Wilman D. J. et al., 2005, MNRAS, 358, 88

Wilman D. J., Erwin P., 2012, ApJ, 746, 160

Wilman D. J., Fontanot F., De Lucia G., Erwin P., Monaco P., 2013, MNRAS, 433, 2986

Wilman D. J., Oemler J. A., Mulchaey J. S., McGee S. L., Balogh M. L., Bower R. G., 2009, ApJ, 692, 298

Wolf C. et al., 2009, MNRAS, 393, 1302

Wright N. J., Drake J. J., Civano F., 2010, ApJ, 725, 480

Wuyts S. et al., 2011, ApJ, 742, 96

Xue Y. Q. et al., 2011, ApJS, 195, 10

Yang X., Mo H. J., Jing Y. P., van den Bosch F. C., Chu Y., 2004, MNRAS, 350, 1153

Yang X., Mo H. J., van den Bosch F. C., 2003, MNRAS, 339, 1057

Yang X., Mo H. J., van den Bosch F. C., 2008, ApJ, 676, 248

Yang X., Mo H. J., van den Bosch F. C., Jing Y. P., 2005, MNRAS, 356, 1293

Yang X., Mo H. J., van den Bosch F. C., Pasquali A., Li C., Barden M., 2007, ApJ, 671, 153

Zabludoff A. I., Mulchaey J. S., 1998, ApJ, 496, 39

Zepf S. E., Whitmore B. C., 1993, ApJ, 418, 72

Ziparo F. et al., 2013, MNRAS, 434, 3089

Ziparo F. et al., 2014, MNRAS, 437, 458

Zwicky F., 1937, ApJ, 86, 217

Cirriculum Vitae

Ghazaleh Erfanianfar

Departmental Address:

Max Planck Institute for Extraterrestrial Physics
Giessenbachstrasse 1
85748 Garching, Germany
+49-89-30000-3210
erfanian@mpe.mpg.de

Educations:

2010–2013: PhD student of the International Max Planck Research School at the Max-Planck-Institut fur extraterrestrische Physik (Garching bei München, Germany).

2010: Master degree in Physics at Sharif university of technology (Tehran, Iran).

2008: Bachelor degree in Physics at Sharif university of technology (Tehran, Iran).

Special honors and awards:

Selected and honored as top five students in B.Sc, Physics department, Sharif University of Technology, 2008.

Publicatios:

1) **G. Erfanianfar**, A. Finoguenov, M. Tanaka, et al. "X-ray groups of galaxies in the AEGIS deep and wide fields", 2013, 756, 117 ApJ.

2) **G. Erfanianfar**, P. Popesso, A. Finoguenov, A. Biviano, D. Wilman, et al. "The evolution of star formation activity in galaxy groups" submitted to MNRAS.

3) G. Mountrichas, G. Georgakakis, A. Finoguenov, **G. Erfanianfar**, M.C. Cooper, A. L. Coil, et al. “Measuring the dark matter halo mass of X-ray AGN at z 1 using photometric redshifts”, 2013, 430, 631, MNRAS.

4) M. Mirkazemi, A. Finoguenov, M. J. Pereira, M. Tanaka, **G. Erfanianfar**, et al. “Brightest Xray clusters of galaxies in the CFHTLS wide fields” submitted to A&A.

Languages:

Persian : Native Speaker

English : Fluent

German : Basic